2014

The Contribution of Fly Ash Components to PCDD/F Formation

Phillip M. Potter
Louisiana State University and Agricultural and Mechanical College, ppotte2@tigers.lsu.edu

THE CONTRIBUTION OF FLY ASH COMPONENTS TO PCDD/F FORMATION

A Dissertation

Submitted to the Graduate Faculty of the
Louisiana State University and
Agricultural and Mechanical College
in partial fulfillment of the
requirements for the degree of
Doctor of Philosophy

in

The Department of Chemistry

by
Phillip M. Potter
B.S., Augusta State University, 2009
May 2015

Table of Contents

List of Tables

List of Figures

List of Schemes

List of Abbreviations

PCDD/Fs	-	polychlorinated dibenzo-*p*-dioxins and dibenzofurans
EPFRs	-	environmentally persistent free radicals
2-MCP	-	2-monochlorophenol
STDS	-	System for Thermal Diagnostic Studies
GC/MS	-	gas chromatograph / mass spectrometer
ICP-OES	-	inductively coupled plasma – optical emission spectroscopy
XRD	-	x-ray diffraction
XPS	-	x-ray photoelectron spectroscopy
SEM-EDS	-	scanning electron microscopy – energy dispersive spectroscopy
BET	-	Brunauer-Emmett-Teller
DF	-	dibenzofuran
DD	-	dibenzo-*p*-dioxin
MCDF	-	monochlorodibenzofuran
MCDD	-	monochlorodibenzo-*p*-dioxin
DCDF	-	dichlorodibenzofuran
DCDD	-	dichlorodibenzo-*p*-dioxin
TriCDD	-	trichlorodibenzo-*p*-dioxin
TeCDD	-	tetrachlorodibenzo-*p*-dioxin

Abstract

Chlorinated aromatics undergo surface-mediated reactions with metal oxides to form environmentally persistent free radicals (EPFRs) which can further react to produce polychlorinated dibenzo-*p*-dioxins and dibenzofurans (PCDD/Fs). Previous work using laboratory-made fly ash surrogates composed of transition metal oxides deposited on silica powder has confirmed their ability to mimic fly ash in the production of PCDD/Fs. However, little is known about the propensity of alumina and aluminosilicates to form PCDD/Fs. Cooperative catalysis between transition metals in the formation of PCDD/Fs has also seen little research.

A fly ash sample containing both alumina and mullite, an aluminosilicate, was tested for PCDD/F formation ability and compared to PCDD/F yields from the thermal degradation of 2-monochlorophenol (2-MCP) precursor over γ-alumina, α-alumina, and mullite. A series of fly ash surrogates with varying amounts of co-deposited iron (III) oxide and copper (II) oxide, both known to increase PCDD/F formation individually, were also investigated. A packed-bed flow reactor was used to investigate the thermal degradation of 2-MCP over the various catalysts at 200-600 ^{0}C.

Fly ash gave similar PCDD/F yields to surrogates made with similar transition metal content. γ-alumina, which is thermodynamically unfavorable, was very catalytically active and gave low PCDD/F yields despite a high destruction of 2-MCP. Mullite and α-alumina, the thermodynamically favorable form of alumina, yielded higher concentrations of dioxins and products with a higher degree of chlorine substitution than γ-alumina. The data suggests that certain aluminas and aluminosilicates, commonly

found in fly ash, are active in the formation of PCDD/Fs in the post-flame cool zones of combustion systems and should be considered as additional catalytic surfaces active in the process. The bimetallic surrogates were found to be extremely catalytically active, suggesting synergistic effects between Fe and Cu in real incineration systems. Under oxidative conditions, the bimetallic surrogates completely catalytically oxidize the 2-MCP precursor and exhibit low yields of PCDD/Fs. Under pyrolytic conditions, the bimetallic surrogates give extremely high yields of PCDD/Fs. The comparisons between transition metal and non-transition metal effects on PCDD/F formation represents a new step forward in our understanding of PCDD/F emissions from incineration systems.

Chapter I. Introduction

1.1 Background and Significance

Polychlorinated dibenzo-*p*-dioxins and dibenzofurans (PCDD/Fs), along with other dioxin-like compounds, are of particular interest because of their extreme toxicity to mammals. Dioxins are teratogenic, mutagenic, and carcinogenic.[1-4] Dioxins are also commonly associated with combustion output, such as fine and ultrafine particulate matter, which has particle diameters below 2.5 ($PM_{2.5}$) and 0.1 ($PM_{0.1}$) micrometers, respectively. This association gives them the unique ability to bypass the defenses of the human respiratory system and deposit deep within lung tissue (see Figure 1.1).

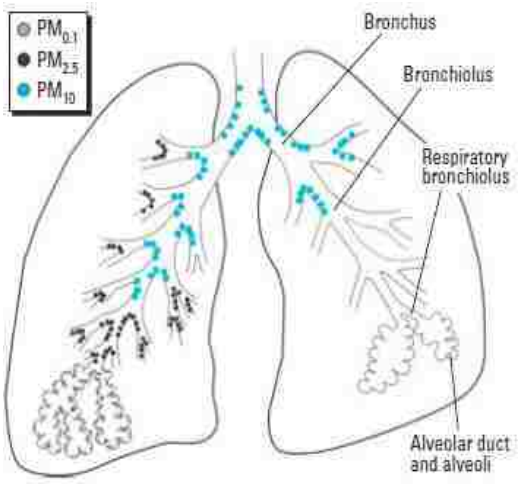

Figure 1.1. Fine ($PM_{2.5}$) and ultrafine ($PM_{0.1}$) particulate matter is able to penetrate human respiratory defenses[19]

In addition to inhalation, humans also encounter dioxins and dioxin-like compounds through ingestion. Lack of a biodegradation pathway causes dioxins to persist in biological systems. Due to this persistence and their lipophilic nature, dioxin-like compounds tend to biomagnify.[5, 6] Dioxins work their way up a food chain, increasing in concentration with each new trophic level.[7, 8]

The vast majority of dioxin-like compounds in the environment originate from anthropogenic sources.[9-18] As seen in Figures 1.2 and 1.3, the primary origin of PCDD/Fs can be traced to the formation of halogenated aromatics and metal-rich fly

ash in the postflame, cool zone of incineration systems. The formation of PCDD/Fs in combustion processes is a preventable hazard to human health and, therefore, the study of PCDD/F formation and ways to inhibit the formation are of utmost importance.

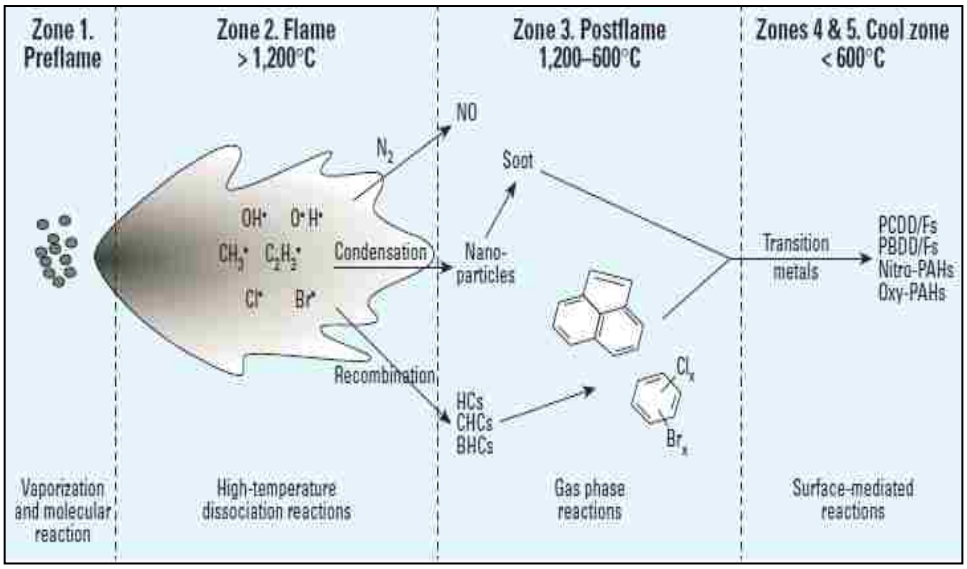

Figure 1.2. The small hydrocarbons from thermal degradation reactions can condense to form halogenated aromatics in the postflame zone[19]

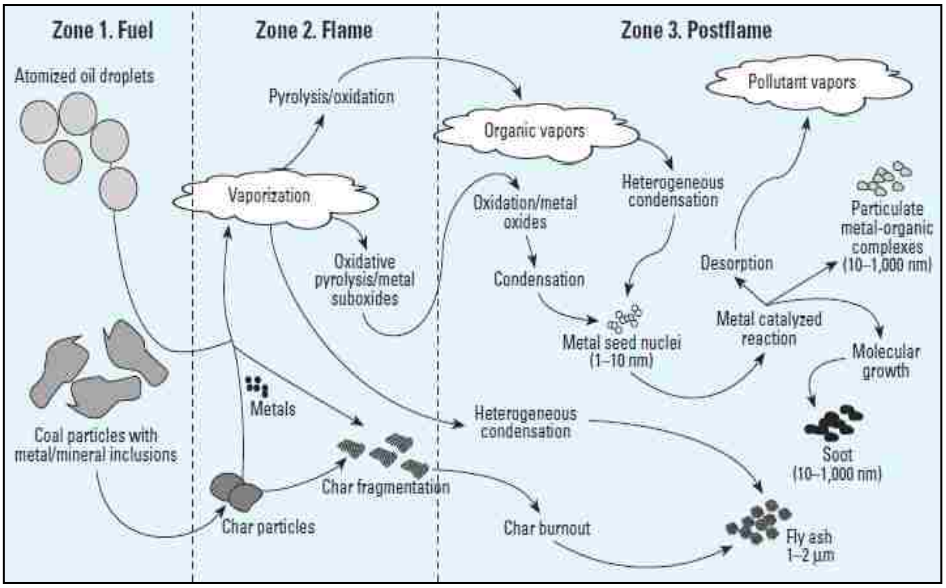

Figure 1.3. Inorganic carbon and metals can condense to form fly ash in the postflame zone[19]

1.2 PCDD/F Formation Pathways

The basic structure of PCDDs and PCDFs is shown in Figure 1.4. PCDD/Fs can be formed by way of three primary pathways: gas-phase formation involving organic precursors, de novo formation from inorganic components, and surface-mediated reactions between organic precursors and catalytic metal oxides.

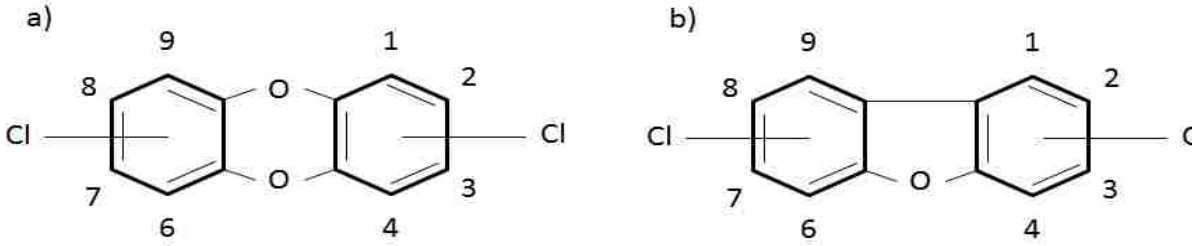

Figure 1.4. Basic structure of a) PCDDs and b) PCDFs depicting numbered substituent positions

1.2.1 Gas-Phase PCDD/F Formation

Homogeneous reactions involving various organic precursors can lead to the formation of gas-phase PCDD/Fs.[22-24] Gas-phase formation of PCDD/Fs typically takes place at higher temperatures between 400-800^{0}C and is responsible for approximately 30% of total PCDD/F emissions.[25, 26] Chlorinated phenols and benzenes are the most common PCDD/F precursors. Condensation of precursor-derived radicals is the accepted mechanism for gas-phase PCDD/F formation.[27-29] Polychlorinated dibenzofurans are formed from condensation of substituted phenyl radicals. In the case of dibenzo-*p*-dioxins, two gas-phase pathways exist. Reactions between chlorophenoxy radicals and substituted phenyl radicals lead to the formation of chlorinated dibenzo-*p*-dioxin. Radical-molecule reactions involving chlorophenoxy radicals forms

nonchlorinated dibenzo-*p*-dioxin. Other precursor-derived radicals, such as phenoxyl diradicals, have been investigated as potential PCDD/F intermediates.

1.2.2 *De Novo* Pathway

The *de novo* pathway yields PCDD/Fs from inorganic combustion byproducts at post-flame conditions. In the *de novo* pathway, the reaction between elemental carbon, oxygen, and chlorine is catalyzed by transition metals to form PCDD/Fs. The *de novo* formation of PCDD/Fs involves chlorination reactions of a carbon matrix followed by oxidation to liberate PCDD/Fs and other chlorinated species.[30-37] Transition metals have been shown to affect PCDD/F formation by way of *de novo* synthesis.[34, 38-41] In particular, transition metal chlorides have seen wide use as *de novo* catalysts.

1.2.3 Surface-Mediated Precursor Pathway

In postflame, cool zones of an incinerator, where temperatures fall between 200-600ºC, reactions between precursor molecules, such as chlorinated benzenes or phenols, are catalyzed by transition metal-oxides.[42-55] These surface-mediated reactions are responsible for up to 70% of all combustion-generated dioxins.[20, 25] Because it generates the largest portion of dioxins, the transition metal-mediated pathway requires the most attention.

The organic radicals that form during incineration of chlorinated hydrocarbons should be short-lived, but electron paramagnetic resonance (EPR) studies have shown that they can persist for days or weeks.[50] A mechanism was deduced in which transition metal oxides that are present in both the waste and/or the combustion reactor stabilize the free radicals and, in fact, catalyze their formation.[50, 56, 57] This mechanism

yields pollutant-particle systems that have been termed environmentally persistent free radicals (EPFRs).[56]

The interaction between 2-monochlorophenol (2-MCP) and transition metal-oxides begins with physisorption. The hydroxyl group of the 2-MCP forms a hydrogen bond with a hydroxyl group on the surface of the transition metal-oxide. Chemisorption of 2-MCP takes place as a covalent bond forms between 2-MCP and the transition metal oxide leading to the loss of a water molecule.[50, 58] Another possible orientation for chemisorption produces a bidentate surface-bound species through the loss of two HCl molecules. The bidentate model of chemisorption is only exhibited by chlorinated benzenes; chlorinated phenols almost exclusively follow the adsorption pathway shown in Scheme 1.1.[59, 60]

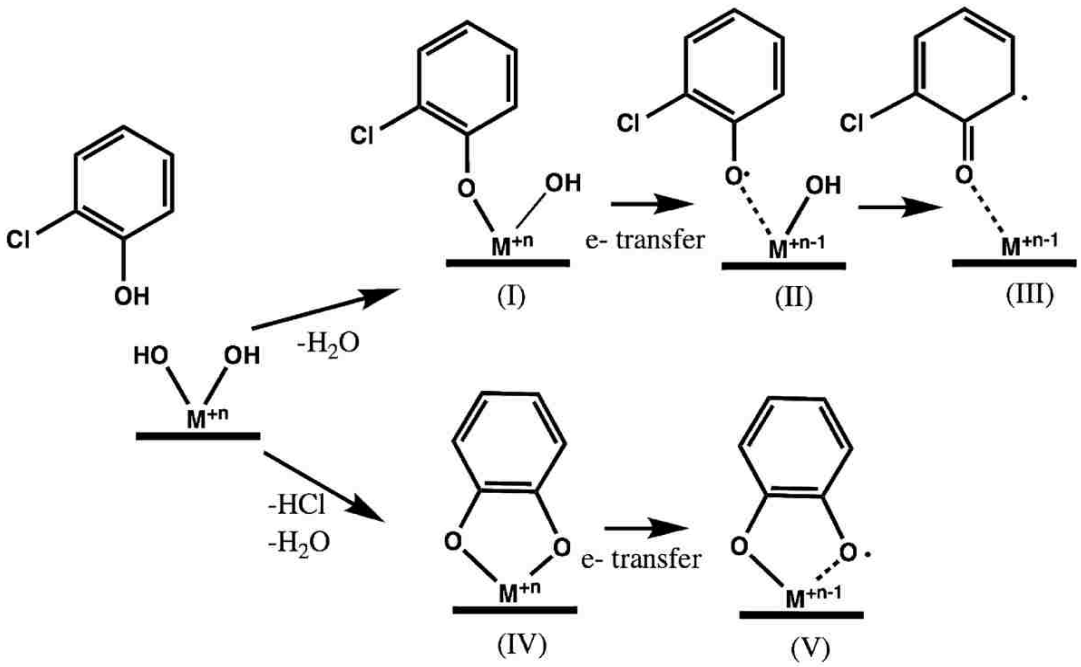

Scheme 1.1. Formation of an EPFR through the adsorption of 2-MCP on a transition metal oxide surface. The symbol, *n*, represents the initial oxidation state of the metal.[21]

Electron-transfer between the transition metal and the oxygen on 2-MCP reduces the metal and creates an oxygen-centered radical. The radical is further stabilized through electron-exchange to create a carbon-centered radical on the ring of 2-MCP. The adsorption of 2-MCP on a transition metal-oxide produces environmentally persistent chlorophenoxy radicals.[50] These EPFRs that are bound to the transition metal-oxide surface are very stable and resistant to reaction.

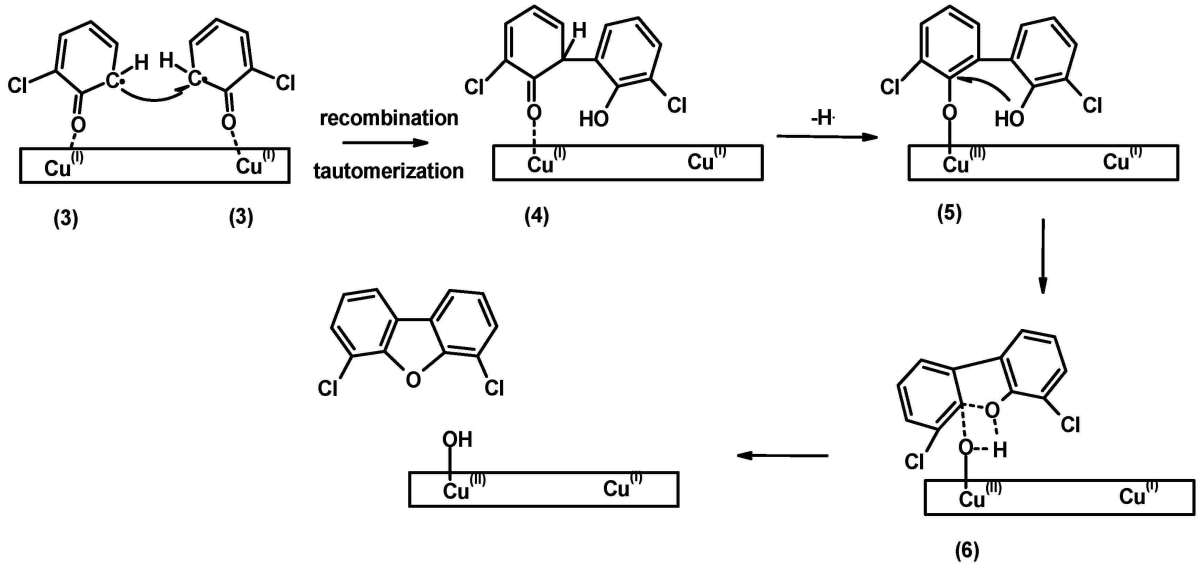

Scheme 1.2. Following the Langmuir-Hinshelwood mechanism, adjacent chlorophenoxy radicals react to form a PCDF.[20]

EPFRs associated with a metal oxide substrate are precursors to PCDD/Fs. EPFRs can react to form dioxins by way of two different mechanisms: (1) the Langmuir-Hinshelwood mechanism, in which two adjacent surface-bound EPFRs react and (2) the Eley-Rideal mechanism in which a surface-bound EPFR reacts with a gas-phase precursor molecule.[20, 59, 61-63] The Langmuir-Hinshelwood mechanism is characterized by an organic ring-closing reaction involving oxygen. This reaction, between two

adjacent surface-bound EPFRs, leads to the formation of a polychlorinated dibenzofuran (see Scheme 1.2). Chlorination/dechlorination reactions take place prior to desorption to form a range of PCDFs.

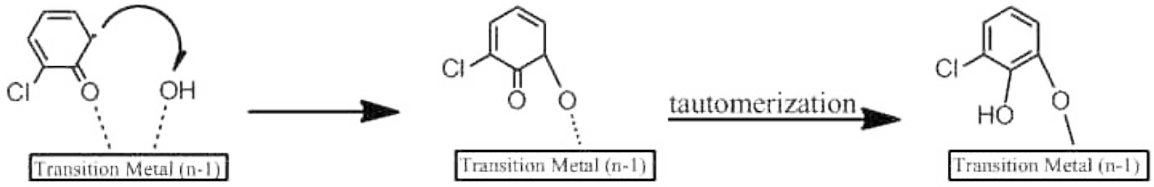

Scheme 1.3. Surface-bound chlorophenoxy radicals react with surface-bound hydroxyl groups to form a chlorohydroxyphenoxy species.

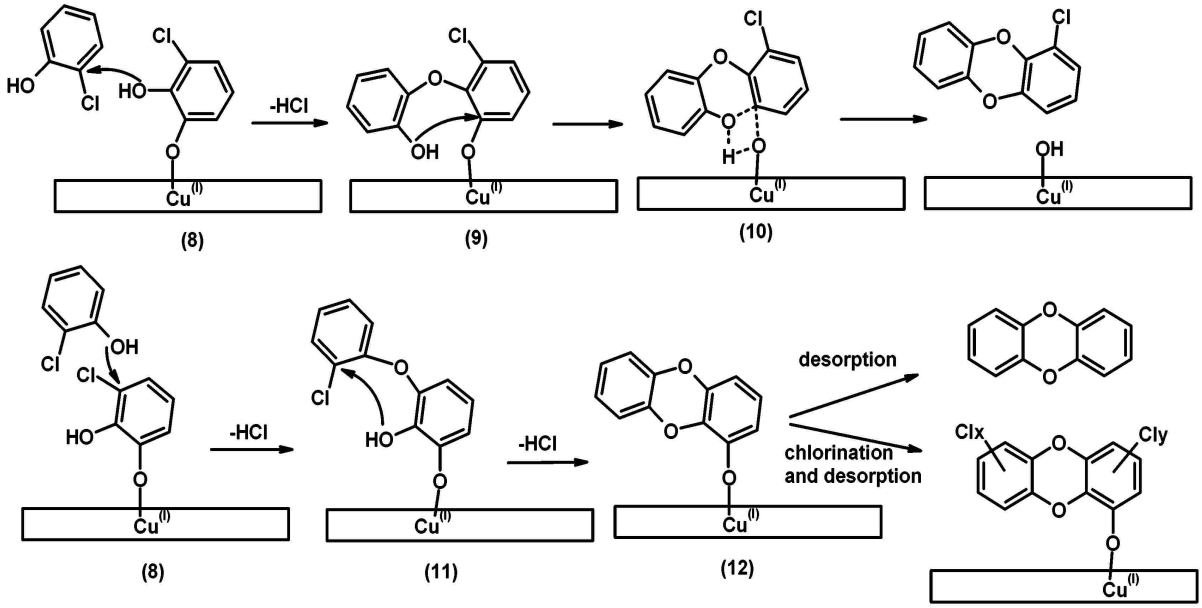

Scheme 1.4. Formation of dibenzo-p-dioxin or a PCDD is determined by which hydroxyl group initiates the reaction.[20]

Surface-bound chlorophenoxy radicals react with surface-bound hydroxyl groups to form a surface-bound chlorohydroxyphenoxy species (see Scheme 1.3). This species is a reactant in the Eley-Rideal mechanism. The Eley-Rideal mechanism is a competitive reaction that can take place depending on the identity of the dioxin

precursor. This reaction involves a surface-bound species reacting with certain gas-phase precursor molecules to form a surface-bound chlorohydroxy biphenyl ether, which undergoes ring-closing to form dibenzo-*p*-dioxin or a PCDD[20] (see Scheme 1.4).

The formation of chlorobenzenes and chlorophenols is due to cleavage of the chlorophenoxy radical from the transition metal-oxide surface. Whether the chlorinated aromatic maintains its hydroxyl group depends upon the cleavage site. If cleavage occurs at the bond between the carbon on the ring and the oxygen, then the oxygen stays on the transition metal surface and the expelled species forms a polychlorinated benzene. If cleavage occurs at the bond between the transition metal and oxygen, then the oxygen stays with the chlorinated aromatic and forms a polychlorinated phenol.

Chlorination during the pyrolysis of 2-MCP is carried out by hypochlorite species adsorbed onto the transition metal surfaces. Surface-bound hypochlorite ions are formed in the presence of O_2, which explains why higher yields of highly chlorinated species are formed from oxidative decomposition rather than pyrolytic decomposition.

1.3 Disagreement Between Lab-scale and Full-scale Experiments

Analysis of full scale combustion systems tends to show significantly higher yields of PCDFs over PCDDs.[9, 12, 64-70] Research with chlorinated precursors has attempted to replicate this ratio with no success.[20, 21, 59, 63, 71-73] The ratio of PCDDs to PCDFs is affected by the identity of both the precursor and the metal oxide. Previous experiments in the Dellinger group have shown a difference in PCDD to PCDF ratios by using chlorinated benzenes as the dioxin precursor. Chlorophenoxy radicals from the chemisorption of chlorophenols have been shown to favor reaction with gas-phase

chlorophenols rather than reaction with other nearby chlorophenoxy radicals. This means that pyrolysis of chlorophenols yields higher amounts of PCDDs than PCDFs. Chlorobenzenes in the gas phase do not react with surface-bound chlorophenoxy radicals. This means that combustion of chlorobenzenes yields low concentrations of PCDDs and much higher concentrations of PCDFs.

1.4 Disadvantages to Model Fly Ash Surrogates

To fully understand the mechanism and yields of PCDD/Fs on the surface of fly ashes, model fly ash surrogates have been investigated. Using a bottom up approach, systems containing either iron or copper oxides impregnated onto a silica matrix were studied extensively and these transition metal oxides were found to contribute to PCDD/F formation.[20, 21, 38, 41, 71, 72, 74] The initial focus on iron and copper oxide was due to their relative high concentrations in fly ashes and their known redox properties.[38, 75-77] These fly ash surrogates were appropriate tools to formulate a reaction mechanism because they are uniform throughout and their chemical makeup is easily reproducible, as opposed to fly ash, whose metal-content can vary wildly depending on its source. The immense focus on transition metals discounts the presence of aluminum-containing compounds in fly ashes.

Aluminas and aluminosilicates are major components of fly ashes where the aluminum concentration can reach 13-16% by mass.[78] Surprisingly, there are very few studies on the surface-mediated formation of PCDD/Fs over alumina, though it is known to be catalytically active.[79] In here, we are presenting pioneering studies on the contribution of aluminas and aluminosilicates to PCDD/F emissions. We have chosen

to study PCDD/F formation from 2-MCP precursor over the following systems: γ-alumina, α-alumina, mullite, and a fly ash sample. 2-MCP was selected due to its extensive use in PCDD/F research leading to well characterized product profiles and high yields. Mullite is an aluminosilicate that is commonly found in fly ash and can reach concentrations of up to 20% by mass.[80] α-alumina is the most thermodynamically stable form of alumina and, unlike γ-alumina, can be found in fly ashes. Although γ-alumina does not occur in fly ash, it is known for possessing strong catalytic activity.

While PCDD/F formation from organic precursors over alumina is a new area of research, the use of alumina in other areas of PCDD/F research is well documented. Due to its prevalence in real fly ash samples, alumina has been used as a support for fly ash surrogates in *de novo* PCDD/F formation experiments.[81, 82] Fly ash surrogates made by Schoonenboom et al. consisted of KCl and $CuCl_2$ impregnated onto alumina along with a carbon source. Alumina has been shown to have promoting effects on *de novo* formation of PCDD/Fs.

Reactions involving PCDD/Fs and PCDD/F precursors on alumina have focused on its ability to dechlorinate certain compounds.[83, 84] Schoonenboom et al. investigated the ability of alumina to dechlorinate octachlorinated PCDD/Fs and found the activity of alumina to vary based on its acidity. Qian et al. report that alumina has a suppressing effect on the formation of PCDD/Fs from a pentachlorophenol precursor which is likely due to its dechlorinating ability.

The use of monometallic surrogates also discounts the presence of synergistic effects between various components in real world fly ash. The effects of cooperative

catalysis on PCDD/F formation have not been studied and could lead to a greater understanding of the roles that various metals play in these reactions. In real fly ash, various transition metals cohabitate particle surfaces. Following previous work with Fe_2O_3 and CuO monometallic surrogates, we investigated the effects of Fe/Cu bimetallic surrogates on surface-mediated PCDD/F formation.

Both iron and copper are known catalysts in various PCDD/F formation pathways. While copper tends to be more catalytically active than iron, iron is typically present in fly ash in much higher concentrations than copper.[75-77] Both Fe_2O_3 and CuO have been shown to form phenoxyl-type EPFRs as intermediates in the formation of PCDD/Fs.[57, 60, 85] Bimetallic catalysis between iron and copper has displayed synergistic effects in a variety of applications,[86-93] but has never been applied to PCDD/F formation.

1.5 Research Aims

The goal of this work is to investigate (i) the contribution to PCDD/F formation from aluminum-containing compounds in fly ash, specifically alumina and aluminosilicates, and (ii) the synergistic effects on PCDD/F formation from Fe/Cu bimetallic model fly ash surrogates. The data obtained from individual fly ash components will also be used to determine whether prediction of PCDD/F yields on fly ash is possible.

1.6 References

1. Kakeyama, M.; Tohyama, C., Developmental neurotoxicity of dioxin and its related compounds. *Ind Health* **2003,** *41*, (3), 215-230.

2. Peterson, R. E.; Theobald, H. M.; Kimmel, G. L., Developmental and Reproductive Toxicity of Dioxins and Related-Compounds - Cross-Species Comparisons. *Crit Rev Toxicol* **1993,** *23*, (3), 283-335.

3. Popp, J. A.; Crouch, E.; McConnell, E. E., A weight-of-evidence analysis of the cancer dose-response characteristics of 2,3,7,8-tetrachlorodibenzodioxin (TCDD). *Toxicol Sci* **2006,** *89*, (2), 361-369.

4. Smith, A. H.; Warner, M. L., Biologically Measured Human Exposure to 2,3,7,8-Tetrachlorodibenzo-P-Dioxin and Human Cancer. *Chemosphere* **1992,** *25*, (1-2), 219-222.

5. Fernandez, P.; Grimalt, J. O., On the global distribution of persistent organic pollutants. *Chimia* **2003,** *57*, (9), 514-521.

6. Simonich, S. L.; Hites, R. A., Global Distribution of Persistent Organochlorine Compounds. *Science* **1995,** *269*, (5232), 1851-1854.

7. Fiedler, H.; Cooper, K.; Bergek, S.; Hjelt, M.; Rappe, C.; Bonner, M.; Howell, F.; Willett, K.; Safe, S., PCDD, PCDF, and PCB in farm-raised catfish from southeast United States - Concentrations, sources, and CYP1A induction. *Chemosphere* **1998,** *37*, (9-12), 1645-1656.

8. Schecter, A.; Cramer, P.; Boggess, K.; Stanley, J.; Papke, O.; Olson, J.; Silver, A.; Schmitz, M., Intake of dioxins and related compounds from food in the US population. *J Toxicol Env Heal A* **2001,** *63*, (1), 1-18.

9. Altwicker, E. R.; Schonberg, J. S.; Konduri, R. K. N. V.; Milligan, M. S., Polychlorinated Dioxin Furan Formation in Incinerators. *Hazard Waste Hazard* **1990,** *7*, (1), 73-87.

10. Brzuzy, L. P.; Hites, R. A., Global mass balance for polychlorinated dibenzo-p-dioxins and dibenzofurans. *Environmental science & technology* **1996,** *30*, (6), 1797-1804.

11. Huang, H.; Buekens, A., On the Mechanisms of Dioxin Formation in Combustion Processes. *Chemosphere* **1995,** *31*, (9), 4099-4117.

12. Thomas, V. M.; Spiro, T. G., Peer reviewed: the u.s. Dioxin inventory: are there missing sources? *Environmental science & technology* **1996,** *30*, (2), 82A-5A.

13. Fiedler, H., Thermal formation of PCDD/PCDF: A survey. *Environ Eng Sci* **1998,** *15*, (1), 49-58.

14. Addink, R.; Altwicker, E. R., Formation of polychlorinated dibenzo-p-dioxins and dibenzofurans on secondary combustor/boiler ash from a rotary kiln burning hazardous waste. *Journal of hazardous materials* **2004,** *114*, (1-3), 53-58.

15. Skodras, G.; Grammelis, P.; Samaras, P.; Vourliotis, P.; Kakaras, E.; Sakellaropoulos, G. P., Emissions monitoring during coal waste wood co-combustion in an industrial steam boiler. *Fuel* **2002,** *81*, (5), 547-554.

16. Gullett, B. K.; Touati, A.; Lee, C. W., Formation of chlorinated dioxins and furans in a hazardous-waste-firing industrial boiler. *Environmental science & technology* **2000,** *34*, (11), 2069-2074.

17. Lindner, G.; Jenkins, A. C.; Mccormack, J.; Adrian, R. C., Dioxins and Furans in Emissions from Medical Waste Incinerators. *Chemosphere* **1990,** *20*, (10-12), 1793-1800.

18. Rappe, C.; Andersson, R.; Bonner, M.; Cooper, K.; Fiedler, H.; Howell, F., PCDDs and PCDFs in municipal sewage sludge and effluent from POTW in the State of Mississippi, USA. *Chemosphere* **1998,** *36*, (2), 315-328.

19. Cormier, S. A.; Lomnicki, S.; Backes, W.; Dellinger, B., Origin and Health Impacts of Emissions of Toxic By-Products and Fine Particles from Combustion and Thermal Treatment of Hazardous Wastes and Materials. *Environmental Health Perspectives* **2006,** *114*, (6), 810-817.

20. Lomnicki, S.; Dellinger, B., A detailed mechanism of the surface-mediated formation of PCDD/F from the oxidation of 2-chlorophenol on a CuO/silica surface. *Journal of Physical Chemistry A* **2003,** *107*, (22), 4387-4395.

21. Nganai, S.; Lomnicki, S.; Dellinger, B., Ferric oxide mediated formation of PCDD/Fs from 2-monochlorophenol. *Environmental science & technology* **2009,** *43*, (2), 368-73.

22. Froese, K. L.; Hutzinger, O., Mechanisms of the formation of polychlorinated benzenes and phenols by heterogeneous reactions of C-2 aliphatics. *Environmental science & technology* **1997,** *31*, (2), 542-547.

23. Taylor, P. H.; Dellinger, B., Pyrolysis and molecular growth of chlorinated hydrocarbons. *J Anal Appl Pyrol* **1999,** *49*, (1-2), 9-29.

24. Altarawneh, M.; Dlugogorski, B. Z.; Kennedy, E. M.; Mackie, J. C., Mechanisms for formation, chlorination, dechlorination and destruction of polychlorinated dibenzo-p-dioxins and dibenzofurans (PCDD/Fs). *Prog Energ Combust* **2009,** *35*, (3), 245-274.

25. Altwicker, E. R., Some laboratory experimental designs for obtaining dynamic property data on dioxins. *The Science of the total environment* **1991,** *104*, (1-2), 47-72.

26. Khachatryan, L.; Asatryan, R.; Dellinger, B., Development of expanded and core kinetic models for the gas phase formation of dioxins from chlorinated phenols. *Chemosphere* **2003,** *52*, (4), 695-708.

27. Evans, C. S.; Dellinger, B., Mechanisms of dioxin formation from the high-temperature pyrolysis of 2-chlorophenol. *Environmental science & technology* **2003,** *37*, (7), 1325-1330.

28. Evans, C. S.; Dellinger, B., Mechanisms of dioxin formation from the high-temperature oxidation of 2-chlorophenol. *Environmental science & technology* **2005,** *39*, (1), 122-7.

29. Louw, R.; Ahonkhai, S. I., Radical/radical vs radical/molecule reactions in the formation of PCDD/Fs from (chloro)phenols in incinerators. *Chemosphere* **2002,** *46*, (9-10), 1273-1278.

30. Addink, R.; Altwicker, E. R., Role of copper compounds in the de novo synthesis of polychlorinated dibenzo-p-dioxins/dibenzofurans. *Environ Eng Sci* **1998,** *15*, (1), 19-27.

31. Luijk, R.; Akkerman, D. M.; Slot, P.; Olie, K.; Kapteijn, F., Mechanism of formation of polychlorinated dibenzo-p-dioxins and dibenzofurans in the catalyzed combustion of carbon. *Environmental science & technology* **1994,** *28*, (2), 312-21.

32. Stieglitz, L.; Zwick, G.; Beck, J.; Roth, W.; Vogg, H., On the De-Novo Synthesis of Pcdd/Pcdf on Fly-Ash of Municipal Waste Incinerators. *Chemosphere* **1989,** *18*, (1-6), 1219-1226.

33. Stieglitz, L., Selected topics on the de novo synthesis of PCDD/PCDF on fly ash. *Environ Eng Sci* **1998,** *15*, (1), 5-18.

34. Stieglitz, L.; Vogg, H.; Zwick, G.; Beck, J.; Bautz, H., On Formation Conditions of Organohalogen Compounds from Particulate Carbon of Fly-Ash. *Chemosphere* **1991,** *23*, (8-10), 1255-1264.

35. Wikstrom, E.; Ryan, S.; Touati, A.; Gullett, B. K., Key parameters for de novo formation of polychlorinated dibenzo-p-dioxins and dibenzofurans. *Environmental science & technology* **2003,** *37*, (9), 1962-1970.

36. Wikstrom, E.; Ryan, S.; Touati, A.; Telfer, M.; Tabor, D.; Gullett, B. K., Importance of chlorine speciation on de Novo formation of polychlorinated dihenzo-p-dioxins and polychlorinated dibenzofurans. *Environmental science & technology* **2003,** *37*, (6), 1108-1113.

37. Huang, H.; Buekens, A., De novo synthesis of polychlorinated dibenzo-p-dioxins and dibenzofurans - Proposal of a mechanistic scheme. *Science of the Total Environment* **1996,** *193*, (2), 121-141.

38. Ryan, S. P.; Altwicker, E. R., Understanding the role of iron chlorides in the de novo synthesis of polychlorinated dibenzo-p-dioxins/dibenzofurans. *Environmental science & technology* **2004,** *38*, (6), 1708-17.

39. Stieglitz, L.; Zwick, G.; Beck, J.; Bautz, H.; Roth, W., Carbonaceous Particles in Fly-Ash - a Source for the De-Novo-Synthesis of Organochlorocompounds. *Chemosphere* **1989,** *19*, (1-6), 283-290.

40. Weber, P.; Dinjus, E.; Stieglitz, L., The role of copper(II) chloride in the formation of organic chlorine in fly ash. *Chemosphere* **2001,** *42*, (5-7), 579-582.

41. Olie, K.; Addink, R.; Schoonenboom, M., Metals as catalysts during the formation and decomposition of chlorinated dioxins and furans in incineration processes. *J Air Waste Manage* **1998,** *48*, (2), 101-105.

42. Tuppurainen, K. A.; Ruokojarvi, P. H.; Asikainen, A. H.; Aatamila, M.; Ruuskanen, J., Chlorophenols, as precursors of PCDD/Fs in incineration processes: Correlations, PLS modeling, and reaction mechanisms. *Environmental science & technology* **2000,** *34*, (23), 4958-4962.

43. Addink, R.; Bakker, W. C. M.; Olie, K., Influence of Hcl and Cl-2 on the Formation of Polychlorinated Dibenzo-P-Dioxins/Dibenzofurans in a Carbon/Fly Ash Mixture. *Environmental science & technology* **1995,** *29*, (8), 2055-2058.

44. Hatanaka, T.; Imagawa, T.; Takeuchi, M., Effects of copper chloride on formation of polychlorinated dibenzofurans in model waste incineration in a laboratory-scale fluidized-bed reactor. *Chemosphere* **2002,** *46*, (3), 393-9.

45. Hell, K.; Stieglitz, L.; Dinjus, E., Mechanistic aspects of the de-novo synthesis of PCDD/PCDF on model mixtures and MSWI fly ashes using amorphous 12C- and 13C-labeled carbon. *Environmental science & technology* **2001,** *35*, (19), 3892-8.

46. Ryu, J. Y.; Mulholland, J. A.; Kim, D. H.; Takeuchi, M., Homologue and isomer patterns of polychlorinated dibenzo-p-dioxins and dibenzofurans from phenol precursors: comparison with municipal waste incinerator data. *Environmental science & technology* **2005,** *39*, (12), 4398-406.

47. Weber, R.; Hagenmaier, H., Mechanism of the formation of polychlorinated dibenzo-p-dioxins and dibenzofurans from chlorophenols in gas phase reactions. *Chemosphere* **1999,** *38*, (3), 529-49.

48. Born, J. G. P.; Mulder, P.; Louw, R., Fly-Ash Mediated Reactions of Phenol and Monochlorophenols - Oxychlorination, Deep Oxidation, and Condensation. *Environmental science & technology* **1993,** *27*, (9), 1849-1863.

49. Hatanaka, T.; Imagawa, T.; Takeuchi, M., Effects of copper chloride on formation of polychlorinated dibenzo-p-dioxins in model waste incineration. *Chemosphere* **2003,** *51*, (10), 1041-6.

50. Lomnicki, S.; Truong, H.; Vejerano, E.; Dellinger, B., Copper oxide-based model of persistent free radical formation on combustion-derived particulate matter. *Environmental science & technology* **2008,** *42*, (13), 4982-8.

51. Milligan, M. S.; Altwicker, E. R., Chlorophenol reactions on fly ash .1. Adsorption desorption equilibria and conversion to polychlorinated dibenzo-p-dioxins. *Environmental science & technology* **1996,** *30*, (1), 225-229.

52. Ghorishi, S. B.; Altwicker, E. R., Formation of polychlorinated dioxins, furans, benzenes, and phenols in the post-combustion region of a heterogeneous combustor: effect of bed material and post-combustion temperature. *Environmental science & technology* **1995,** *29*, (5), 1156-62.

53. Karasek, F. W.; Dickson, L. C., Model studies of polychlorinated dibenzo-p-dioxin formation during municipal refuse incineration. *Science* **1987,** *237*, (4816), 754-6.

54. Shaub, W. M.; Tsang, W., Dioxin formation in incinerators. *Environmental science & technology* **1983,** *17*, (12), 721-30.

55. Dickson, L. C.; Lenoir, D.; Hutzinger, O., Surface-Catalyzed Formation of Chlorinated Dibenzodioxins and Dibenzofurans during Incineration. *Chemosphere* **1989,** *19*, (1-6), 277-282.

56. Dellinger, B.; Loninicki, S.; Khachatryan, L.; Maskos, Z.; Hall, R. W.; Adounkpe, J.; McFerrin, C.; Truong, H., Formation and stabilization of persistent free radicals. *Proceedings of the Combustion Institute* **2007,** *31*, 521-528.

57. Vejerano, E.; Lomnicki, S.; Dellinger, B., Formation and stabilization of combustion-generated environmentally persistent free radicals on an Fe(III)2O3/silica surface. *Environmental science & technology* **2011,** *45*, (2), 589-94.

58. Alderman, S. L.; Dellinger, B., FTIR investigation of 2-chlorophenol chemisorption on a silica surface from 200 to 500 degrees C. *The journal of physical chemistry. A* **2005,** *109*, (34), 7725-31.

59. Lomnicki, S.; Dellinger, B., Formation of PCDD/F from the pyrolysis of 2-chlorophenol on the surface of dispersed copper oxide particles. *Proceedings of the Combustion Institute* **2002,** *29*, 2463-2468.

60. Alderman, S. L.; Farquar, G. R.; Poliakoff, E. D.; Dellinger, B., An infrared and X-ray spectroscopic study of the reactions of 2-chlorophenol, 1,2-dichlorobenzene, and chlorobenzene with model cuO/silica fly ash surfaces. *Environmental science & technology* **2005,** *39*, (19), 7396-401.

61. Addink, R.; Olie, K., Mechanisms of Formation and Destruction of Polychlorinated Dibenzo-p-dioxins and Dibenzofurans in Heterogeneous Systems. *Environmental science & technology* **1995,** *29*, (6), 1425-35.

62. Lippert, T.; Wokaun, A.; Lenoir, D., Surface-Reactions of Brominated Arenes as a Model for the Formation of Chlorinated Dibenzodioxins and Dibenzofurans in

Incineration - Inhibition by Ethanolamine. *Environmental science & technology* **1991,** *25*, (8), 1485-1489.

63. Lomnicki, S.; Dellinger, B., Formation of PCDD/F from 2-chlorophenol catalyzed by CuO in combustion exhaust. *Abstr Pap Am Chem S* **2003,** *225*, U819-U819.

64. Clement, R. E.; Tosine, H. M.; Osborne, J.; Ozvacic, V.; Wong, G., Gas-Chromatographic Mass-Spectrometric Determination of Chlorinated Dibenzo-Para-Dioxins and Dibenzofurans in Incinerator Stack Emissions and Fly-Ash - a 13-Test Study. *Biomed Environ Mass* **1988,** *17*, (2), 81-96.

65. Everaert, K.; Baeyens, J., The formation and emission of dioxins in large scale thermal processes. *Chemosphere* **2002,** *46*, (3), 439-48.

66. Giugliano, M.; Cernuschi, S.; Grosso, M.; Aloigi, E.; Miglio, R., The flux and mass balance of PCDD/F in a MSW incineration full scale plant. *Chemosphere* **2001,** *43*, (4-7), 743-50.

67. Mariani, G.; Benfenati, E.; Fanelli, R., Concentrations of Pcdd and Pcdf in Different Points of a Modern Refuse Incinerator. *Chemosphere* **1990,** *21*, (4-5), 507-517.

68. Sakai, S. I.; Hayakawa, K.; Takatsuki, H.; Kawakami, I., Dioxin-like PCBs released from waste incineration and their deposition flux. *Environmental science & technology* **2001,** *35*, (18), 3601-3607.

69. Blumenstock, M.; Zimmermann, R.; Schramm, K. W.; Kettrup, A., Identification of surrogate compounds for the emission of PCdd/F (I-TEQ value) and evaluation of their on-line real-time detectability in flue gases of waste incineration plants by REMPI-TOFMS mass spectrometry. *Chemosphere* **2001,** *42*, (5-7), 507-18.

70. Hell, K.; Stieglitz, L.; Altwicker, E. R.; Addink, R.; Will, R., Reactions of 2,4,6-trichlorophenol on model fly ash: oxidation to CO and CO2, condensation to PCDD/F and conversion into related compounds. *Chemosphere* **2001,** *42*, (5-7), 697-702.

71. Nganai, S.; Lomnicki, S.; Dellinger, B., Formation of PCDD/Fs from oxidation of 2-monochlorophenol over an Fe2O3/silica surface. *Chemosphere* **2012,** *88*, (3), 371-6.

72. Nganai, S.; Lomnicki, S. M.; Dellinger, B., Formation of PCDD/Fs from the copper oxide-mediated pyrolysis and oxidation of 1,2-dichlorobenzene. *Environmental science & technology* **2011,** *45*, (3), 1034-40.

73. Mester, Z.; Angelone, M.; Brunori, C.; Cremisini, C.; Muntau, H.; Morabito, R., Digestion methods for analysis of fly ash samples by atomic absorption spectrometry. *Anal Chim Acta* **1999,** *395*, (1-2), 157-163.

74. Gullett, B. K.; Bruce, K. R.; Beach, L. O., The Effect of Metal-Catalysts on the Formation of Polychlorinated Dibenzo-Para-Dioxin and Polychlorinated Dibenzofuran Precursors. *Chemosphere* **1990,** *20*, (10-12), 1945-1952.

75. Cains, P. W.; McCausland, L. J.; Fernandes, A. R.; Dyke, P., Polychlorinated dibenzo-p-dioxins and dibenzofurans formation in incineration: Effects of fly ash and carbon source. *Environmental science & technology* **1997,** *31*, (3), 776-785.

76. Seames, W. S., An initial study of the fine fragmentation fly ash particle mode generated during pulverized coal combustion. *Fuel Process Technol* **2003,** *81*, (2), 109-125.

77. Takasuga, T.; Makino, T.; Tsubota, K.; Takeda, N., Formation of dioxins (PCDDs/PCDFs) by dioxin-free fly ash as a catalyst and relation with several chlorine-sources. *Chemosphere* **2000,** *40*, (9-11), 1003-1007.

78. Ahmaruzzaman, M., A review on the utilization of fly ash. *Prog Energ Combust* **2010,** *36*, (3), 327-363.

79. Corma, A., From Microporous to Mesoporous Molecular Sieve Materials and Their Use in Catalysis. *Chemical reviews* **1997,** *97*, (6), 2373-2420.

80. Jankowski, J.; Ward, C. R.; French, D.; Groves, S., Mobility of trace elements from selected Australian fly ashes and its potential impact on aquatic ecosystems. *Fuel* **2006,** *85*, (2), 243-256.

81. Schoonenboom, M. H.; Olie, K., Formation of Pcdds and Pcdfs from Anthracene and Chloroanthracene in a Model Fly-Ash System. *Environmental science & technology* **1995,** *29*, (8), 2005-2009.

82. Schoonenboom, M. H.; Tromp, P. C.; Olie, K., The Formation of Coplanar Pcbs, Pcdds and Pcdfs in a Fly-Ash Model System. *Chemosphere* **1995,** *30*, (7), 1341-1349.

83. Qian, Y.; Zheng, M. H.; Liu, W. B.; Ma, X. D.; Zhang, B., Influence of metal oxides on PCDD/Fs formation from pentachlorophenol. *Chemosphere* **2005,** *60*, (7), 951-958.

84. Schoonenboom, M. H.; Zoetemeijer, H. E.; Olie, K., Dechlorination of Octachlorodibenzo-P-Dioxin and Octachlorodibenzofuran on an Alumina Support. *Appl Catal B-Environ* **1995,** *6*, (1), 11-20.

85. Kiruri, L. W.; Khachatryan, L.; Dellinger, B.; Lomnicki, S., Effect of Copper Oxide Concentration on the Formation and Persistency of Environmentally Persistent Free Radicals (EPFRs) in Particulates. *Environmental science & technology* **2014,** *48*, (4), 2212-2217.

86. Deng, W. Q.; Xu, X.; Goddard, W. A., A two-stage mechanism of bimetallic catalyzed growth of single-walled carbon nanotubes. *Nano Lett* **2004,** *4*, (12), 2331-2335.

87. He, M. S.; Chernov, A. I.; Obraztsova, E. D.; Jiang, H.; Kauppinen, E. I.; Lehtonen, J., Synergistic effects in FeCu bimetallic catalyst for low temperature growth of single-walled carbon nanotubes. *Carbon* **2013,** *52*, 590-594.

88. Koutsospyros, A.; Pavlov, J.; Fawcett, J.; Strickland, D.; Smolinski, B.; Braida, W., Degradation of high energetic and insensitive munitions compounds by Fe/Cu bimetal reduction. *Journal of hazardous materials* **2012,** *219*, 75-81.

89. Santos, M. M.; Schuchardt, U., The Synergistic Effect in Oxidative Lignin Degradation by the Biomimetic Gif System. *J Brazil Chem Soc* **1995,** *6*, (3), 257-260.

90. Schuchardt, U.; Pereira, R.; Krahembuhl, C. E. Z.; Rufo, M.; Buffon, R., Synergistic Effect of Iron and Copper Oxides Supported on Silica in the Room-Temperature Oxidation of Cyclohexane. *Appl Catal a-Gen* **1995,** *131*, (1), 135-141.

91. Shirakawa, E.; Ikeda, D.; Masui, S.; Yoshida, M.; Hayashi, T., Iron-Copper Cooperative Catalysis in the Reactions of Alkyl Grignard Reagents: Exchange Reaction with Alkenes and Carbometalation of Alkynes. *Journal of the American Chemical Society* **2012,** *134*, (1), 272-279.

92. Siriwardane, R.; Tian, H. J.; Simonyi, T.; Poston, J., Synergetic effects of mixed copper-iron oxides oxygen carriers in chemical looping combustion. *Fuel* **2013,** *108*, 319-333.

93. Zhu, N. R.; Luan, H. W.; Yuan, S. H.; Chen, J.; Wu, X. H.; Wang, L. L., Effective dechlorination of HCB by nanoscale Cu/Fe particles. *Journal of hazardous materials* **2010,** *176*, (1-3), 1101-1105.

Chapter II. Experimental

2.1 System for Thermal Diagnostic Studies

The System for Thermal Diagnostic Studies (STDS) was designed to facilitate the efficiency and reliability of thermal decomposition analysis.[1] The STDS is able to simulate a variety of incineration conditions through the control of temperature, gas flow rate, and fuel injection rate. The system is modular in nature, being composed of several instruments that are each responsible for specific duties. A diagram of the STDS can be viewed in Figure 2.1. The instrument can be seen in Figure 2.2.

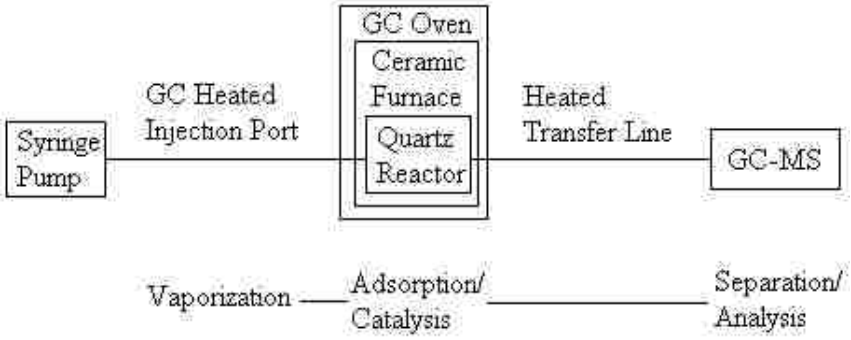

Figure 2.1. Block diagram of the System for Thermal Diagnostic Studies (STDS)

Figure 2.2. The current form of the STDS

All reactions take place in a packed-bed, plug flow quartz reactor, as seen in Figure 2.3, heated by an electric furnace manufactured by Omega. The furnace is capable of maintaining temperatures between 30-1000 ^{0}C to simulate various post-incineration conditions or areas of a flame. The reactor and furnace are held within a Varian 3800 Gas Chromatograph oven. The purpose of this housing is to provide a constant and controllable temperature outside the furnace and to heat the transfer-lines leading to and from the quartz reactor. The gas chromatograph also has a heated injector system of its own that allows fast and reproducible injections. The exit port of the first gas chromatograph leads to the injection port of a second gas chromatograph of identical make and model. The transfer line that connects the two gas chromatographs consists of deactivated, silica-lined stainless steel guard column wrapped in heat rope and well-insulated with fiberglass. The transfer line is capable of maintaining temperatures up to 240 ºC, but is typically kept at 185 ºC during reactions to prevent condensation of combustion products during transport.

Figure 2.3 Inside view of the reactor and furnace housed within a GC oven

The second gas chromatograph performs the separation of the decomposition products. The column installed in the gas chromatograph is a 30 m, 0.25 mm i.d., 0.25 µm film thickness HP-5MS (Agilent). A Varian Saturn 2000 Mass Spectrometer is

installed on the second gas chromatograph and serves to analyze the decomposition products. The Saturn 2000 is equipped with an ion trap and an electron multiplier detector. Mass spectra were taken from 40 to 450 amu.

The temperature program for the first gas chromatograph consists of a constant flow rate and constant temperature that is dependent on the vaporization temperature of the chemical precursor. The flow rate for the reaction gas is 13.2 mL/min of carrier gas and the first oven and injector are kept at 185 ºC to maintain the organic precursor, 2-monochlorophenol (2-MCP), in the gas phase. The temperature program for the second gas chromatograph begins at -60 ºC and the mass spectrometer is deactivated during a 75 minute collection phase. During this phase, 2-MCP is automatically injected into the first gas chromatograph with a syringe pump at a rate of 0.18 microliters per hour. The 2-MCP is vaporized and passes through and interacts with a catalyst substrate in the quartz reactor.

The quartz reactor is packed with an appropriate mass of catalyst to give a catalytic bed length of 3.5 mm. The catalytic bed is packed on both ends with fine quartz wool and has an average volume of 0.044 cm^3.

The combustion products, along with any unreacted precursor, are transferred into the head of the capillary column in the second gas chromatograph and cryogenically trapped at -60 ºC. At the end of the 75 minute collection phase, the syringe is retracted from the first gas chromatograph and the transfer line is retracted from the second gas chromatograph. The instrument now enters the separation/analysis phase. The second gas chromatograph begins heating its column

and the mass spectrometer detector is turned on. The oven heats to 300 ºC at a rate of 15 ºC per minute and then holds for 6.00 minutes.

The injection rate of the syringe pump was calculated so as to maintain a constant 2-MCP concentration of 50.0 ppm within the catalytic bed. The size of the catalytic bed in the reactor and the flowrate of the carrier gas are used to calculate the precursor concentration in the gas phase.

The experiments are performed using a carrier gas of either ultrapure helium or a mixture of 20% oxygen in helium. The pure helium simulates incineration in an oxygen-starved environment, also known as pyrolytic conditions. The oxygen mixture simulates incineration in a well-mixed, aerated environment, also known as oxidative conditions.

Standards of dioxins were purchased from Cambridge Isotope Laboratories. Retention times for analytes were confirmed using an identical temperature program without the 75 minute collection period.

The following equation was used to determine the percent yields of the various products:

$$\% \text{ yield} = [\text{product}]A / [\text{2-MCP}]_0$$

where [product] is the moles of product formed and $[\text{2-MCP}]_0$ is the total number of moles of 2-MCP that is injected into the reactor. The molar stoichiometric ratio of reactant to product, A, is equal to 1 for chlorobenzenes and chlorophenols and equal to 2 for dioxins. Every plotted point on the percent yield graphs represents the average of four experimental runs. All error bars represent one standard deviation.

2.2 Fly Ash Desorption

The STDS was used to analyze the inherent dioxin content of the fly ash prior to introduction of additional dioxin precursor. The desorption procedure follows the same steps for loading the reactor and activating the sample under air flow for 1 hr. The desorption was performed at various temperatures to ensure that activation at 450 ^{0}C would sufficiently clean the surface of adsorbed dioxin. Both fresh fly ash and a sample that had undergone activation were used. The sample would first be subjected to air flow for 1 hr at 250 ^{0}C and then the process would be repeated on the same sample while increasing the temperature in 50 ^{0}C increments.

2.3 ICP-OES Digestion & Analysis

Prior to elemental analysis, the fly ash was digested in a mixture of HNO_3, HCl, and HF (Fisher) in a CEM Mars 5 Microwave Reaction System. Approximately 100 mg of flyash was digested in 10.00 mL of a 3:1:1 ratio of HNO_3, HCl, and HF. The CEM Mars 5 was programmed to ramp to 200 ^{0}C over 5.0 minutes and then to hold for 25 minutes. The microwave program was run on the fly ash samples two times to ensure there was no residue remaining on the reaction vessels. Without the use of hydrofluoric acid in the reaction matrix, complete digestion cannot be attained and a residue of silica and alumina will always remain. If one does not need quantitative information on Si/Al content, then simply digesting in concentrated nitric acid is sufficient to digest other elements and leech any transition metals out of the sample. Prior to ICP-OES analysis, the samples must be diluted to approximately 5% total acid content to prevent damaging the instrument. ICP-OES analysis was performed on a Spectro Ciros CCD.

2.4 XRD Analysis

The fly ash was analyzed with a Bruker-Siemens D5000 XRD using Cu-Kα radiation and a solid state detector while operating in θ-2θ mode with a diffraction angle scanning range of 10-45^0 at a rate of 1^0 min^{-1}. Diffrac AT software was used to qualitatively analyze the crystalline components within the fly ash.

2.5 XPS Analysis

Elemental composition of the fly ash surface was determined using a Kratos Axis-165 XPS using a monochromatic Al-Kα radiation source. Survey scans were taken over the range of 0-1000 eV with a step size of 1 eV and a dwell time of 70 ms. High resolution scans were taken of various elements of interest using a step size of 0.1 eV and a dwell time of 100 ms. The Kratos charge neutralizing module was used to remove the effects of the surface charge on the sample. Kratos Vision software was used to match peaks with their corresponding elements.

2.6 SEM-EDS Analysis

The particle morphology of the fly ash was investigated using a Hitachi S-3600N Variable Pressure scanning electron microscope with an integrated EDAX energy dispersive spectroscopy system. The acceleration voltage was 20 kV and images were taken at magnifications of x500 and x1500. To ensure better quantification of element concentration, the fly ash was not coated with any conductive substance. Leaving the sample uncoated leads to decreased image quality, but the images still easily allow identification of particle size and shape. Team EDS Software Suite was used to identify peaks and quantify elemental composition.

2.7 BET Analysis

A Quantachrome Autosorb-1 was used to analyze the surface properties of the catalytic material. Samples were dried under air at 120 ^{0}C for 12 hrs prior to analysis to ensure removal of all adsorbed moisture. A 10-point isotherm was constructed using nitrogen as the sorbent gas on a dried powder sample. Surface area, total pore volume, and average pore diameter were calculated using the Brunauer-Emmett-Teller method.

2.8 Fly Ash Surrogate Preparation

The Fe/Cu mixed metal oxide catalysts were prepared using incipient wetness co-impregnation. Silica gel (mesh 100-125) was used as the support matrix. Iron (III) nitrate ($Fe(NO_3)_3 \cdot 9H_2O$) (Sigma-Aldrich) and copper (II) nitrate ($Cu(NO_3)_2 \cdot 2.5H_2O$) (Sigma-Aldrich) were used as transition metal oxide precursors. The metal nitrates were dissolved in an appropriate volume of water to allow incipient wetness and the solution was left on the silica gel for 24 hrs. A rotary evaporator was used to remove the water and deposit the metal nitrates followed by 12 h in a 120 ^{0}C drying oven. Calcination in air at 450 ^{0}C for 5 h leads to the oxidation of the metal nitrates and the formation of the transition metal oxides.

2.9 References

1. Rubey, W. A.; Grant, R. A., Design Aspects of a Modular Instrumentation System for Thermal Diagnostic Studies. *Review of Scientific Instruments* **1988,** *59*, (2), 265-269.

Chapter III. Results

3.1 Fly Ash Characterization

3.1.1 Fly Ash Desorption

In an effort to keep experimental procedures consistent with previous work, the activation phase of the experimental procedure was tested on the fly ash to ensure it would fully desorb any adsorbed dioxins inherent to the sample. The results show that the majority of the small concentration of dioxins on the fly ash is desorbed when exposed to air flow for 1 hr at 450^{0}C. The fly ash that had already undergone activation showed no increase of dioxin desorption with temperature. While the concentration of dioxins inherent to the fly ash is too small to cause any major interference with the concentrations being formed during catalysis, the prior desorption of the fly ash surface will lead to more accurate results. The activation step of the experimental procedure was kept consistent with previous work. PCDD/F desorption over the entire studied temperature range can be seen in Figure 3.1.

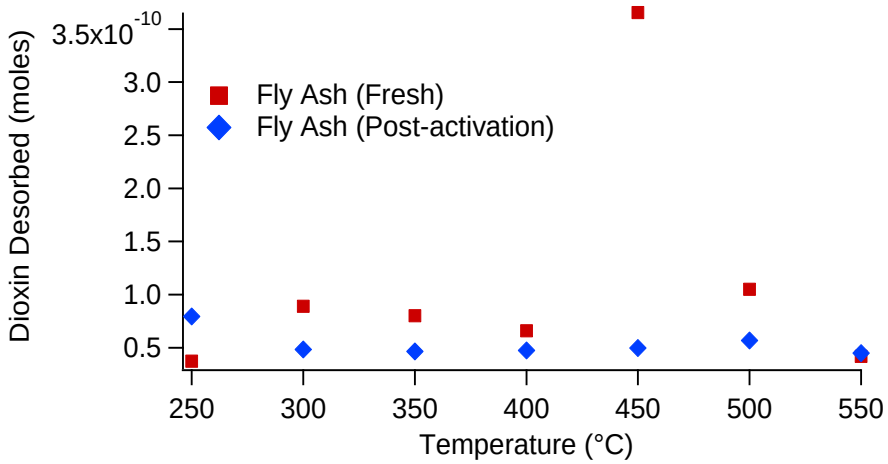

Figure 3.1. PCDD/F background emissions from fly ash

3.1.2 Elemental Analysis of Fly Ash

The elemental composition of the studied fly ash in this work is presented in Table 3.1. The composition is quite typical compared to other fly ashes presented in literature[1-5] with iron being the most abundant transition metal component at ~4.5% by mass. The concentration of other transition metals falls within bounds typically found in fly ashes. From the perspective of PCDD/F formation, the concentration of copper in fly ashes is of importance, as copper is considered one of the most potent PCDD/F formation catalysts and has been studied extensively in the past.[6-10] The fly ash studied in here contains only 0.02 % Cu, which is within the range observed in fly ashes from waste incineration processes. Copper concentration can be as high as ~4.5%, especially in e-waste reclamation systems.[11] Since iron content is so dominant in the fly ash, it is anticipated to be a driving force in PCDD/F formation from precursors. Our previous experiments have been performed using a Fe_2O_3/silica system containing 5% iron oxide that translates to ~3.5% Fe in the synthetic fly ash (see Table 3.1), and showed a high yield of PCDD/Fs from such systems.[10, 12, 13]

Table 3.1. Elemental composition of fly ash and fly ash surrogates

	Fly Ash Surrogates	Fly Ash
Si	44.41	46.49
Al	-	10.43
Fe	3.50	4.46
Ti	-	1.01
Ca	-	0.28
Mg	-	0.16
Mn	-	0.034
Cu	3.99	0.020
Zn	-	0.016

The two other primary components of fly ash, as listed in Table 3.1, are Al and Si. Though the concentrations of those elements are high, little is known on their propensity to catalyze the formation of PCDD/Fs from precursors. These two elements, Si and Al, form the inorganic matrix of the fly ashes and are usually in the form of

oxides. SiO_2 is believed to be inert in the PCDD/F formation; however, other forms of the oxide can exist.

3.1.3 X-ray Crystallography of Fly Ash

The x-ray diffraction spectrum obtained from fly ash is shown in Figure 3.2. XRD analysis of the fly ash confirmed the majority of Si is present in the form of quartz (SiO_2). The presence of aluminosilicates has also been detected in the form of mullite ($Al_6Si_2O_{13}$). Silica and mullite are commonly found in fly ashes in considerable quantities as they are formed during the particle inception process during cooling in the post-flame zone from vaporized Si and Al from fuel. Though no crystalline forms of aluminum oxides were detected (except of aluminosilicates), it does not exclude small crystallite or amorphous phases of other aluminum oxides to be present. In particular, one would anticipate α-alumina to be present, as this is the most thermodynamically stable form of aluminum oxides.

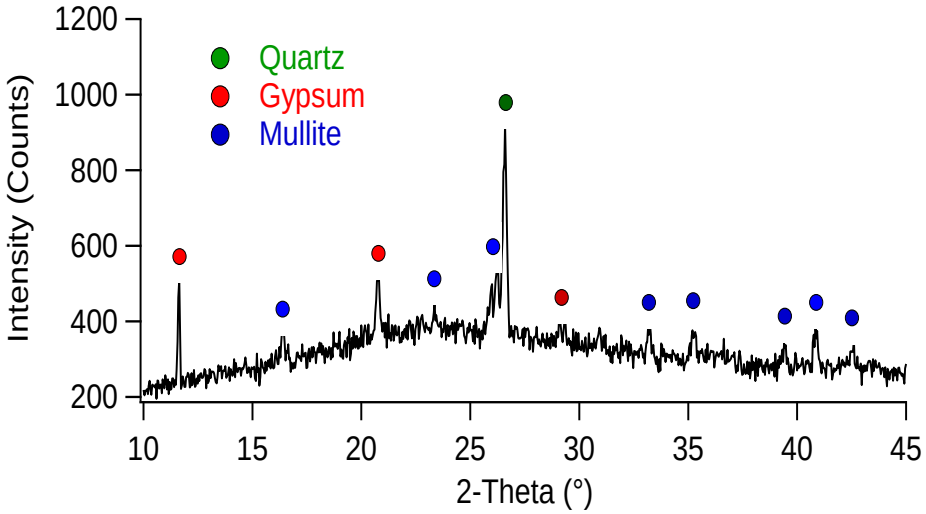

Figure 3.2. XRD peak analysis of crystalline phases in the studied fly ash

3.1.4 X-ray Photoelectron Spectroscopy of Fly Ash

X-ray photoelectron spectroscopy (XPS) is an instrumental technique that will yield information about the identity and oxidation state of surface elements. The technique has a penetration depth of 1-10 nm and was used to qualitatively identify the surface species on the fly ash. A survey scan confirmed the presence of large amounts of carbon (C-C bonds), oxygen (SiO_2, Al_2O_3, and C-O bonds), and silicon (SiO_2). High resolution scans were focused on various elements of particular interest. The presence of both Al_2O_3 and Fe_2O_3 were confirmed on the surface of the fly ash particles and their spectra can be seen in Figures 3.3 and 3.4. XPS typically has a detection limit of ppth. The presence of copper oxide on the surface of the fly ash could not be confirmed due to the concentration falling below the detection limit.

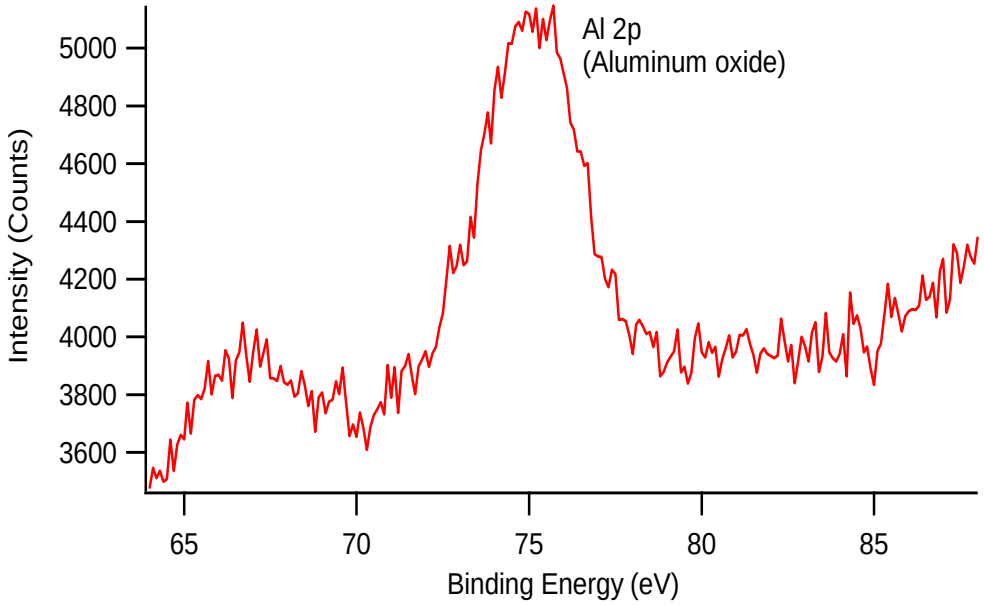

Figure 3.3. High-resolution x-ray photoelectron spectrum of fly ash centered on signal region for alumina

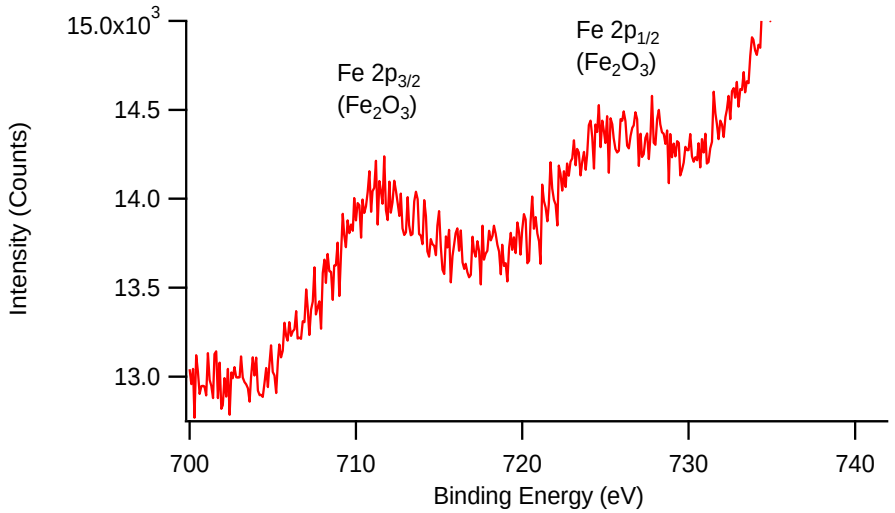

Figure 3.4. High-resolution x-ray photoelectron spectrum of fly ash centered on signal region for iron (III) oxide

3.1.5 Electron Microscopy of Fly Ash

Scanning electron microscopy was used to take images of the fly ash to investigate the size of the particles and their morphology. Figures 3.5 and 3.6 show images taken at x500 and x1500 magnification. While there are some larger agglomerates, most of the fly ash particles fall below 10 micrometers.

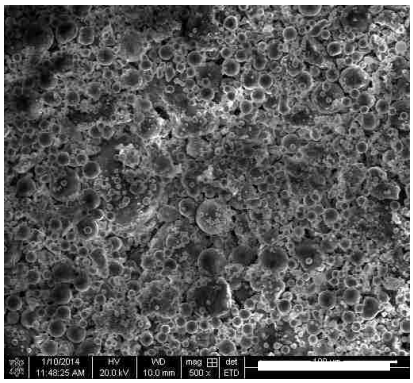

Figure 3.5. SEM image of fly ash particles at x500 magnification. Scale bar is equal to 100 µm.

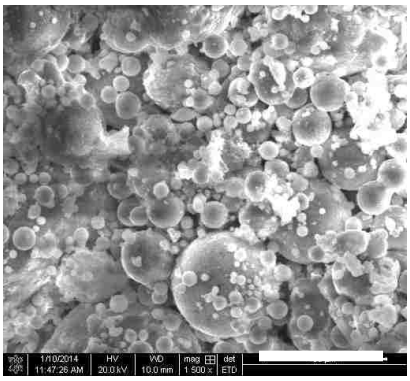

Figure 3.6. SEM image of fly ash particles at x1500 magnification. Scale bar is equal to 10µm.

Energy-dispersive x-ray spectroscopy (EDS) was used to obtain elemental information that could be correlated with the ICP-OES data. EDS has a typical penetration depth of 0.5-3 micrometers. Because most of the fly ash particles are thicker than 3 micrometers, there may be some degree of error in the EDS data. Table 3.2 shows the EDS data compared to the ICP-OES results. Similar transition metal values indicate that these elements are closer to the surface. The large discrepancy in silicon content is likely due to a majority of silicon being nearer to the core of the particles where the technique cannot penetrate. The full EDS spectrum can be viewed in Figure 3.7.

Table 3.2. Quantitative elemental analysis from EDS and ICP-OES techniques.

	Weight %	
	EDS	ICP-OES
O	47.89	-
Si	21.06	46.49
Al	13.33	10.43
Fe	6.75	4.46
Ca	4.41	0.28
K	1.99	-
C	1.22	-
Ti	1.19	1.01
Mg	0.96	0.16
F	0.52	-
Na	0.36	-
Cu	0.33	0.02

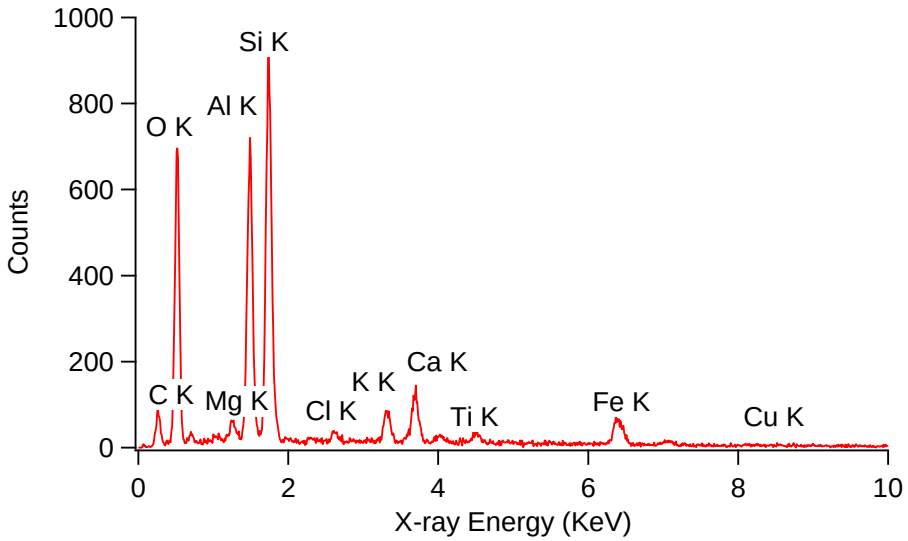

Figure 3.7. Energy-dispersive x-ray spectrum of fly ash

3.1.6 Surface Morphology of Fly Ash

Surface area of the fly ash has been found to be relatively small at 13.65m^2/g (see Table 3.3) when compared to the aluminas and aluminosilicates. Similarly, the mullite sample has a very small surface area of <2m^2/g. In addition to their extremely low surface area, fly ash and mullite also have low total pore volume of 6.49x$10^{-3}$$cm^3$/g and 7.44x$10^{-4}$$cm^3$/g, respectively. Due to their low surface area and pore volume, both the fly ash and mullite can be considered systems without significant pore structure. Thus, surface activity in these two catalysts is most likely related to the external surface of the particles. The average pore diameter of α-alumina is ~2 Å and though the pore system is very well developed, it is essentially not accessible for aromatic molecules (>2.5Å). It is difficult to consider the overall surface area of α-alumina as a contributing factor, as most of the surface is unavailable. Therefore, α-alumina has available surface area similar to that of fly ash and mullite.

Table 3.3. Surface morphology parameters of materials used in the experiments

Sample	Surface Area (m^2/g)	Total Micropore Volume (cm^3/g)	Average Pore Diameter (Å)
Fly Ash	13.65	6.49 x 10^{-3}	19.03
α-Alumina	175.70	9.49 x 10^{-3}	2.16
γ-Alumina	267.50	1.29 x 10^{-1}	19.37
Mullite	1.57	7.44 x 10^{-4}	21.28

3.2 Thermal Degradation of 2-Monochlorophenol over Fly Ash

3.2.1 Pyrolytic Conditions

The product yields from the surface-mediated pyrolysis of 2-MCP over fly ash are presented in Figures 3.8-3.10 as a function of temperature. The decomposition of 2-MCP reaches 90% between 250-300 ºC and reaches a maximum of ~98% at 500 ºC.

The yields of chlorinated benzenes can be seen in Figure 3.8. MCBz, DCBz, and TriCBz were obtained with yields of 0.002%, 0.005%, and 0.00003% respectively, at 250ºC. The yields of MCBz and DCBz both increased with increasing temperature, reaching maximum yields of 0.001% and 0.00008% at 500ºC respectively. The yield of TriCBz did not significantly change with temperature.

The yields of chlorinated phenols can be seen in Figure 3.9. DCP and TriCP were obtained with yields of 0.04% and 0.0002% respectively, at 250ºC. The yields of DCP and TriCP both reached maximum yields of 0.07% and 0.004% respectively, at 350ºC. The lower temperature of formation indicates that the chlorination of the 2-MCP precursor is a simple reaction that requires little energy.

The yields of PCDD/Fs can be seen in Figure 3.10. DF, DD, MCDF, MCDD, DCDF, and DCDD were obtained with yields of 0.000008%, 0.0002%, 0.0001%, 0.0001%, 0.0001%, and 0.0001%, respectively, at 250ºC. DF and DD both increased significantly with increasing temperature, reaching maximums of 0.002% and 0.02% at 550ºC, respectively. The yield of MCDD plateaued at 0.002% at 400^0C. Table 3.4 gives the yields of all chlorinated benzenes, phenols, and dioxin products.

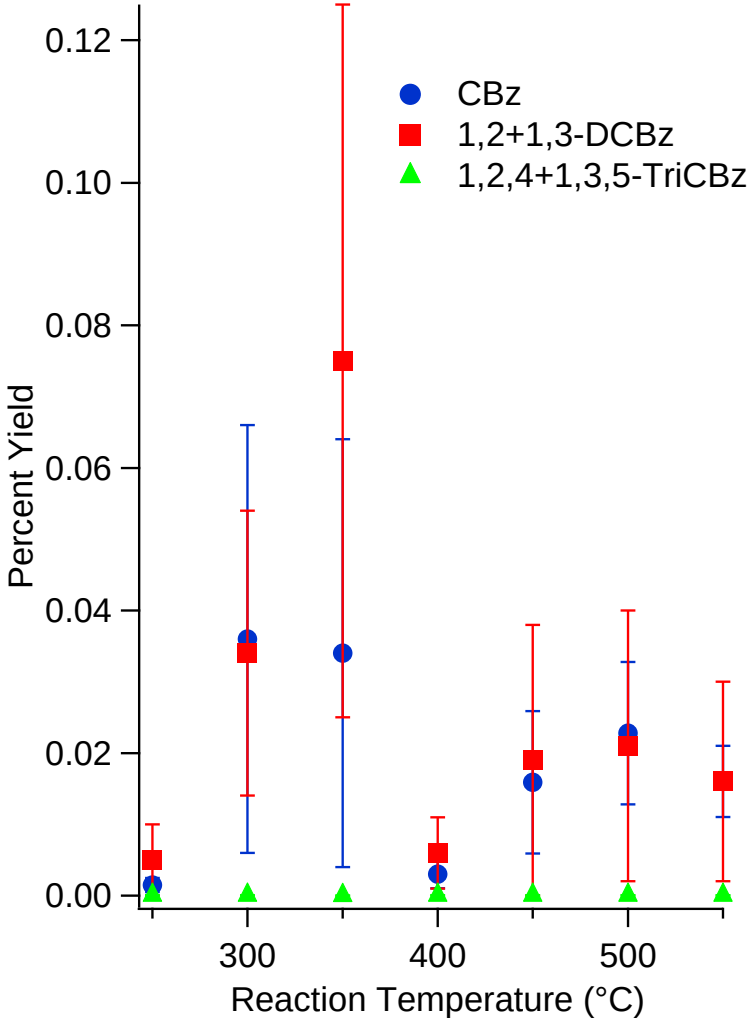

Figure 3.8. Chlorinated benzene yields from the pyrolysis of 2-MCP over fly ash.

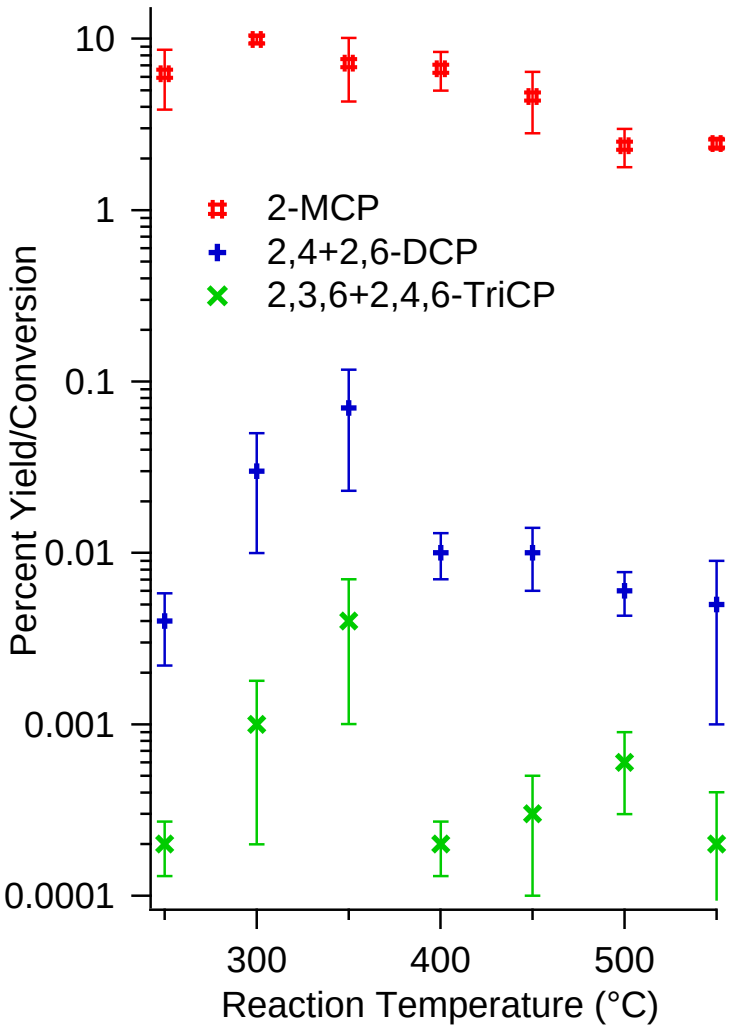

Figure 3.9. Chlorinated phenol yields and precursor conversion from the pyrolysis of 2-MCP over fly ash.

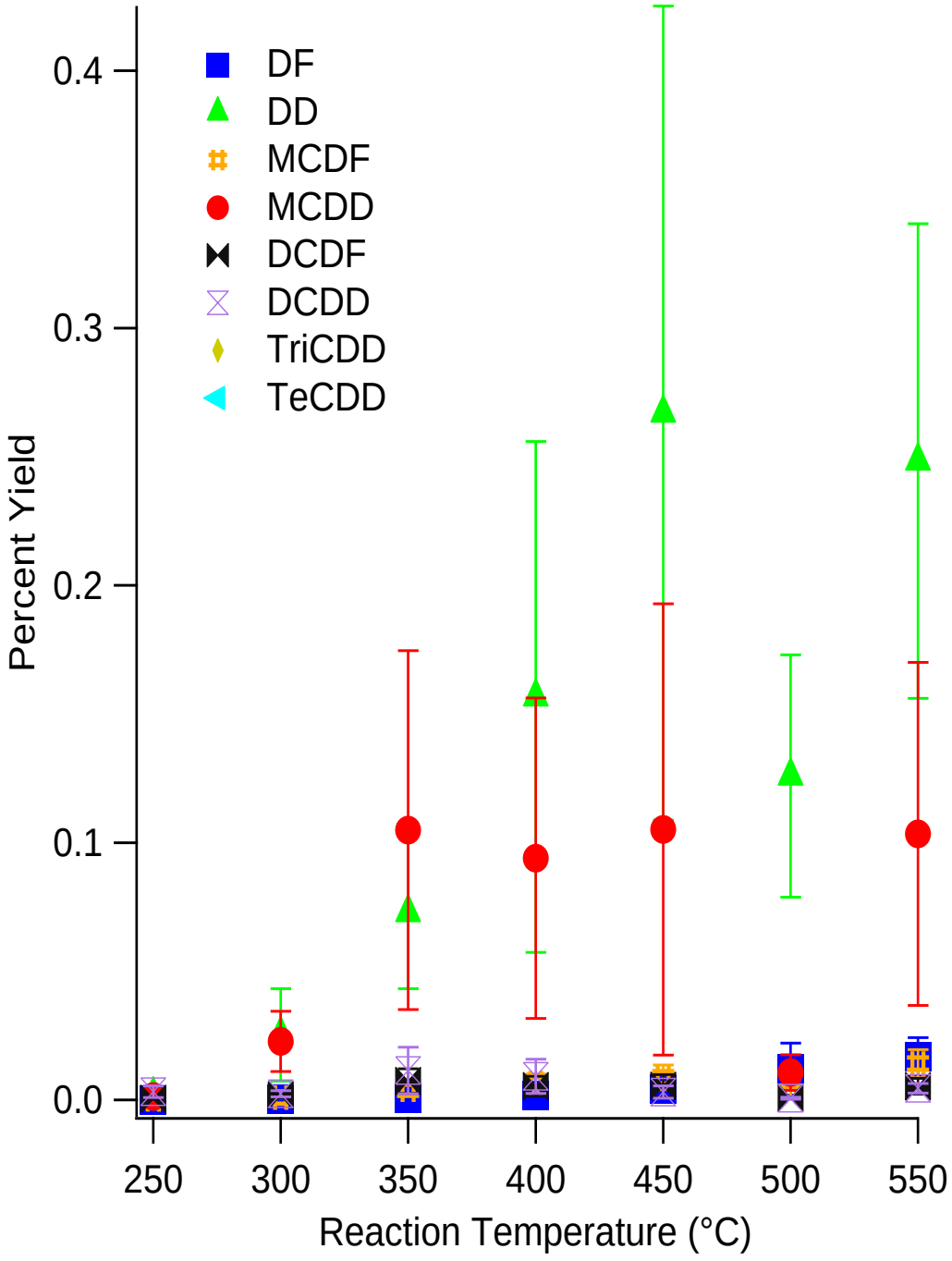

Figure 3.10. Major PCDD/F yields from the pyrolysis of 2-MCP over fly ash.

Table 3.4. Dioxin and nondioxin products from the pyrolysis of 2-MCP over fly ash.

	Reaction Temperature (^{0}C)					
	250	300	350	400	450	500
MCB	0.0015	0.036	0.034	0.0025	0.016	0.023
2-MCP	6.2	9.9	7.2	6.7	4.6	2.4
DCBz	0.005	0.034	0.05	0.0055	0.019	0.021
DCP	0.0038	0.028	0.065	0.013	0.014	0.0058
TriCP	0.00016	0.0011	0.0041	0.00021	0.00029	0.00063
DF	0.00011	0.00025	0.00069	0.0018	0.0042	0.012
DD	0.0019	0.025	0.073	0.16	0.27	0.13
MCDF	0.00027	0.001	0.0041	0.0066	0.0089	0.0033
MCDD	0.0014	0.023	0.1	0.094	0.11	0.011
DCDF	0.00049	0.0019	0.0073	0.0055	0.0056	0.00089
DCDD	0.0032	0.0024	0.011	0.0093	0.0031	0.00068
bdl - Below Detection Limit						

3.2.2 Oxidative Conditions

The product yields from the surface-mediated oxidation of 2-MCP over fly ash are presented in Figures 3.11-3.13 as a function of temperature. The decomposition of precursor was less than under pyrolytic conditions at low temperatures. Thermal degradation of 2-MCP reached approximately 70% between 250-300ºC but surpassed pyrolytic conditions to a maximum of >99.5% at 550ºC.

The yields of chlorinated benzenes can be seen in Figure 3.11. MCBz and DCBz were obtained with yields of 0.0009% and 0.1% respectively, at 250ºC. The yields of MCBz and DCBz both increased with increasing temperature, reaching maximum yields of 0.03% and 1.8% at 450ºC respectively. No higher chlorinated species were formed.

The yields of chlorinated phenols can be seen in Figure 3.12. DCP was the only chlorophenol product and was obtained with a yield of 0.1% at 250ºC. The yield of DCP reached a maximum of 0.9% at 350ºC, indicating a lower temperature required for chlorinating the 2-MCP precursor.

The yields of PCDD/Fs can be seen in Figure 3.13. DF, DD, MCDF, MCDD, DCDF, and DCDD were obtained with yields of 0.00005%, 0.000003%, 0.002%, 0.1%, 0.002%, and 0.01% respectively, at 250ºC. All dioxin products increased with temperature to reach maximums at 450^{0}C. DD and DF were formed in the least amounts. The two chlorinated dibenzo-p-dioxin species, MCDD and DCDD were formed in the highest concentrations, reaching yields of 0.8% and 0.1% respectively. Table 3.5 gives the yields of all chlorinated benzenes, phenols, and dioxin products.

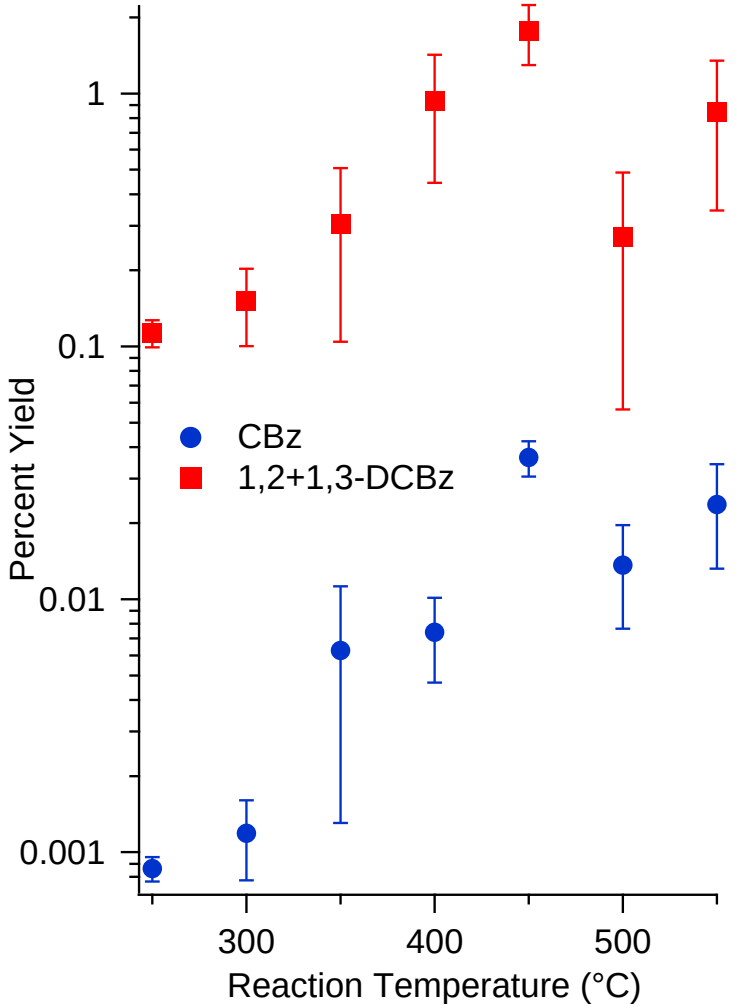

Figure 3.11. Chlorinated benzene yields from the oxidation of 2-MCP over fly ash.

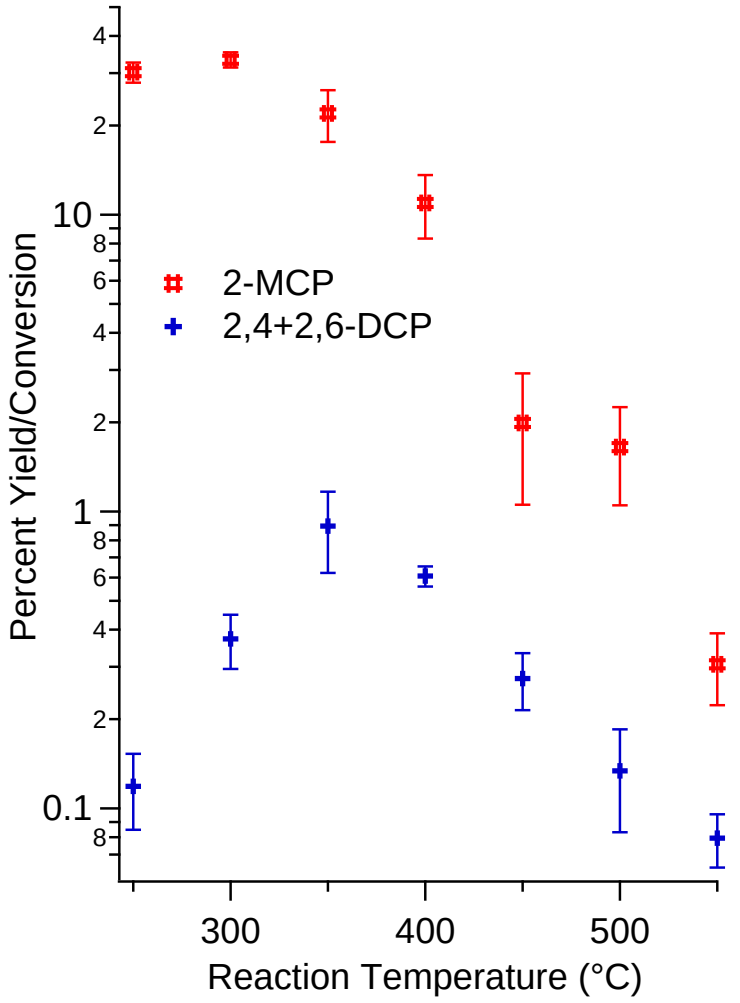

Figure 3.12. Chlorinated phenol yields and precursor conversion from the oxidation of 2-MCP over fly ash.

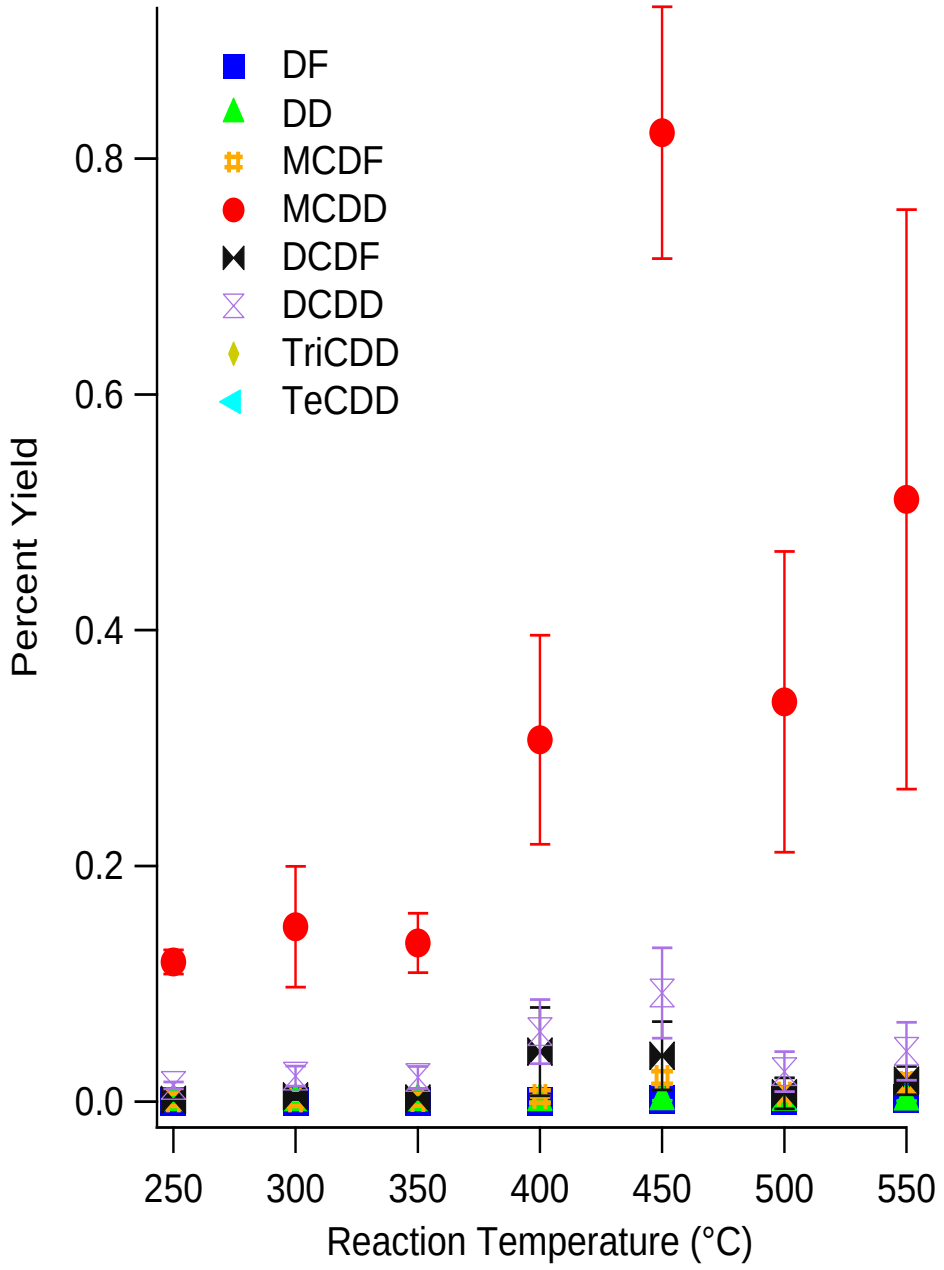

Figure 3.13. Major PCDD/F yields from the oxidation of 2-MCP over fly ash.

Table 3.5. Dioxin and nondioxin products from the oxidation of 2-MCP over fly ash.

	Reaction Temperature (^{0}C)						
	250	300	350	400	450	500	550
CBz	0.00086	0.0012	0.0063	0.0074	0.036	0.014	0.024
2-MCP	30	33	22	11	2	1.6	0.31
DCBz	0.11	0.15	0.31	0.94	1.8	0.27	0.85
DCP	0.12	0.37	0.89	0.61	0.27	0.13	0.079
DF	0.000049	0.000087	0.0002	0.0004	0.002	bdl	0.0027
DD	0.000003	0.000019	0.00013	0.00017	0.0009	0.00036	0.00067
MCDF	0.0015	0.0015	0.0018	0.0044	0.021	0.0065	0.016
MCDD	0.12	0.15	0.13	0.31	0.82	0.34	0.51
DCDF	0.0016	0.0045	0.0027	0.042	0.039	0.0071	0.018
DCDD	0.014	0.022	0.021	0.06	0.092	0.025	0.043
bdl - Below Detection Limit							

3.3 Thermal Degradation of 2-Monochlorophenol over α-Alumina

3.3.1 Pyrolytic Conditions

The product yields from the pyrolysis of 2-MCP over α-alumina are shown in Figures 3.14-3.16. The α-alumina was less active than γ-alumina in the destruction of 2-MCP precursor. While α-alumina was more active than fly ash at low temperatures, it did not reach the same destruction capacity as fly ash at high temperatures. Thermal degradation of 2-MCP reached 84% at 250ºC and increased to >90% at 550ºC.

MCBz, DCBz, and TriCBz were obtained with yields of 0.002%, 0.01%, and 0.00003% respectively, at 250ºC (see Figure 3.14). TeCBz, PentaCBz, and HexaCBz were identified in low yields and only formed at temperatures >350^{0}C. Chlorobenzene yields did not change significantly with temperature.

DCP and TriCP were obtained with yields of 0.01% and 0.0002% respectively, at 250ºC (see Figure 3.15). Chlorophenols were formed in higher concentrations than chlorobenzenes. The yields of DCP and TriCP both increased with increasing temperature, reaching maximum yields of 0.05% and 0.005% respectively, at 500ºC.

DF, DD, MCDF, MCDD, DCDF, and DCDD, TriCDD, and TeCDD were obtained, with low yields, at 250ºC (see Figure 3.16). The nonchlorinated DF and DD increased across the entire temperature range and reached maximums of 0.0006% and 0.00008%, respectively, at 550^{0}C. Chlorinated dioxins reached local maximums between 300-350^{0}C and then began increasing rapidly at 550^{0}C. Table 3.6 gives the yields of all chlorinated benzenes, phenols, and dioxin products.

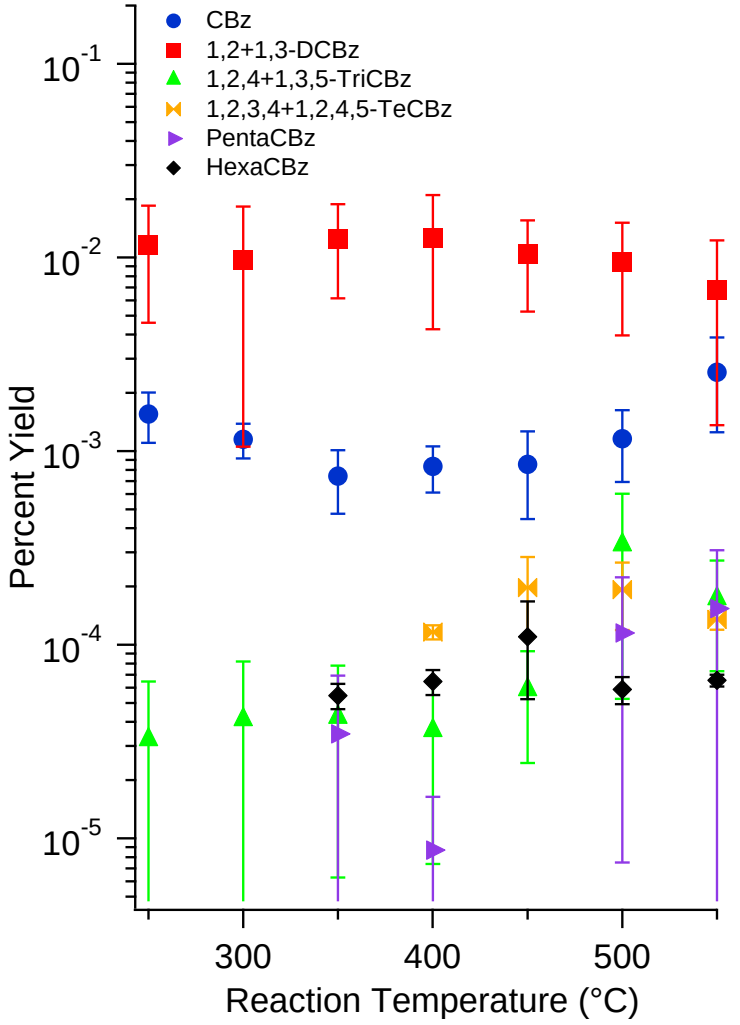

Figure 3.14. Chlorinated benzene yields from the pyrolysis of 2-MCP over α-alumina.

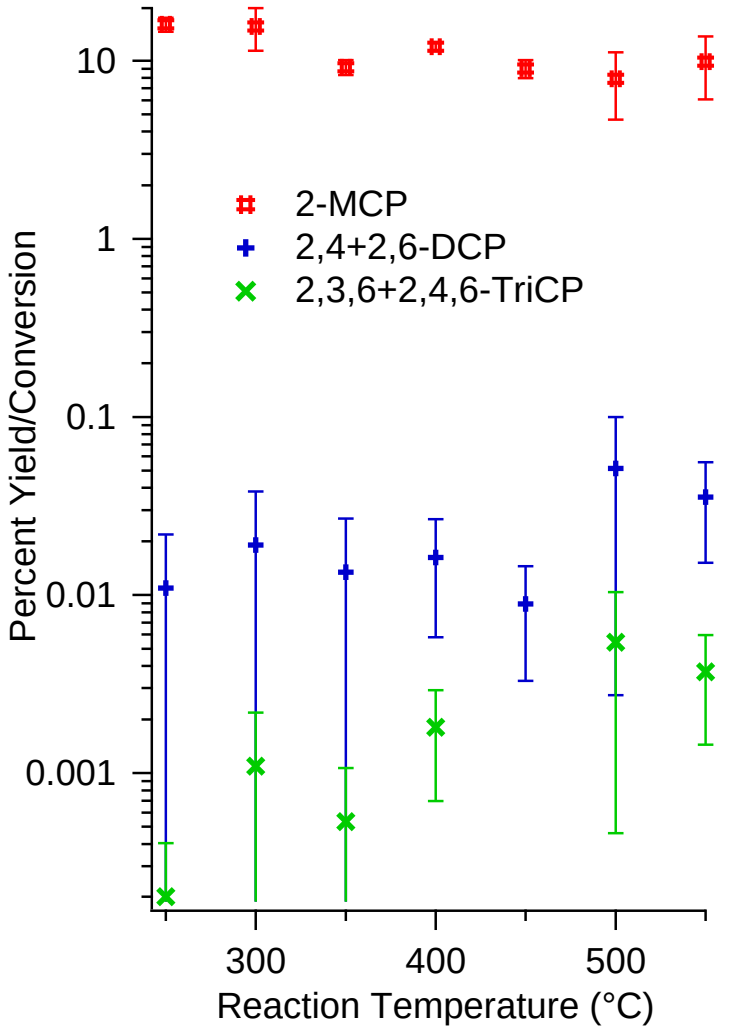

Figure 3.15. Chlorinated phenol yields and precursor conversion from the pyrolysis of 2-MCP over α-alumina.

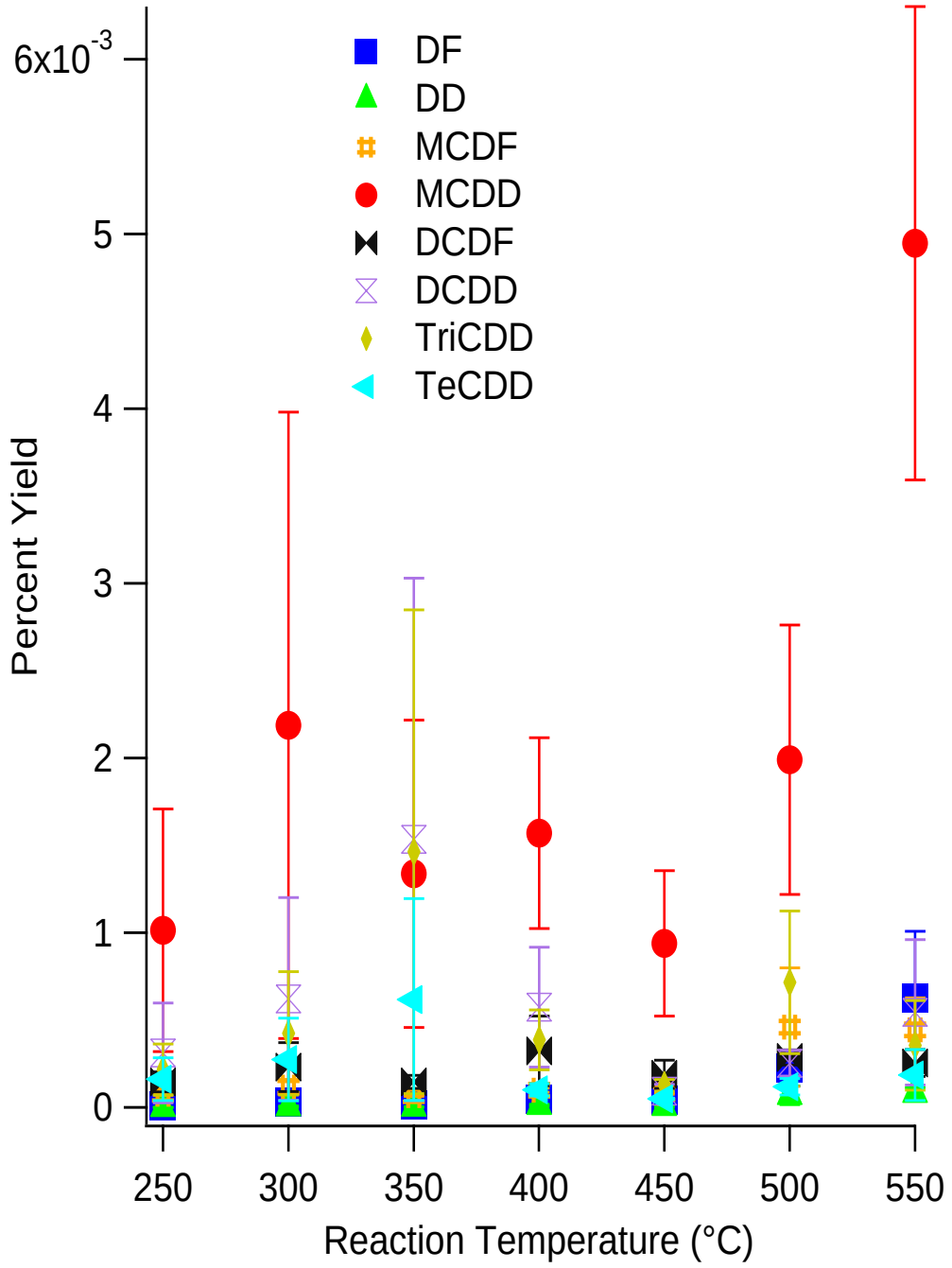

Figure 3.16. Major PCDD/F yields from the pyrolysis of 2-MCP over α-alumina.

Table 3.6. Dioxin and nondioxin products from the pyrolysis of 2-MCP over α-alumina.

	Reaction Temperature (^{0}C)						
	250	300	350	400	450	500	550
CBz	0.0016	0.0012	0.00074	0.00084	0.00085	0.0012	0.0026
2-MCP	16	16	8.2	16	9	7.9	9.9
DCBz	0.012	0.0097	0.013	0.013	0.01	0.0095	0.0068
DCP	0.011	0.019	0.013	0.016	0.0089	0.051	0.035
TriCBz	0.000032	0.000041	0.000042	3.6E-05	0.000059	0.00033	0.00017
TetraCBz	bdl	bdl	bdl	0.00012	0.0002	0.00019	0.00014
TriCP	0.0002	0.0011	0.00053	0.0018	bdl	0.0054	0.0037
PentaCBz	bdl	bdl	0.000035	8.7E-06	bdl	0.00012	0.00015
HexaCBz	bdl	bdl	0.000055	6.5E-05	0.00011	5.9E-05	6.6E-05
DF	0.000011	0.000032	0.000014	4.9E-05	0.000039	0.00022	0.00063
DD	8.3E-07	3.4E-06	1.9E-06	1.1E-05	5.8E-06	6.9E-05	8.1E-05
MCDF	0.000075	0.00012	0.000068	9.8E-05	0.000079	0.00046	0.00044
MCDD	0.001	0.0022	0.0013	0.0016	0.00094	0.002	0.0049
DCDF	0.00015	0.00023	0.00015	0.00032	0.00019	0.00029	0.00025
DCDD	0.00031	0.00062	0.0015	0.00057	0.000093	0.00025	0.00054
TriCDD	0.00022	0.00042	0.0015	0.00039	0.00013	0.00072	0.00036
TetraCDD	0.00016	0.00028	0.00062	0.0001	0.00005	0.00012	0.00019
bdl - Below Detection Limit							

3.3.2 Oxidative Conditions

The product yields from the oxidation of 2-MCP over α-alumina are shown in Figures 3.17-3.19. The α-alumina was less active than γ-alumina in the destruction of 2-MCP . While α-alumina was more active than fly ash at low temperatures, it did not reach the same destruction capacity as fly ash at high temperatures. Oxidative conditions led to α-alumina being less active at lower temperatures and more active at higher temperatures. Thermal degradation of 2-MCP began at approximately 75% but increased to >96% at 550ºC.

Oxidative conditions led to a greater variety of chlorinated products (see Figure 3.17). MCBz, DCBz, TriCBz, TeCBz, and HexaCBz were obtained with yields of 0.001%, 0.04%, 0.00003%, 0.0002%, and 0.00005% respectively, at 250ºC. All chlorobenzenes showed increased yields with increased.

DCP and TriCP were obtained with yields of 0.03% and 0.003% respectively, at 250ºC. Chlorophenols were formed in higher concentrations than chlorobenzenes (see Figure 3.18). The yields of DCP and TriCP increased with increasing temperature, reaching maximum yields of 0.5% and 0.1% respectively, at 450ºC.

DF and DD were the lowest concentration dioxin congeners, (see Figure 3.19) but increased and reached maximums of 0.001% and 0.0005%, respectively, at 550^0C. MCDD was the highest concentration product formed and reached a maximum yield of 0.3% at 500^0C. The higher chlorinated dibenzo-p-dioxins showed no significant increase of yield with increased temperature. Table 3.7 gives the yields of all chlorinated benzenes, phenols, and dioxin products.

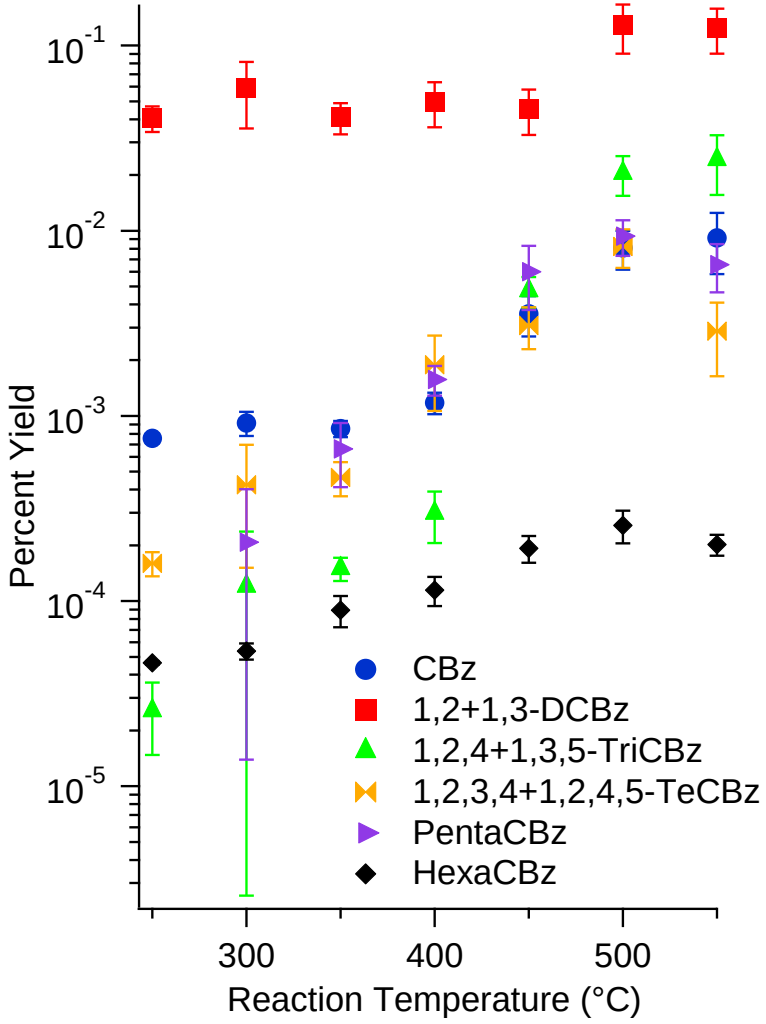

Figure 3.17. Chlorinated benzene yields from the oxidation of 2-MCP over α-alumina.

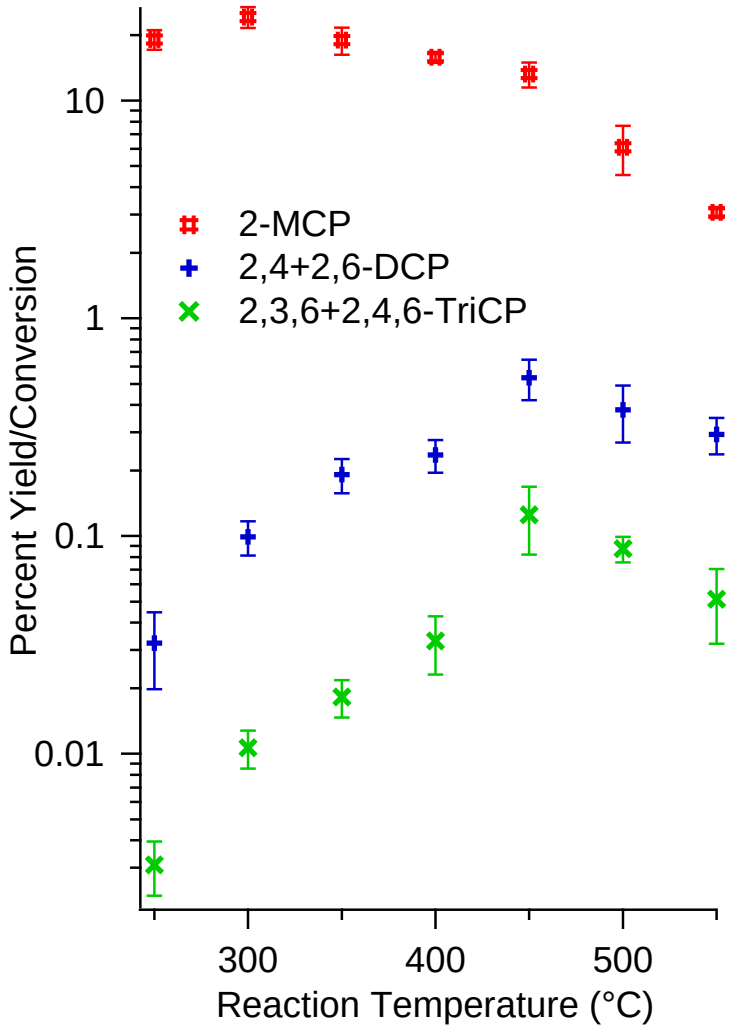

Figure 3.18. Chlorinated phenol yields and precursor conversion from the oxidation of 2-MCP over α-alumina.

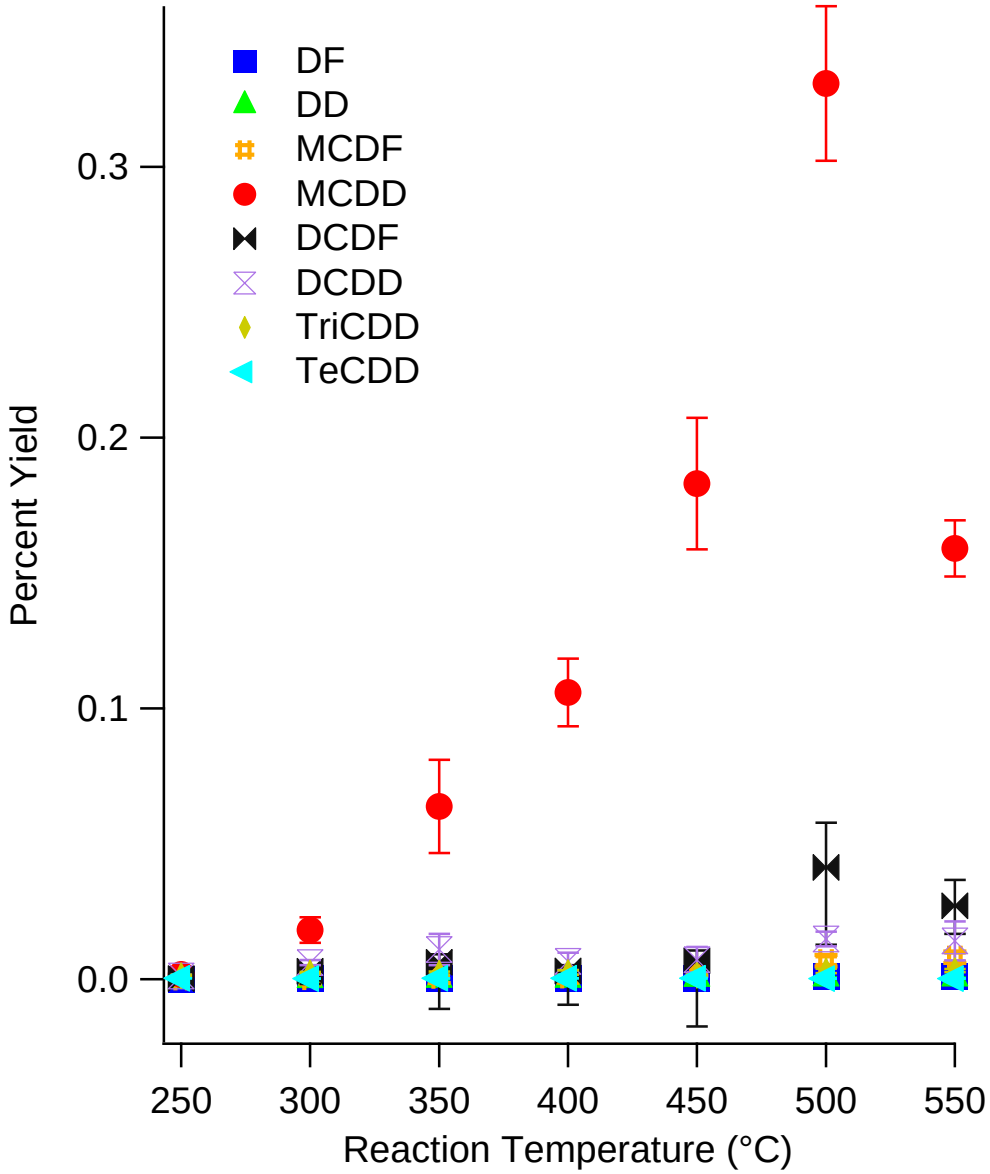

Figure 3.19. Major PCDD/F yields from the oxidation of 2-MCP over α-alumina.

Table 3.7. Dioxin and nondioxin products from the oxidation of 2-MCP over α-alumina.

	Reaction Temperature (^{0}C)						
	250	300	350	400	450	500	550
CBz	0.00076	0.00092	0.00085	0.0012	0.0036	0.0081	0.0091
2-MCP	19	24	19	16	13	6.1	3.1
DCBz	0.041	0.059	0.041	0.05	0.045	0.13	0.12
DCP	0.032	0.099	0.19	0.24	0.53	0.38	0.29
TriCBz	0.000026	0.00012	0.00015	0.0003	0.0047	0.02	0.024
TetraCBz	0.00016	0.00042	0.00046	0.0019	0.0031	0.0082	0.0029
TriCP	0.0031	0.011	0.018	0.033	0.13	0.087	0.051
PentaCBz	bdl	0.00021	0.00066	0.0016	0.006	0.0093	0.0066
HexaCBz	0.000046	0.000054	0.000089	0.00011	0.00019	0.00026	0.0002
DF	0.0000087	0.000021	0.000028	0.000038	0.00031	0.00082	0.00095
DD	0.0000008	0.0000068	0.000055	0.00012	0.00037	0.00054	0.00048
MCDF	0.000086	0.00022	0.00064	0.00081	0.0033	0.0068	0.0081
MCDD	0.0018	0.018	0.064	0.11	0.18	0.33	0.16
DCDF	0.00017	0.0029	0.0062	0.0031	0.0068	0.041	0.027
DCDD	0.0011	0.0061	0.011	0.0066	0.0071	0.015	0.014
TriCDD	0.0013	0.0023	0.0022	0.0024	0.0014	0.003	0.0032
TetraCDD	0.00033	0.00023	0.00025	0.00034	0.00026	0.00022	0.00023
bdl - Below Detection Limit							

3.4 Thermal Degradation of 2-Monochlorophenol over γ-Alumina

3.4.1 Pyrolytic Conditions

The product yields from the surface-mediated pyrolysis of 2-MCP over γ-alumina are presented in Figures 3.20-3.22 as a function of temperature. γ-Alumina was extremely active in the decomposition of 2-MCP and reached >99.9% destruction efficiency across the entire range of 250-550 ^{0}C. The high catalytic activity of γ-alumina also led to low product yields.

The yields of chlorinated benzenes can be seen in Figure 3.20. MCBz, DCBz, TriCBz, TeCBz, PentaCBz, and HexaCBz were obtained with yields of 0.002%, 0.01%, 0.000004%, 0.00002%, 0.00005%, and 0.00002% respectively, at 200ºC. All chlorobenzene yields stayed constant at higher temperatures.

The yields of chlorinated phenols can be seen in Figure 3.21. DCP and TriCP were obtained with yields of 0.0001% and 0.00001% respectively, at 200ºC. The yields of DCP and TriCP both increased slightly with increasing temperature, reaching maximum yields of 0.01% and 0.002% respectively, at 400ºC.

PCDD/F yields were extremely low over γ-alumina (see Figure 3.22). DF, DD, MCDF, MCDD, DCDF, DCDD, TriCDD, and TeCDD were obtained with yields of 0.00008%, 0.000001%, 0.00007%, 0.0005%, 0.00009%, 0.00002%, 0.00007%, and 0.00004% respectively, at 200ºC. All dibenzo-p-dioxins had constant yields across the entire temperature range. The nonchlorinated DF and, to a lesser degree, DCDF were the only dioxin products to show a significant increase. Table 3.8 gives the yields of all chlorinated benzenes, phenols, and dioxin products.

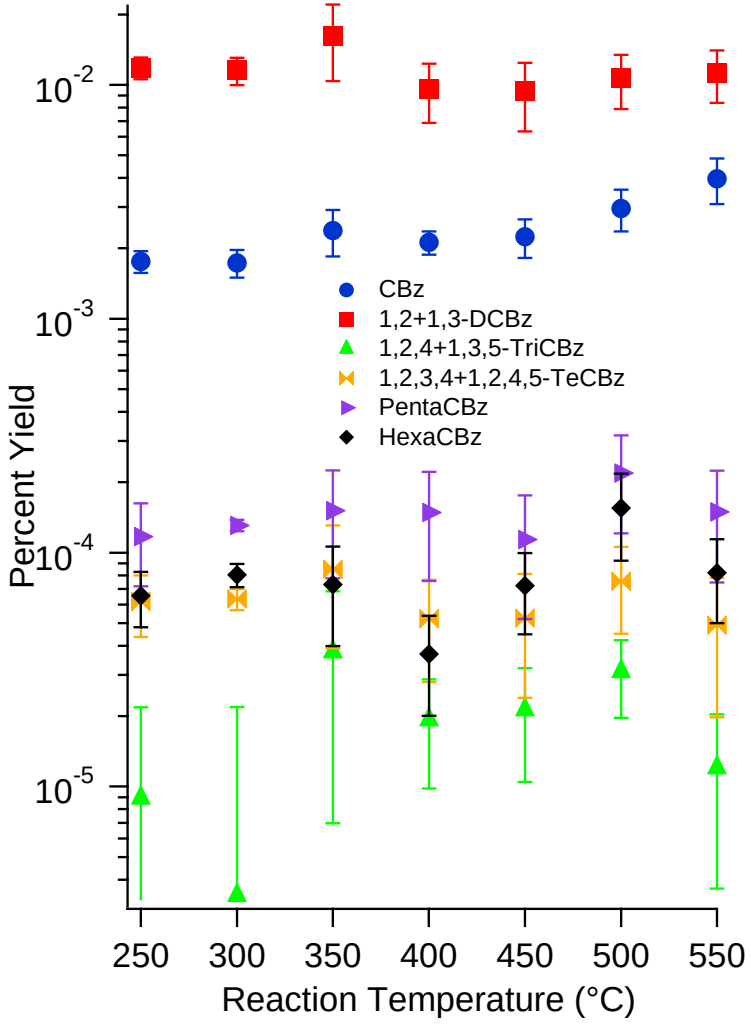

Figure 3.20. Chlorinated benzene yields from the pyrolysis of 2-MCP over γ-alumina.

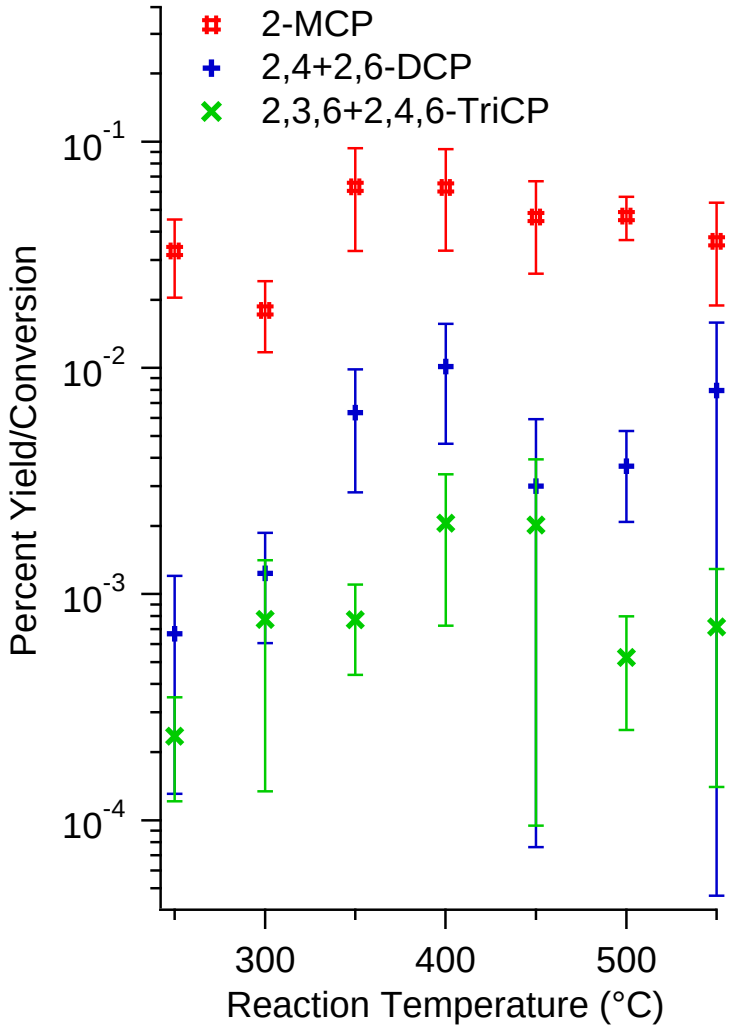

Figure 3.21. Chlorinated phenol yields and precursor conversion from the pyrolysis of 2-MCP over γ-alumina.

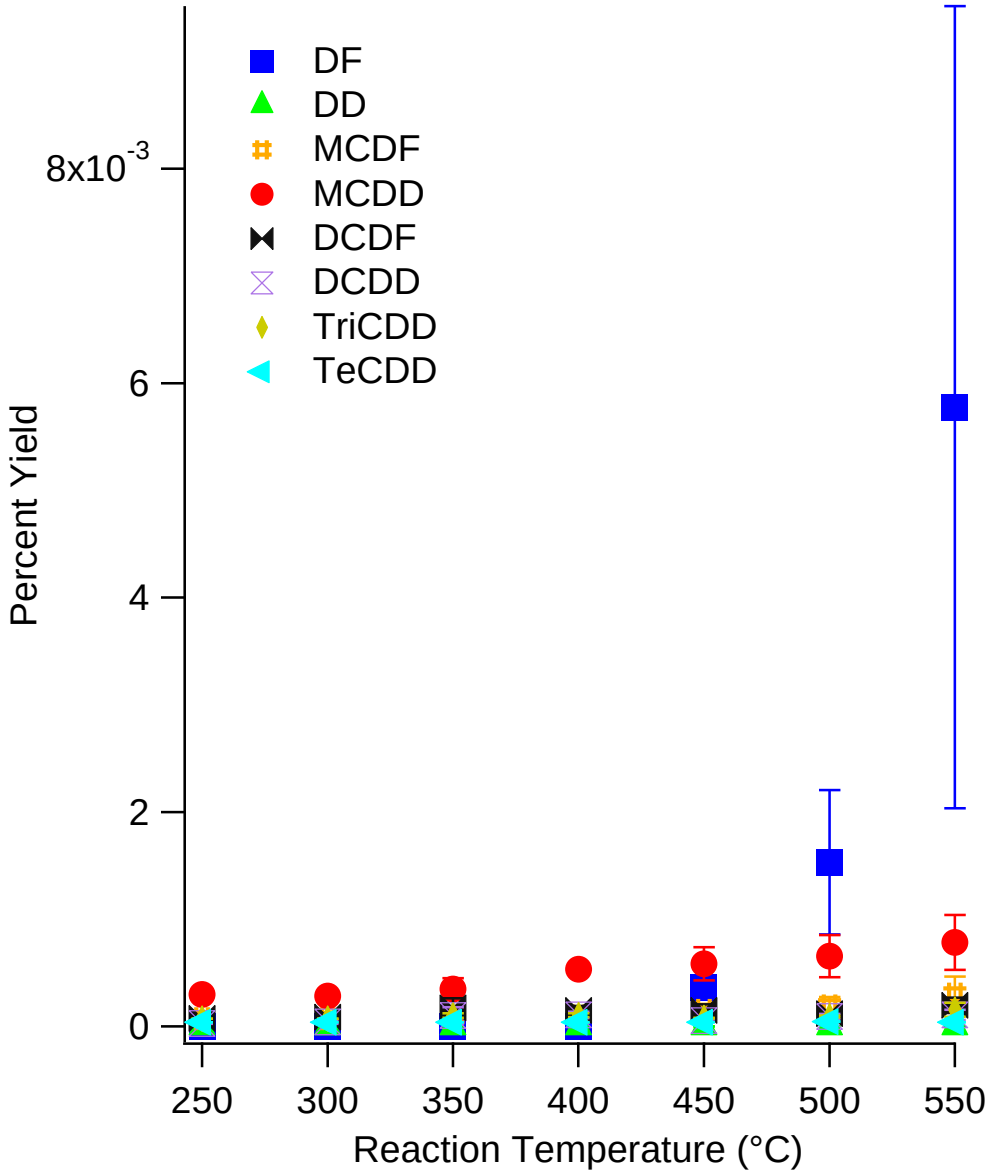

Figure 3.22. Major PCDD/F yields from the pyrolysis of 2-MCP over γ-alumina.

Table 3.8. Dioxin and nondioxin products from the pyrolysis of 2-MCP over γ-alumina.

	Reaction Temperature (^{0}C)						
	250	300	350	400	450	500	550
CBz	0.0022	0.0017	0.0024	0.0021	0.0022	0.003	0.004
2-MCP	0.066	0.018	0.086	0.087	0.064	0.067	0.14
DCBz	0.016	0.012	0.016	0.0096	0.0094	0.011	0.011
DCP	0.00066	0.0012	0.0063	0.01	0.003	0.0037	0.0079
TriCBz	6.80E-05	3.40E-06	3.80E-05	1.90E-05	2.10E-05	3.10E-05	1.20E-05
TetraCBz	1.40E-04	6.30E-05	8.50E-05	5.20E-05	5.30E-05	7.50E-05	4.90E-05
TriCP	0.00023	0.00077	0.00077	0.0021	0.002	0.00052	0.00072
PentaCBz	0.00022	0.00013	0.00015	0.00015	0.00011	0.00022	0.00015
HexaCBz	0.00011	0.00008	0.000073	3.7E-05	0.000072	0.00015	8.2E-05
DF	8.70E-06	0.00E+00	0.00E+00	0.00E+00	3.60E-04	1.50E-03	5.80E-03
DD	7.60E-07	4.00E-07	6.00E-07	5.90E-07	7.60E-07	8.30E-07	1.20E-06
MCDF	8.40E-05	7.00E-05	9.20E-05	9.70E-05	1.50E-04	1.90E-04	3.00E-04
MCDD	4.60E-04	2.80E-04	3.50E-04	5.30E-04	5.80E-04	6.60E-04	7.80E-04
DCDF	1.70E-03	8.60E-05	1.70E-04	1.50E-04	1.50E-04	1.20E-04	2.00E-04
DCDD	1.50E-03	4.20E-05	1.00E-04	1.10E-04	5.40E-05	9.20E-05	1.10E-04
TriCDD	1.10E-04	7.20E-05	1.00E-04	1.00E-04	7.80E-05	9.30E-05	1.60E-04
TetraCDD	4.40E-05	bdl	4.00E-05	3.90E-05	3.90E-05	4.40E-05	bdl
bdl - Below Detection Limit							

3.4.2 Oxidative Conditions

The product yields from the surface-mediated oxidation of 2-MCP over γ-alumina are presented in Figures 3.23-3.25 as a function of temperature. The reaction gas did not have an effect on the destruction of the 2-MCP precursor. Thermal degradation of 2-MCP reached >99.9% across the entire temperature range of 250-550ºC. The high catalytic activity of the γ-alumina led to low product yields.

The yields of chlorinated benzenes can be seen in Figure 3.23. MCBz and DCBz were obtained with yields of 0.0007% and 0.02% respectively, at 250ºC. The product profile was more limited under oxidative conditions. The higher catalytic activity under oxidative conditions likely resulted in less opportunity for chlorination of products. The yields of MCBz and DCBz increased slightly with increasing temperature, reaching maximums at 475ºC of 0.02% and 0.2% respectively.

The yields of chlorinated phenols can be seen in Figure 3.24. DCP was obtained with a yield of 0.0005% at 250ºC. The yield of DCP increased slightly with increasing temperature, reaching a maximum of 0.001% at 500ºC.

The yields of PCDD/Fs can be seen in Figure 3.25. DF, DD, MCDF, MCDD, DCDF, and DCDD were obtained with yields of 0.00004%, 0.0000005%, 0.0004%, 0.006%, 0.002%, and 0.005% respectively, at 250ºC. Dioxin products were extremely low for γ-alumina. Most of the dioxin products showed no significant increase across the temperature range. MCDD increased slightly with increasing temperature, reaching a maximum yield of 0.01% at 450ºC. Table 3.9 gives the yields of all chlorinated benzenes, phenols, and dioxin products.

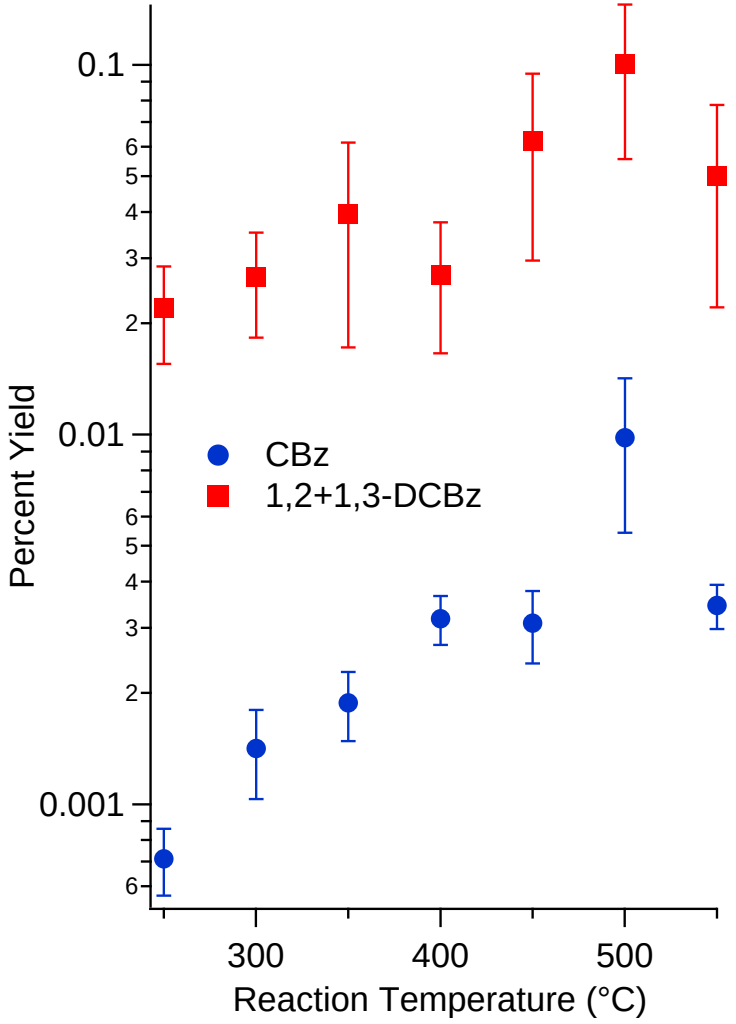

Figure 3.23. Chlorinated benzene yields from the oxidation of 2-MCP over γ-alumina.

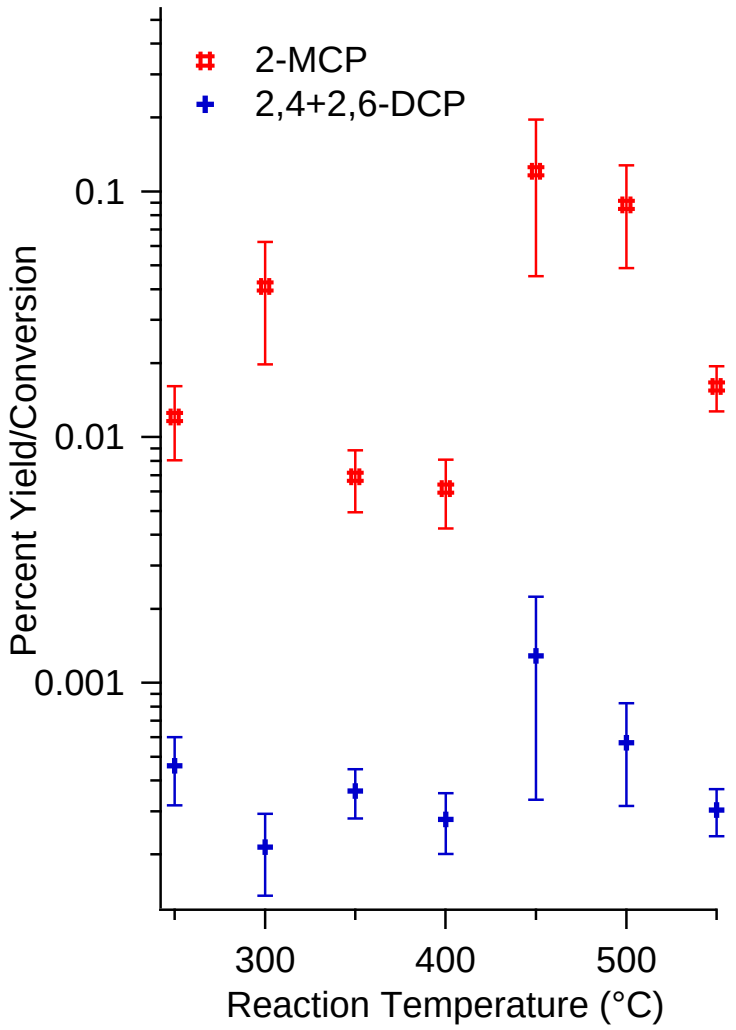

Figure 3.24. Chlorinated phenol yields and precursor conversion from the oxidation of 2-MCP over γ-alumina.

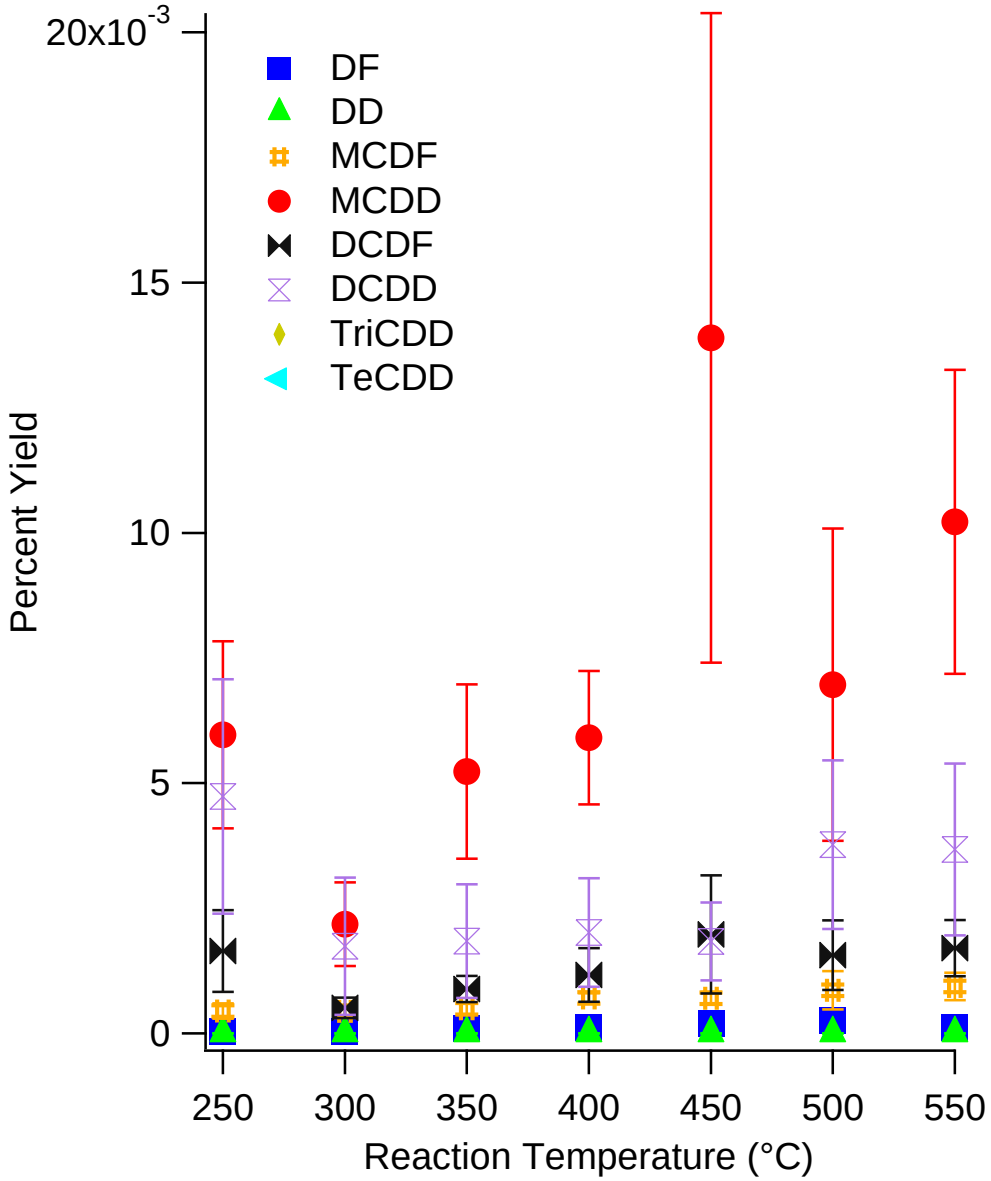

Figure 3.25. Major PCDD/F yields from the oxidation of 2-MCP over γ-alumina.

Table 3.9. Dioxin and nondioxin products from the oxidation of 2-MCP over γ-alumina.

	Reaction Temperature (^{0}C)						
	250	300	350	400	450	500	550
MCB	0.00071	0.0014	0.0019	0.0032	0.0031	0.0098	0.0034
2-MCP	0.012	0.041	0.0069	0.0062	0.12	0.088	0.016
DCBz	0.022	0.027	0.039	0.027	0.062	0.1	0.05
DCP	0.00046	0.00021	0.00036	0.00028	0.0013	0.00057	0.0003
DF	0.000042	0.000031	0.000092	0.00012	0.00021	0.00025	0.00012
DD	5E-07	1.6E-07	7.2E-07	6.3E-07	1.6E-06	5.4E-07	8.3E-07
MCDF	0.00045	0.00044	0.00049	0.00071	0.0007	0.00086	0.00094
MCDD	0.006	0.0022	0.0052	0.0059	0.014	0.007	0.01
DCDF	0.0016	0.00051	0.00089	0.0012	0.002	0.0016	0.0017
DCDD	0.0047	0.0017	0.0018	0.002	0.0018	0.0038	0.0037
bdl - Below Detection Limit							

3.5 Thermal Degradation of 2-Monochlorophenol over Mullite

3.5.1 Pyrolytic Conditions

The product yields from the surface-mediated pyrolysis of 2-MCP over mullite are presented in Figures 3.26-3.28 as a function of temperature. Mullite was fairly active in the destruction of 2-MCP precursor under pyrolytic conditions. Thermal degradation of 2-MCP was >95% at 250ºC and increased to >99.9% at 500ºC.

The yields of chlorinated benzenes can be seen in Figure 3.26. MCBz, DCBz, TriCBz, TeCBz, and PentaCBz were obtained with yields of 0.003%, 0.01%, 0.00006%, 0.00004%, and 0.00003%, respectively, at 250ºC. HexaCBz was formed in extremely small amounts starting at 300^0C. The yields of all chlorinated benzenes showed no significant change with increased temperature.

The yields of chlorinated phenols can be seen in Figure 3.27. DCP was formed in small concentrations at various temperatures with no clear trend. No other chlorinated phenols were formed.

DF, DD, MCDF, MCDD, DCDF, DCDD, TriCDD, and TeCDD were obtained with yields of 0.0001%, 0.000001%, 0.0001%, 0.0003%, 0.0001%, 0.0001%, 0.0001%, and 0.00004% respectively, at 250ºC (see Figure 3.28). DF, MCDF, and DCDF yields increased with temperature and reached maximums of 0.01%, 0.002%, and 0.001% at 600^0C. MCDD was the second highest product yield and reached a maximum of 0.01% at 600^0C. All other chlorinated dibenzo-p-dioxins showed no significant increase with temperature. Table 3.10 gives the yields of all chlorinated benzenes, phenols, and dioxin products.

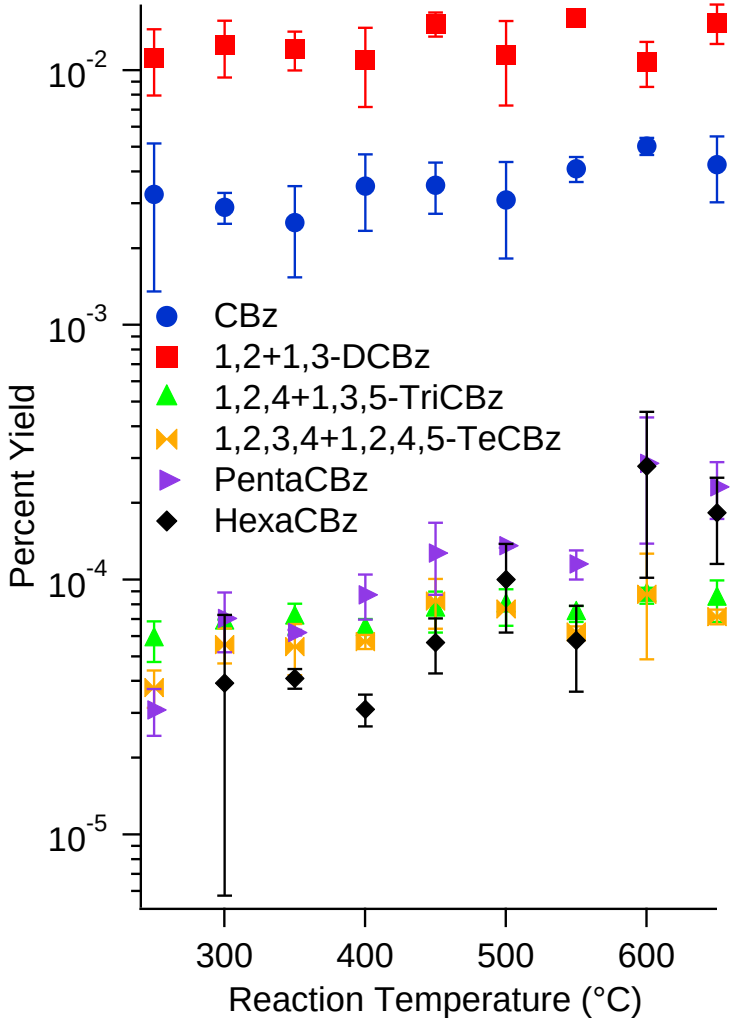

Figure 3.26. Chlorinated benzene yields from the pyrolysis of 2-MCP over mullite.

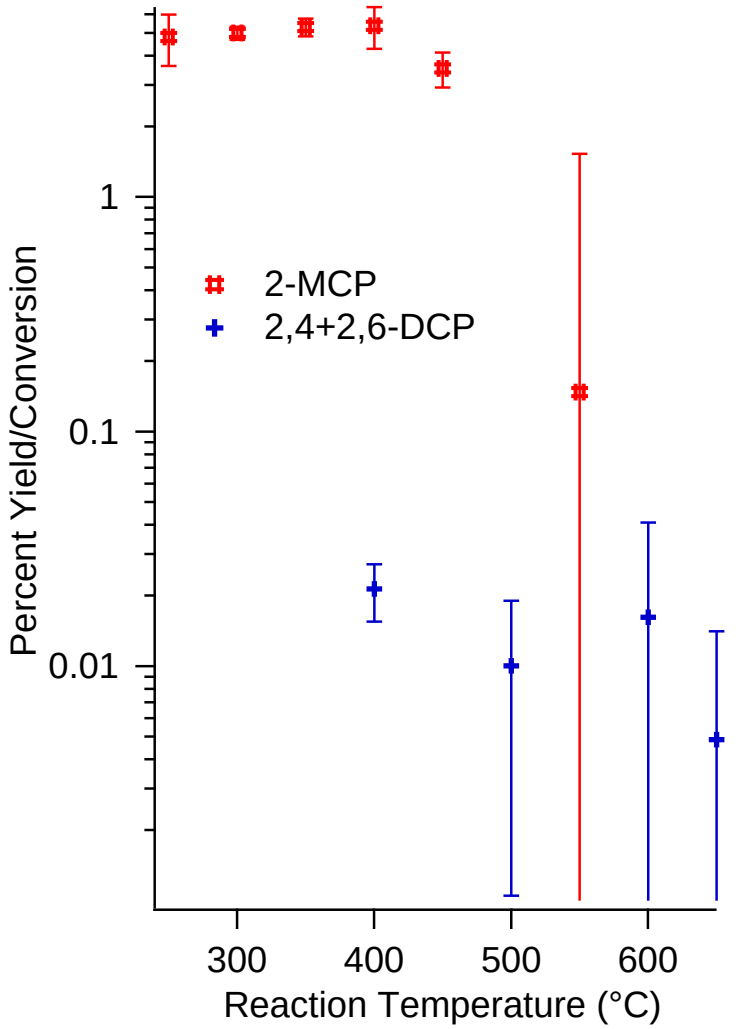

Figure 3.27. Chlorinated phenol yields and precursor conversion from the pyrolysis of 2-MCP over mullite.

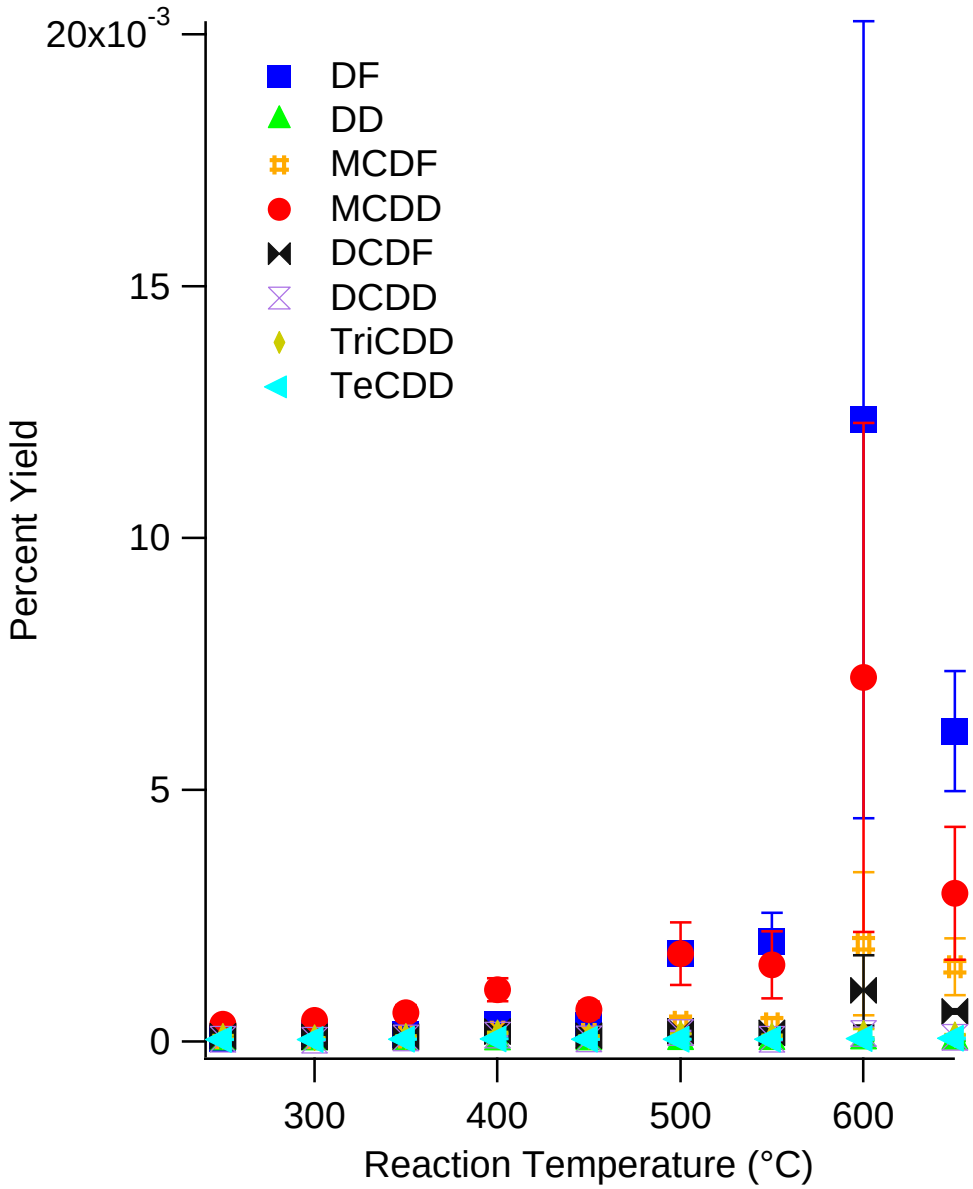

Figure 3.28. Major PCDD/F yields from the pyrolysis of 2-MCP over mullite.

Table 3.10. Dioxin and nondioxin products from the pyrolysis of 2-MCP over mullite.

	Reaction Temperature (^{0}C)						
	300	350	400	450	500	550	600
CBz	0.0029	0.0025	0.0035	0.0035	0.0031	0.0041	0.005
2-MCP	5	5.3	5.4	3.5	bdl	0.15	bdl
DCBz	0.012	0.012	0.011	0.015	0.011	0.016	0.011
DCP	bdl	bdl	0.021	bdl	0.01	bdl	0.016
TriCBz	6.70E-05	7.10E-05	6.40E-05	7.60E-05	7.90E-05	7.30E-05	8.70E-05
TetraCBz	5.60E-05	5.50E-05	5.70E-05	8.20E-05	7.70E-05	6.20E-05	8.70E-05
PentaCBz	7.00E-05	6.20E-05	8.70E-05	1.30E-04	1.40E-04	1.20E-04	2.90E-04
HexaCBz	3.90E-05	4.10E-05	3.10E-05	5.70E-05	1.00E-04	5.80E-05	2.80E-04
DF	1.50E-04	1.30E-04	3.40E-04	3.20E-04	1.80E-03	2.00E-03	1.20E-02
DD	6.40E-07	8.90E-07	1.50E-06	1.20E-06	4.80E-06	5.70E-06	2.20E-05
MCDF	7.90E-05	9.20E-05	1.80E-04	1.40E-04	3.80E-04	3.50E-04	1.90E-03
MCDD	0.00042	0.00057	0.001	0.00063	0.0017	0.0015	0.0072
DCDF	8.60E-05	9.40E-05	2.00E-04	1.20E-04	2.00E-04	1.70E-04	1.00E-03
DCDD	2.70E-05	7.10E-05	1.30E-04	5.10E-05	1.80E-04	4.40E-05	1.60E-04
TriCDD	7.60E-05	1.00E-04	1.70E-04	1.00E-04	1.50E-04	1.10E-04	1.60E-04
TetraCDD	3.90E-05	4.20E-05	4.90E-05	4.30E-05	4.70E-05	4.20E-05	6.00E-05
bdl - Below Detection Limit							

3.5.2 Oxidative Conditions

The product yields from the surface-mediated oxidation of 2-MCP over mullite are presented in Figures 3.29-3.31 as a function of temperature. The decomposition of precursor was less than under pyrolytic conditions at low temperatures. Under oxidative conditions, mullite had similar catalytic activity to α-alumina. Thermal degradation of 2-MCP reached approximately 70% at 250ºC and increased to >98% at 600ºC.

The yields of chlorinated benzenes can be seen in Figure 3.29. MCBz, DCBz, TriCBz, TeCBz, and PentaCBz were obtained with yields of 0.001%, 0.001%, 0.0001%, 0.00004%, and 0.00003% respectively, at 200ºC. Tri-, Te-, Penta-, and HexaCBz reached maximums of 0.001%, 0.002%, 0.001%, and 0.001%. No other chlorinated benzene surpassed the yield of DCBz, which stayed constant.

DCP and TriCP were obtained with yields of 0.01% at 200^0C and 0.01% at 200ºC, respectively. Chlorophenols were produced in much higher concentrations than chlorobenzenes (see Figure 3.30). The yields of DCP and TriCP increased with temperature, reaching maximum yields of 0.2% and 0.05% respectively, at 500ºC.

Under oxidative conditions, mullite showed similar patterns of dioxin formation to α-alumina (see Figure 3.31). DF, DD, MCDF, MCDD, DCDF, DCDD, TriCDD, and TeCDD were obtained with yields of 0.0005%, 0.000001%, 0.0001%, 0.001%, 0.0001%, 0.0001%, 0.0002%, and 0.0001% respectively, at 200ºC. All dioxin congeners showed increased yields with increased temperatures but the mono- and dichlorinated species had the highest concentrations. Table 3.11 gives the yields of all chlorinated benzenes, phenols, and dioxin products.

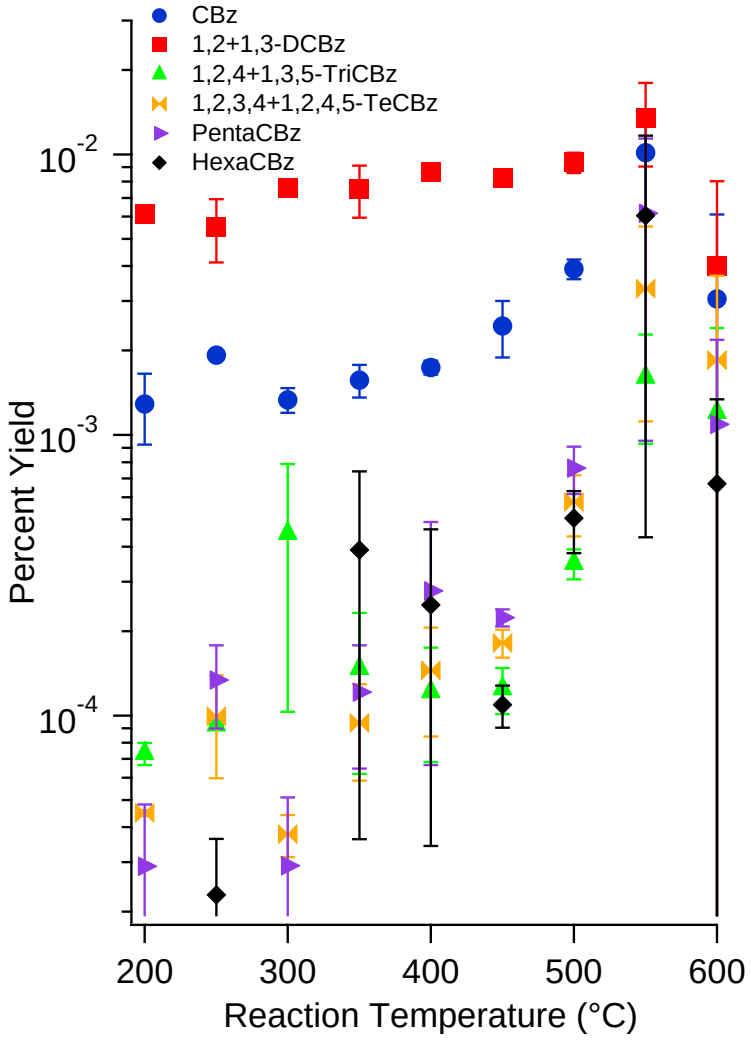

Figure 3.29. Chlorinated benzene yields from the oxidation of 2-MCP over mullite.

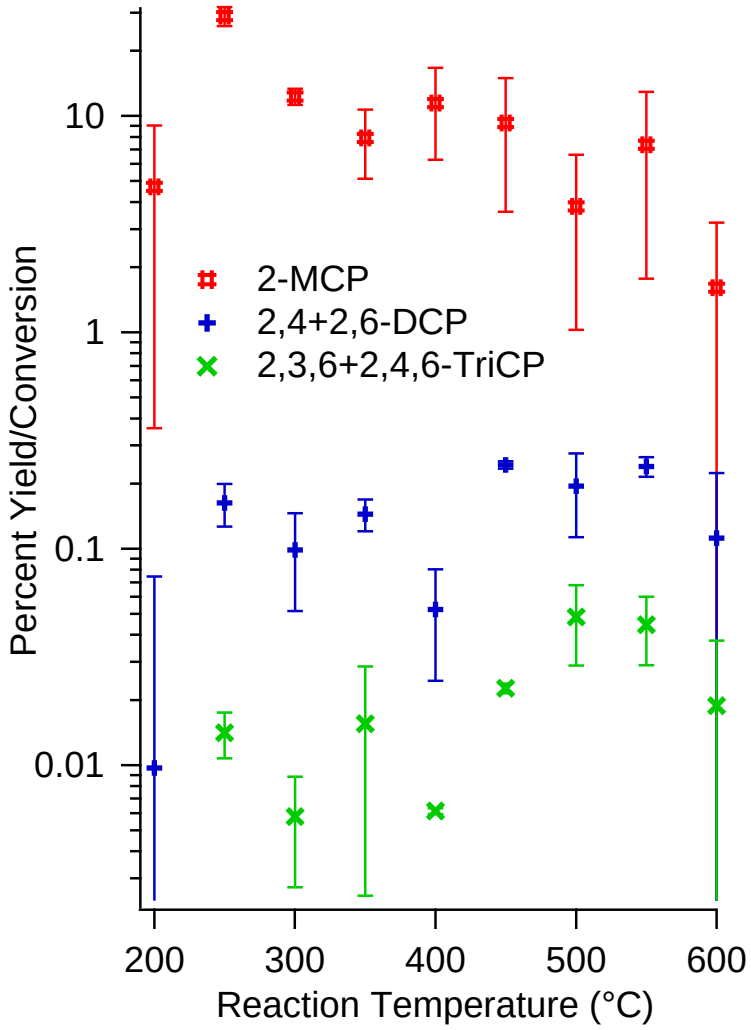

Figure 3.30. Chlorinated phenol yields and precursor conversion from the oxidation of 2-MCP over mullite.

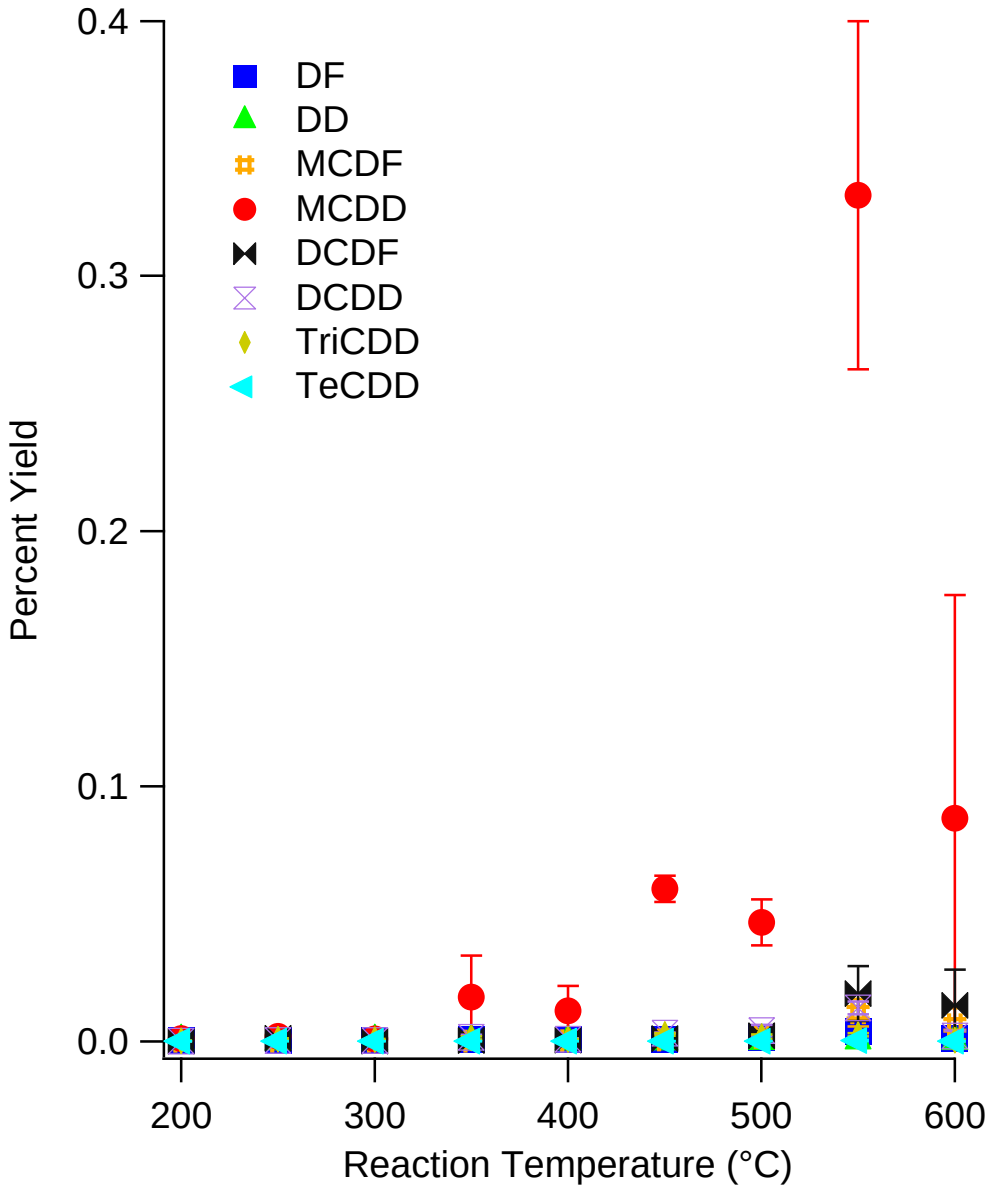

Figure 3.31. Major PCDD/F yields from the pyrolysis of 2-MCP over mullite.

Table 3.11. Dioxin and nondioxin products from the oxidation of 2-MCP over mullite.

	Reaction Temperature (^{0}C)						
	300	350	400	450	500	550	600
CBz	0.0013	0.0016	0.0017	0.0024	0.0039	0.01	0.0031
2-MCP	12	7.9	11	9.3	3.8	7.4	1.6
DCBz	0.0076	0.0075	0.0086	0.0083	0.0094	0.014	0.004
DCP	0.099	0.14	0.052	0.24	0.19	0.24	0.11
TriCBz	0.00045	0.00015	0.00012	0.00012	0.00035	0.0016	0.0012
TetraCBz	0.000038	0.000094	0.00014	0.00018	0.00058	0.0033	0.0018
TriCP	0.0058	0.016	0.0061	0.023	0.048	0.045	0.019
PentaCBz	0.000029	0.00012	0.00028	0.00022	0.00076	0.0062	0.0011
HexaCBz	bdl	0.00039	0.00025	0.00011	0.0005	0.0061	0.00067
DF	0.00026	0.0008	0.00068	0.00077	0.0015	0.0039	0.001
DD	1.90E-06	4.30E-06	4.30E-06	1.90E-05	6.40E-05	3.10E-04	9.40E-05
MCDF	0.00012	0.00015	0.00018	0.0006	0.0016	0.011	0.0065
MCDD	0.001	0.017	0.012	0.06	0.047	0.33	0.087
DCDF	0.00015	0.0003	0.00044	0.0011	0.0023	0.019	0.014
DCDD	0.00032	0.0016	0.00087	0.0032	0.0042	0.013	0.0021
TriCDD	0.00073	0.0014	0.00071	0.0027	0.0018	0.0026	0.00043
TetraCDD	6.10E-05	7.70E-05	7.40E-05	1.10E-04	1.30E-04	4.20E-04	9.50E-05
bdl - Below Detection Limit							

3.6 Thermal Degradation of 2-Monochlorophenol over a 1% Fe_2O_3 + 4% CuO / silica Surrogate

3.6.1 Pyrolytic Conditions

The product yields from the surface-mediated pyrolysis of 2-MCP over a 1% Fe_2O_3 + 4% CuO / silica surrogate are presented in Figures 3.32-3.34 as a function of temperature. The surrogate was fairly active in the destruction of 2-MCP precursor under pyrolytic conditions. Thermal degradation of 2-MCP was >95% at 200ºC and increased to >99.9% at 300ºC.

MCBz and DCBz were obtained with yields of 0.002% and 0.00004%, respectively, at 200ºC (see Figure 3.32). TriCBz, TeCBz, and PentaCBz were obtained with yields of 0.00007%, 0.0002%, and 0.0003% at 250ºC, 225ºC, and 250ºC, respectively. Only MCBz and DCBz exhibited clear trends between yield and temperature, reaching maximums of 0.007% and 0.0007%, respectively, at 275ºC.

The yields of chlorinated phenols can be seen in Figure 3.33. DCP was obtained with a maximum yield of 0.03% at 225 ºC. TriCP was formed in a small temperature range between 300-400 ºC and reached a maximum yield of 0.005%.

The yields of PCDD/Fs can be seen in Figure 3.34. DF, DD, MCDF, MCDD, DCDF, DCDD, and TriCDD were obtained with yields of 0.0003%, 0.0002%, 0.005%, 0.3%, 0.05%, 0.03%, and 0.0009%, respectively, at 200ºC. MCDD and DCDD reached maximum yields of 1.3% at 225^{0}C and 0.16% at 250^{0}C, respectively. DCDF was the primary PCDF and reached a maximum yield of 0.13% at 250^{0}C. All other PCDD/Fs showed no significant increase with temperature. Table 3.12 gives the yields of all chlorinated benzenes, phenols, and dioxin products.

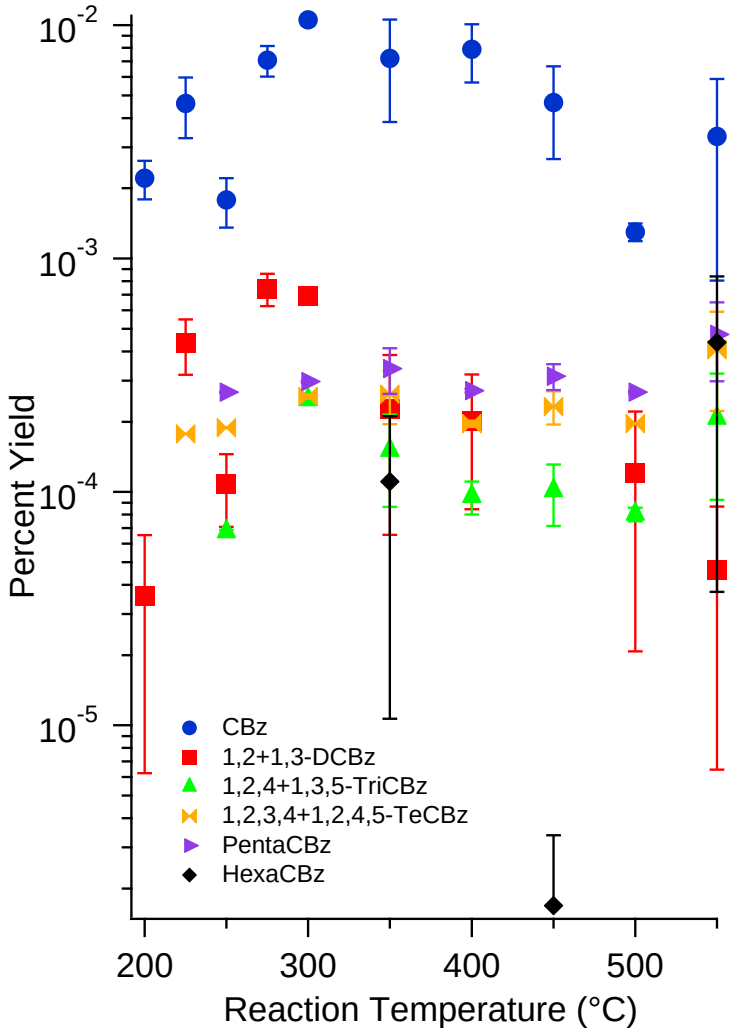

Figure 3.32. Chlorinated benzene yields from the pyrolysis of 2-MCP over a 1% Fe_2O_3 + 4% CuO / silica surrogate.

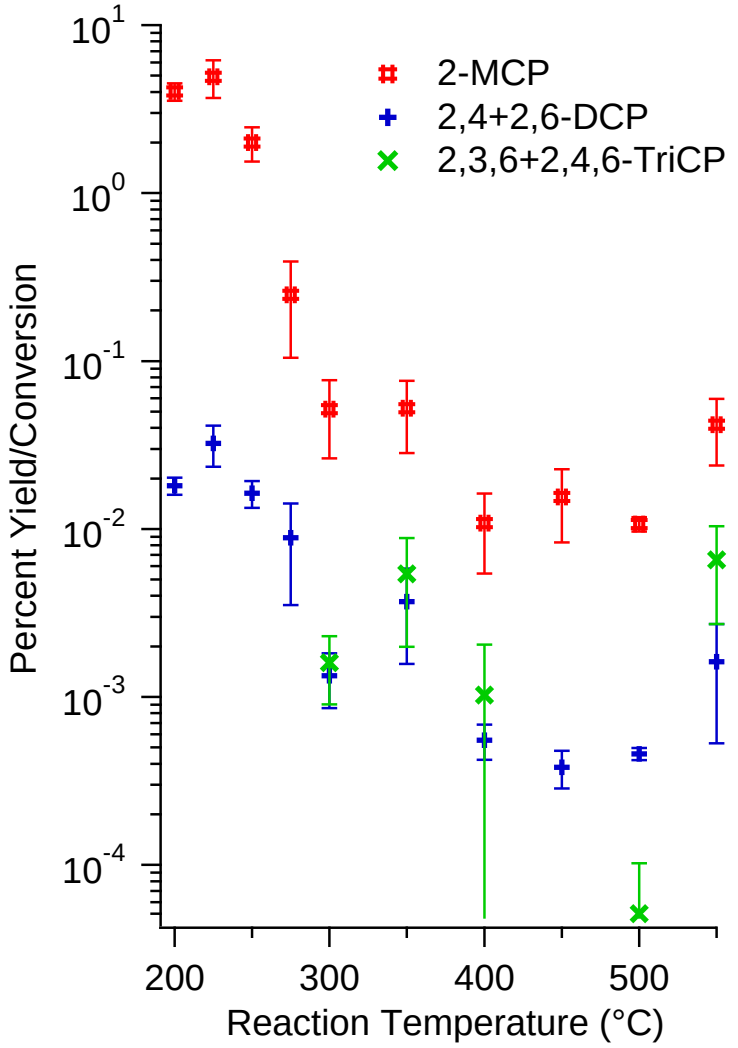

Figure 3.33. Chlorinated phenol yields and precursor conversion from the pyrolysis of 2-MCP over a 1% Fe_2O_3 + 4% CuO / silica surrogate.

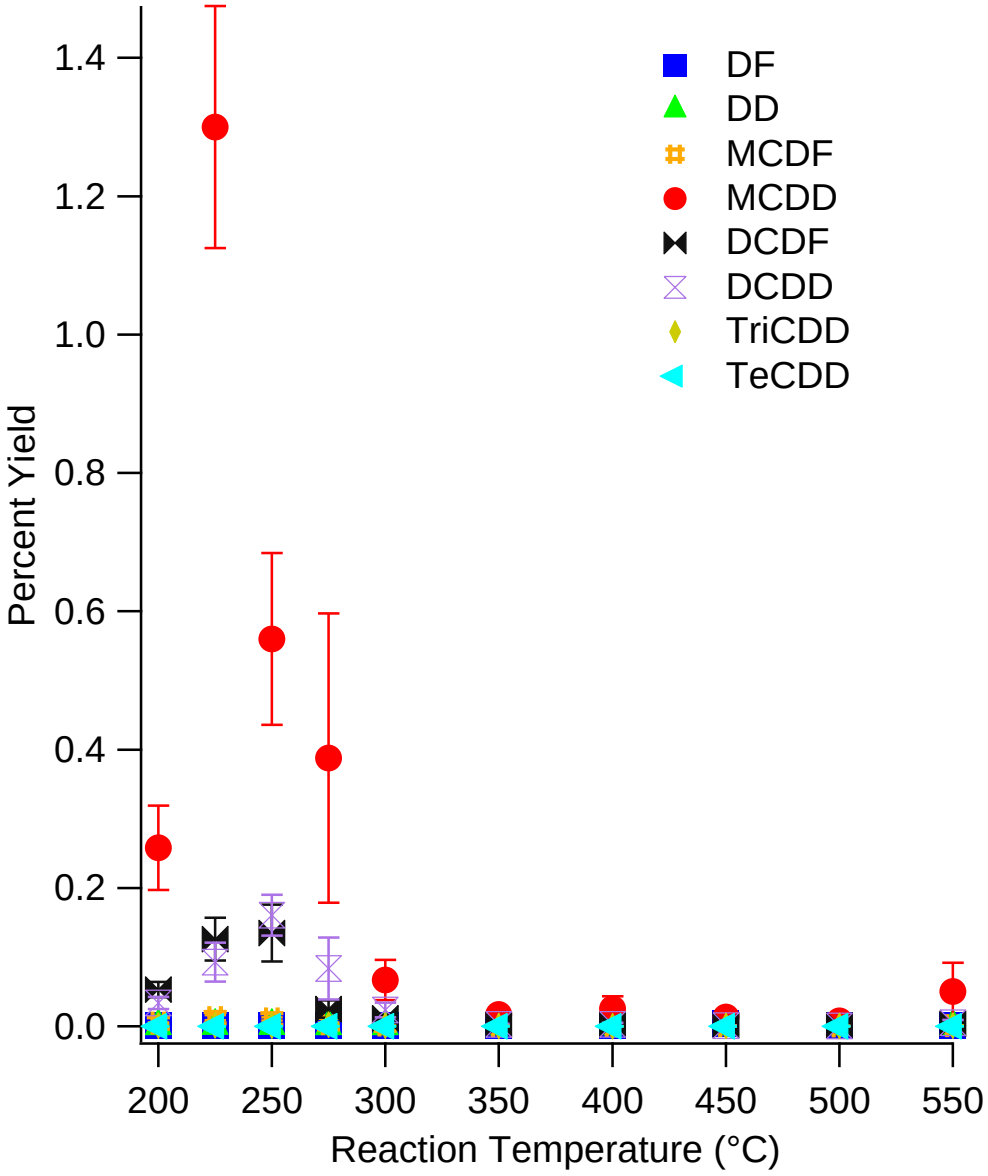

Figure 3.34. Major PCDD/F yields from the pyrolysis of 2-MCP over a 1% Fe_2O_3 + 4% CuO / silica surrogate.

Table 3.12. Dioxin and nondioxin products from the pyrolysis of 2-MCP over a 1% Fe_2O_3 + 4% CuO / silica surrogate.

	Reaction Temperature (^{0}C)						
	200	225	250	275	300	350	400
CBz	0.0022	0.0046	0.0018	0.0071	0.011	0.0072	0.0079
2-MCP	4	4.9	2	0.25	0.052	0.052	0.011
DCBz	0.000036	0.00043	0.00011	0.00074	0.00069	0.00023	0.0002
DCP	0.018	0.032	0.016	0.0089	0.0013	0.0037	0.00055
TriCBz	bdl	bdl	0.000067	bdl	0.00025	0.00015	9.6E-05
TetraCBz	bdl	0.00018	0.00019	bdl	0.00026	0.00026	0.0002
TriCP	bdl	bdl	bdl	bdl	0.0016	0.0054	0.001
PentaCBz	bdl	bdl	0.00027	bdl	0.0003	0.00034	0.00027
HexaCBz	bdl	bdl	bdl	bdl	bdl	0.00011	bdl
DF	0.00027	0.00046	0.00058	0.00043	0.0003	0.0003	0.00057
DD	1.50E-04	5.60E-04	5.40E-04	1.70E-04	5.90E-05	1.60E-05	3.50E-05
MCDF	0.0047	0.013	0.01	0.0038	0.0019	0.00062	0.00095
MCDD	0.26	1.3	0.56	0.39	0.067	0.017	0.025
DCDF	0.053	0.13	0.13	0.025	0.011	0.002	0.0021
DCDD	0.034	0.093	0.16	0.084	0.023	0.0026	0.0029
TriCDD	0.00085	0.0013	0.00089	0.0022	0.00086	0.00029	bdl
bdl - Below Detection Limit							

3.6.2 Oxidative Conditions

The product yields from the surface-mediated oxidation of 2-MCP over a 1% Fe_2O_3 + 4% CuO / silica surrogate are presented in Figures 3.35-3.37 as a function of temperature. The catalyst was extremely active in the decomposition of the precursor under oxidative conditions and displayed >99.9% conversion across the entire temperature range.

The yields of chlorinated benzenes can be seen in Figure 3.35. Lower chlorinated benzenes had higher concentrations at lower temperatures with MCBz and DCBz reaching maximum yields of 0.005% at 275^{0}C and 0.001% at 250^{0}C, respectively. From 350-450^{0}C, higher chlorinated benzenes were the most prevalent. All chlorinated benzenes showed decreasing yields at temperatures above 500^{0}C.

The yields of chlorinated phenols can be seen in Figure 3.36. DCP and TriCP exhibited high yields with maximums of 0.05% and 0.07%, respectively, at 250ºC. Chlorophenols were produced in much higher concentrations than chlorobenzenes.

The yields of PCDD/Fs can be seen in Figure 3.37. Under oxidative conditions, the 1% Fe_2O_3 + 4% CuO / silica surrogate yielded low concentrations of PCDD/Fs. MCDD and DCDD were the most prevalent congeners with maximum yields of 0.04% at 275^{0}C and 0.03% at 250^{0}C, respectively. TriCDD and DCDF also showed significant increase with temperature and held maximums of 0.007% and 0.004%, respectively, at 250^{0}C. Table 3.13 gives the yields of all chlorinated benzenes, phenols, and dioxin products.

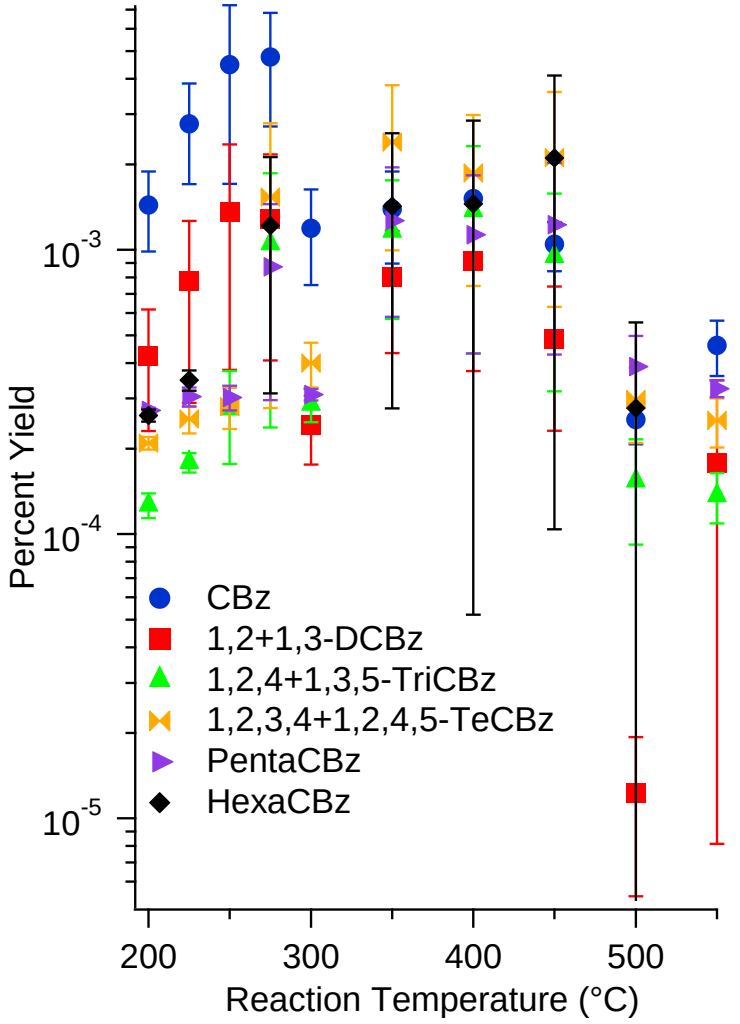

Figure 3.35. Chlorinated benzene yields from the oxidation of 2-MCP over a 1% Fe_2O_3 + 4% CuO / silica surrogate.

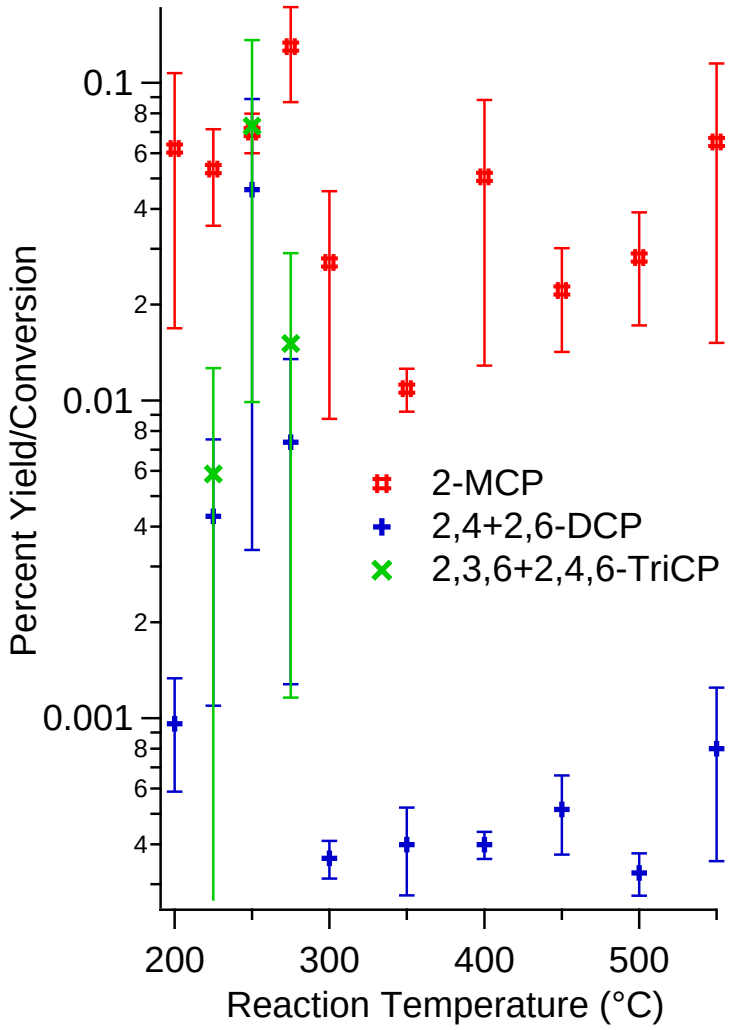

Figure 3.36. Chlorinated phenol yields and precursor conversion from the oxidation of 2-MCP over a 1% Fe_2O_3 + 4% CuO / silica surrogate.

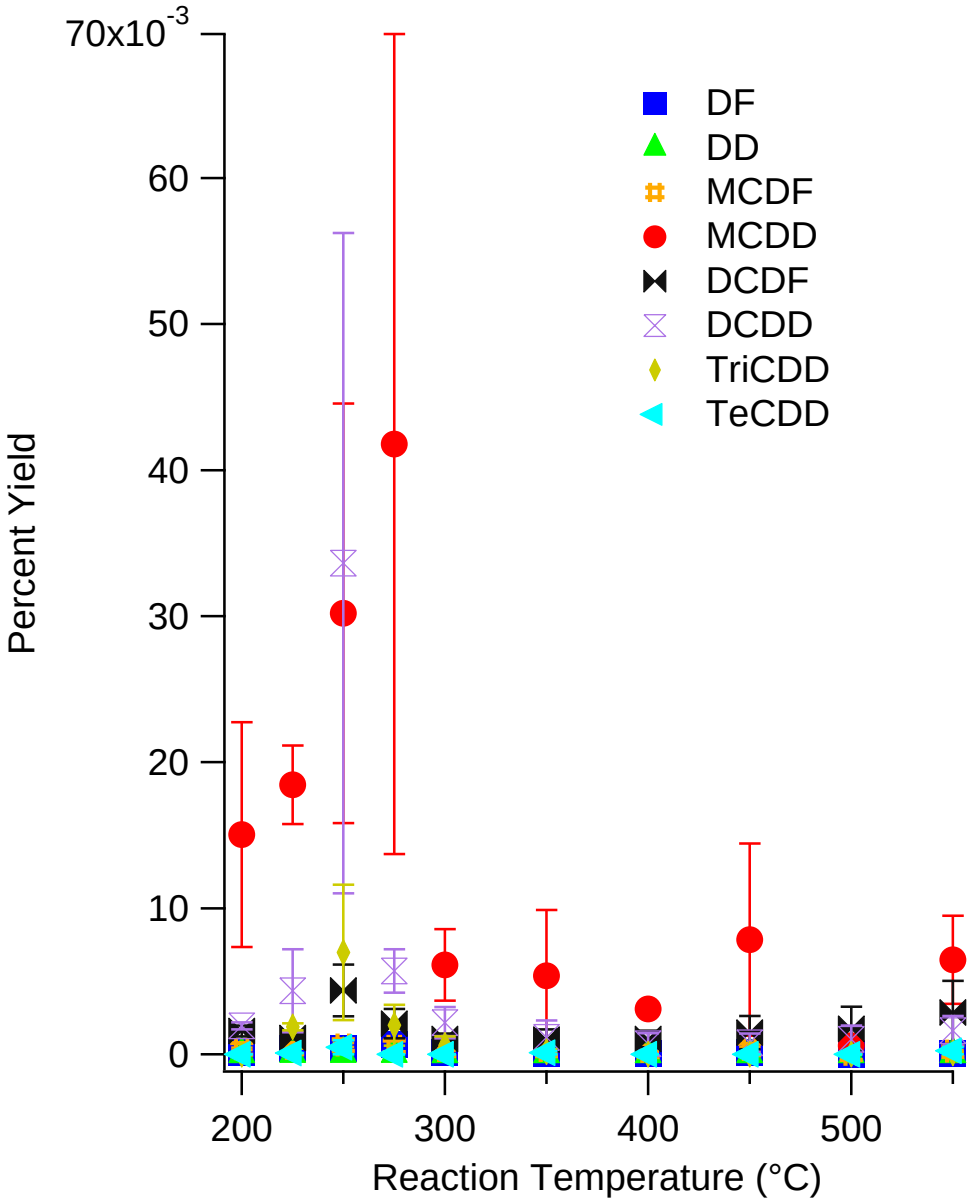

Figure 3.37. Major PCDD/F yields from the oxidation of 2-MCP over 1% Fe_2O_3 + 4% CuO / silica surrogate.

Table 3.13. Dioxin and nondioxin products from the oxidation of 2-MCP over a 1% Fe_2O_3 + 4% CuO / silica surrogate.

	Reaction Temperature (^{0}C)						
	200	225	250	275	300	350	400
CBz	0.0014	0.0028	0.0045	0.0048	0.0012	0.0014	0.0015
2-MCP	0.062	0.053	0.07	0.13	0.027	0.011	0.051
DCBz	0.00042	0.00078	0.0014	0.0013	0.00024	0.0008	0.00091
DCP	0.00096	0.0043	0.046	0.0074	0.00036	0.0004	0.0004
TriCBz	0.00013	0.00018	0.00028	0.0011	0.00029	0.0012	0.0014
TetraCBz	0.00021	0.00025	0.00028	0.0015	0.0004	0.0024	0.0019
TriCP	bdl	0.0059	0.073	0.015	bdl	bdl	bdl
PentaCBz	0.00027	0.0003	0.0003	0.00087	0.00031	0.0013	0.0011
HexaCBz	0.00026	0.00035	bdl	0.0012	bdl	0.0014	0.0015
DF	0.00012	0.0004	0.00037	0.00065	0.00011	6.6E-05	8.7E-05
DD	3.50E-06	1.10E-05	1.50E-05	2.00E-05	3.60E-06	2.50E-06	1.60E-06
MCDF	0.00037	0.00038	0.00063	0.00055	0.00026	0.00026	0.00019
MCDD	0.015	0.018	0.03	0.042	0.0061	0.0054	0.0031
DCDF	0.0016	0.0011	0.0044	0.0021	0.0011	0.001	0.001
DCDD	0.0019	0.0043	0.034	0.0057	0.0022	0.0012	0.00073
TriCDD	bdl	0.0019	0.007	0.002	0.00061	0.00017	bdl
TetraCDD	bdl	9.00E-05	4.80E-04	bdl	bdl	1.20E-04	bdl
bdl - Below Detection Limit							

3.7 Thermal Degradation of 2-Monochlorophenol over a 2.5% Fe_2O_3 + 2.5% CuO / silica Surrogate

3.7.1 Pyrolytic Conditions

The product yields from the surface-mediated pyrolysis of 2-MCP over a 2.5% Fe_2O_3 + 2.5% CuO / silica surrogate are presented in Figures 3.38-3.40 as a function of temperature. The surrogate was fairly active in the destruction of 2-MCP precursor under pyrolytic conditions. Conversion of 2-MCP was 96% at 200ºC and increased to >99.0% at 300ºC.

The yields of chlorinated benzenes can be seen in Figure 3.38. While MCBz was the most prevalent with a maximum of 0.07% at 400^0C, higher chlorinated species also exhibited high yields, such as TeCBz (0.002% at 400^0C), PentaCBz (0.001% at 300^0C), and HexaCBz (0.003% at 300^0C).

The yields of chlorinated phenols can be seen in Figure 3.39. DCP was obtained with a yield of 0.06% at 200ºC and exhibited a downward trend in yield with increasing temperature. TriCP reached a maximum yield of 0.09% at 300^0C and also exhibited a general decrease in yield with increasing temperature.

The yields of PCDD/Fs can be seen in Figure 3.40. MCDD was the most prevalent congener with a maximum yield of 4.4% at 300^0C. DCDF and DCDD were also obtained in significant yields with maximums of 0.8% and 0.6%, respectively, at 300ºC. Table 3.14 gives the yields of all chlorinated benzenes, phenols, and dioxin products.

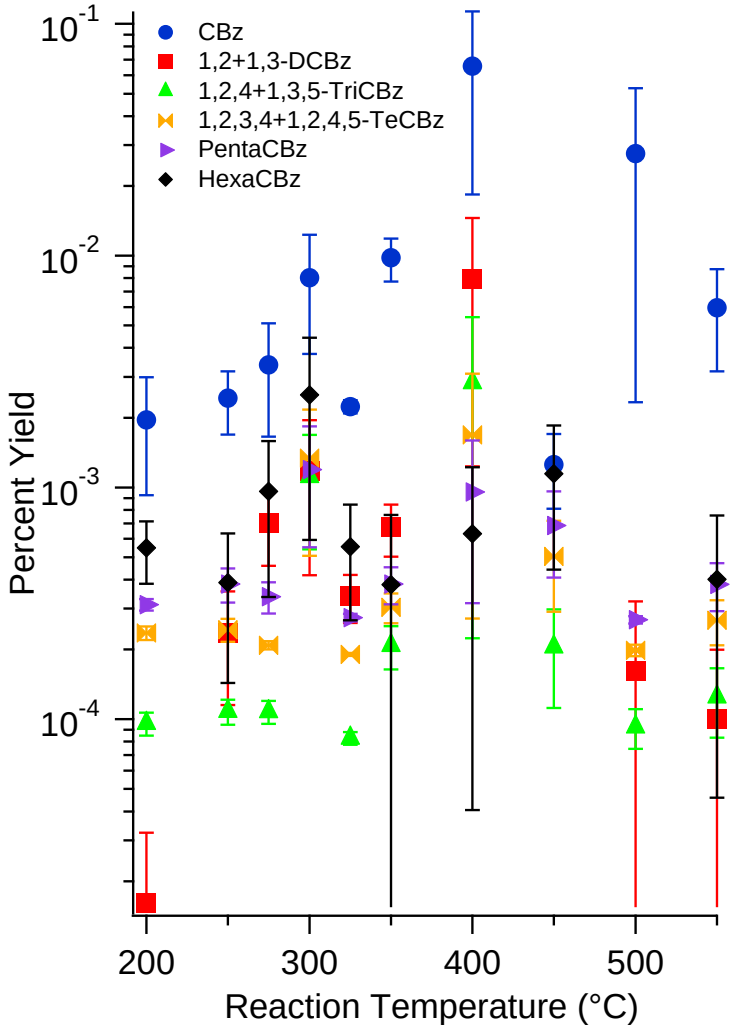

Figure 3.38. Chlorinated benzene yields from the pyrolysis of 2-MCP over a 2.5% Fe_2O_3 + 2.5% CuO / silica surrogate.

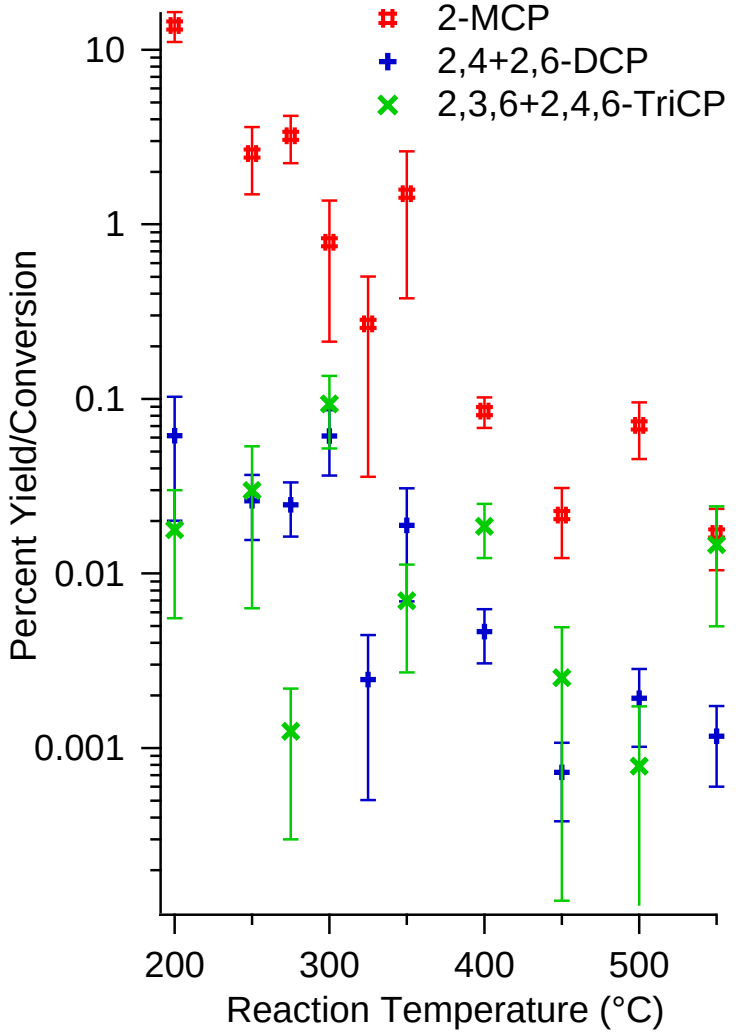

Figure 3.39. Chlorinated phenol yields and precursor conversion from the pyrolysis of 2-MCP over a 2.5% Fe_2O_3 + 2.5% CuO / silica surrogate.

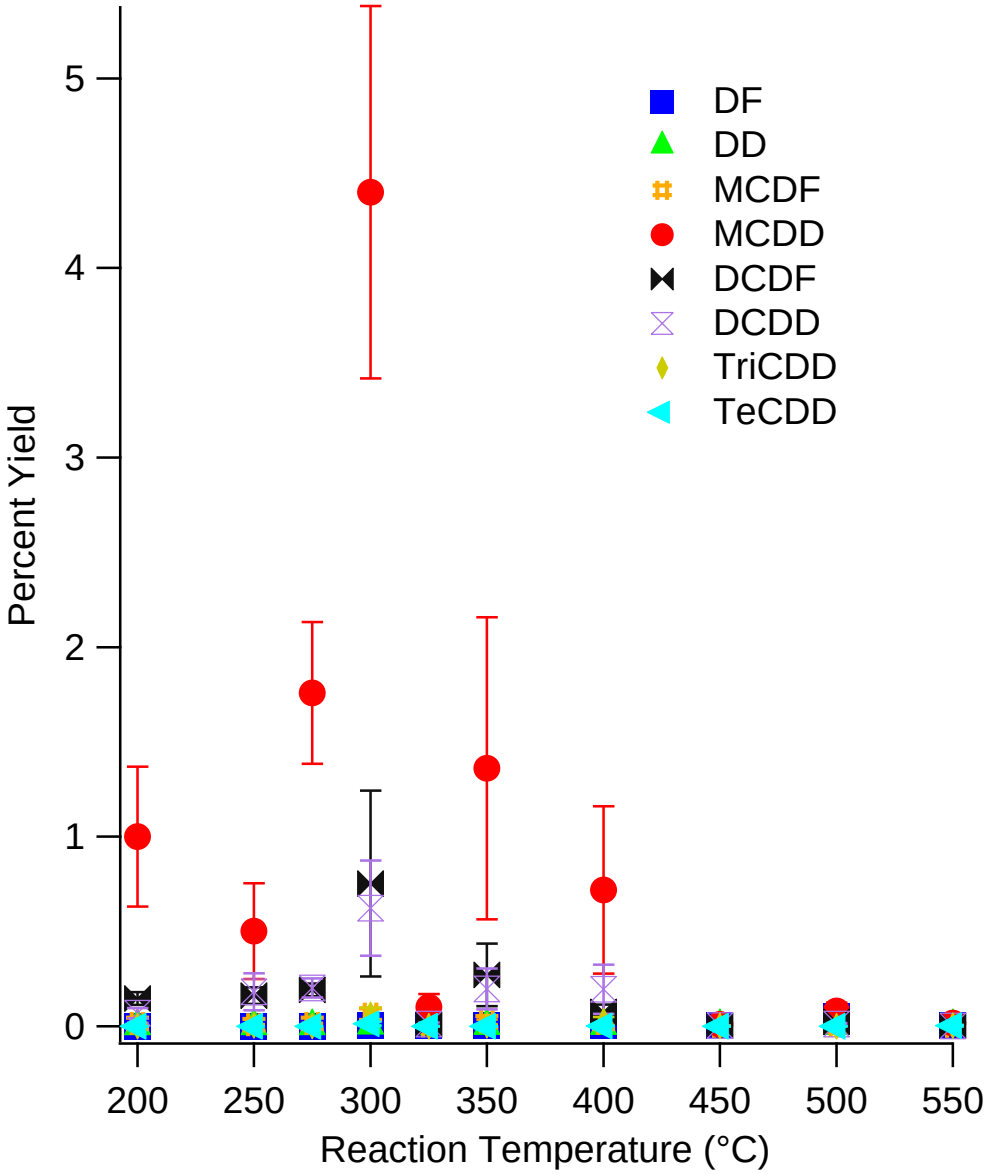

Figure 3.40. Major PCDD/F yields from the pyrolysis of 2-MCP over a 2.5% Fe_2O_3 + 2.5% CuO / silica surrogate.

Table 3.14. Dioxin and nondioxin products from the pyrolysis of 2-MCP over a 2.5% Fe_2O_3 + 2.5% CuO / silica surrogate.

	Reaction Temperature (^{0}C)						
	200	250	275	300	325	350	400
CBz	0.002	0.0024	0.0034	0.008	0.0022	0.0098	0.066
2-MCP	14	2.5	3.2	0.79	0.27	1.5	0.085
DCBz	0.000016	0.00024	0.0007	0.0012	0.00034	0.00067	0.0079
DCP	0.062	0.026	0.025	0.061	0.0025	0.019	0.0046
TriCBz	0.000096	0.00011	0.00011	0.0011	8.3E-05	0.00021	0.0028
TetraCBz	0.00024	0.00024	0.00021	0.0013	0.00019	0.0003	0.0017
TriCP	0.018	0.03	0.0012	0.094	bdl	0.007	0.019
PentaCBz	0.00031	0.00038	0.00034	0.0012	0.00027	0.00038	0.00096
HexaCBz	0.00055	0.00039	0.00096	0.0025	0.00056	0.00038	0.00063
DF	0.00046	0.0006	0.00064	0.0055	0.0014	0.0017	0.0047
DD	4.40E-04	3.20E-04	7.50E-04	3.20E-03	1.10E-04	2.00E-03	8.70E-04
MCDF	0.015	0.0082	0.015	0.063	0.0021	0.023	0.015
MCDD	1	0.5	1.8	4.4	0.1	1.4	0.72
DCDF	0.15	0.16	0.19	0.75	0.0076	0.27	0.075
DCDD	0.069	0.18	0.2	0.62	0.012	0.2	0.2
TriCDD	0.00046	0.0048	0.0016	0.06	bdl	0.0052	0.027
TetraCDD	bdl	2.40E-04	bdl	1.40E-02	bdl	7.20E-05	2.30E-03
bdl - Below Detection Limit							

3.7.2 Oxidative Conditions

The product yields from the surface-mediated oxidation of 2-MCP over a 2.5% Fe_2O_3 + 2.5% CuO / silica surrogate are presented in Figures 3.41-3.43 as a function of temperature. Similar to the 1% Fe_2O_3 + 4% CuO / silica surrogate, this catalyst was extremely active in the decomposition of 2-MCP precursor with a conversion of >99.5% across the entire studied temperature region.

The yields of chlorinated benzenes can be seen in Figure 3.41. All chlorinated benzenes were obtained across the entire temperature range, but higher chlorinated benzenes were found in greater yields. TeCBz, PentaCBz, and HexaCBz were obtained with maximums of 0.01% at 400^{0}C, 0.006% at 400^{0}C, and 0.01% at 500^{0}C, respectively.

The yields of chlorinated phenols can be seen in Figure 3.42. Chlorophenols exhibited higher yields than benzenes at lower temperatures with TriCP reaching a maximum of 0.05% at 250^{0}C and decreased at higher temperatures. The yield of DCP decreased sharply across the entire temperature range.

The yields of PCDD/Fs can be seen in Figure 3.43. Under oxidative conditions, the 2.5% Fe_2O_3 + 2.5% CuO / silica surrogate showed similar yields of PCDD/Fs to the 1% Fe_2O_3 + 4% CuO / silica surrogate. Most congeners held maximum yields at 250^{0}C. Higher chlorinated species, like DCDD, DCDF, TriCDD, and TeCDD were more prevalent than usual. Table 3.15 gives the yields of all chlorinated benzenes, phenols, and dioxin products.

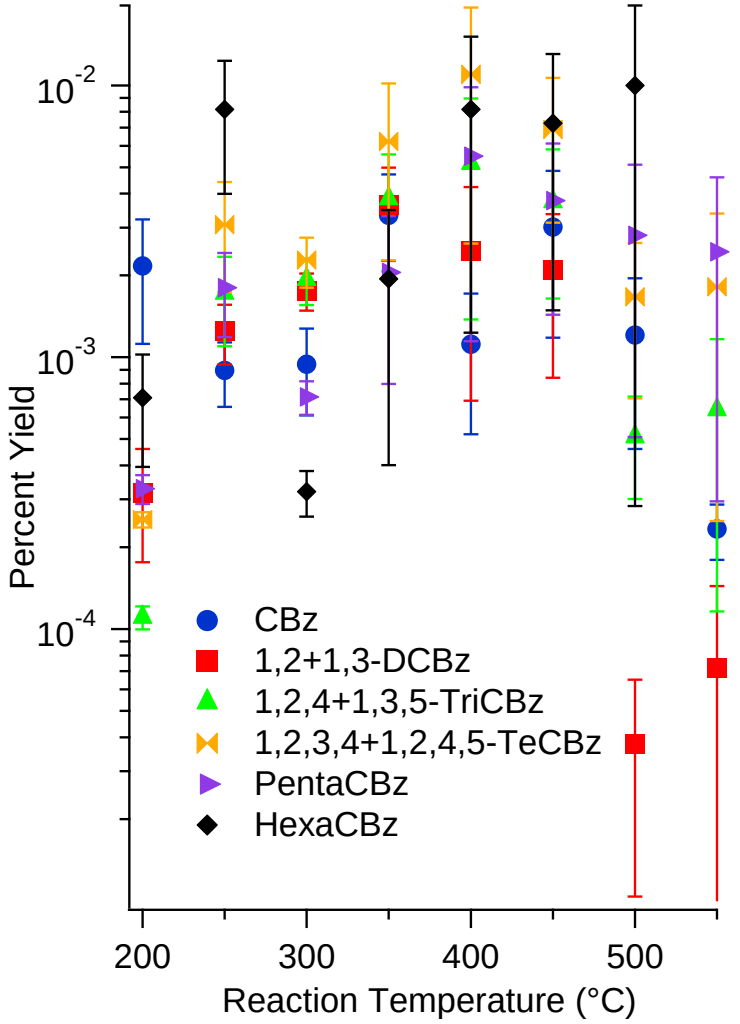

Figure 3.41. Chlorinated benzene yields from the oxidation of 2-MCP over a 2.5% Fe_2O_3 + 2.5% CuO / silica surrogate.

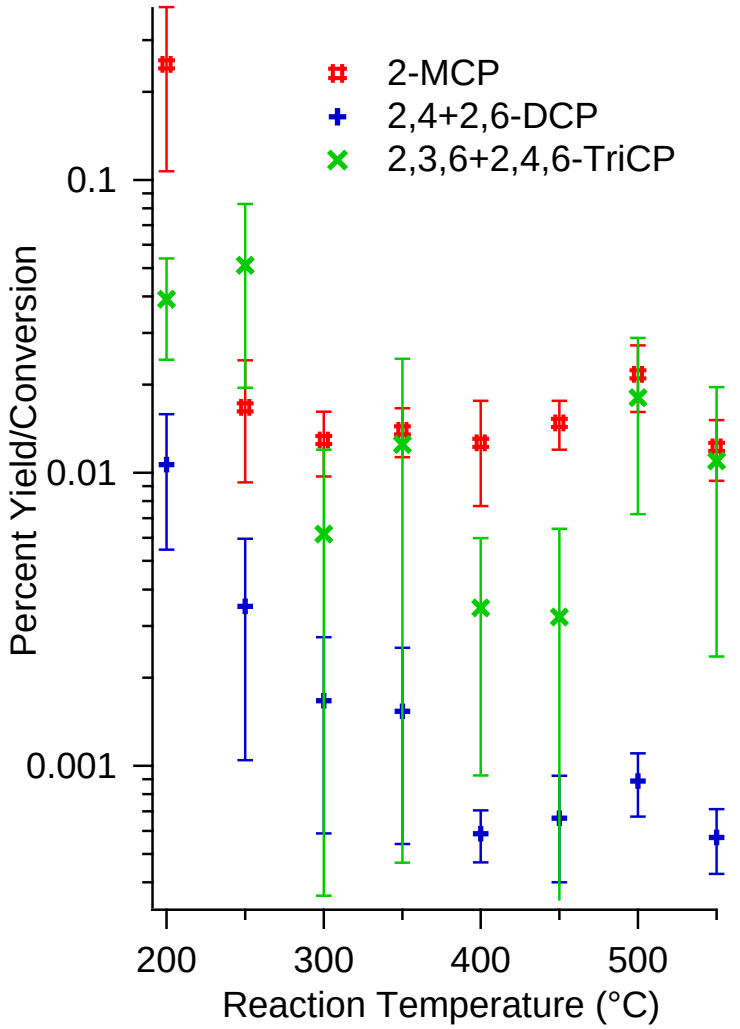

Figure 3.42. Chlorinated phenol yields and precursor conversion from the oxidation of 2-MCP over a 2.5% Fe_2O_3 + 2.5% CuO / silica surrogate.

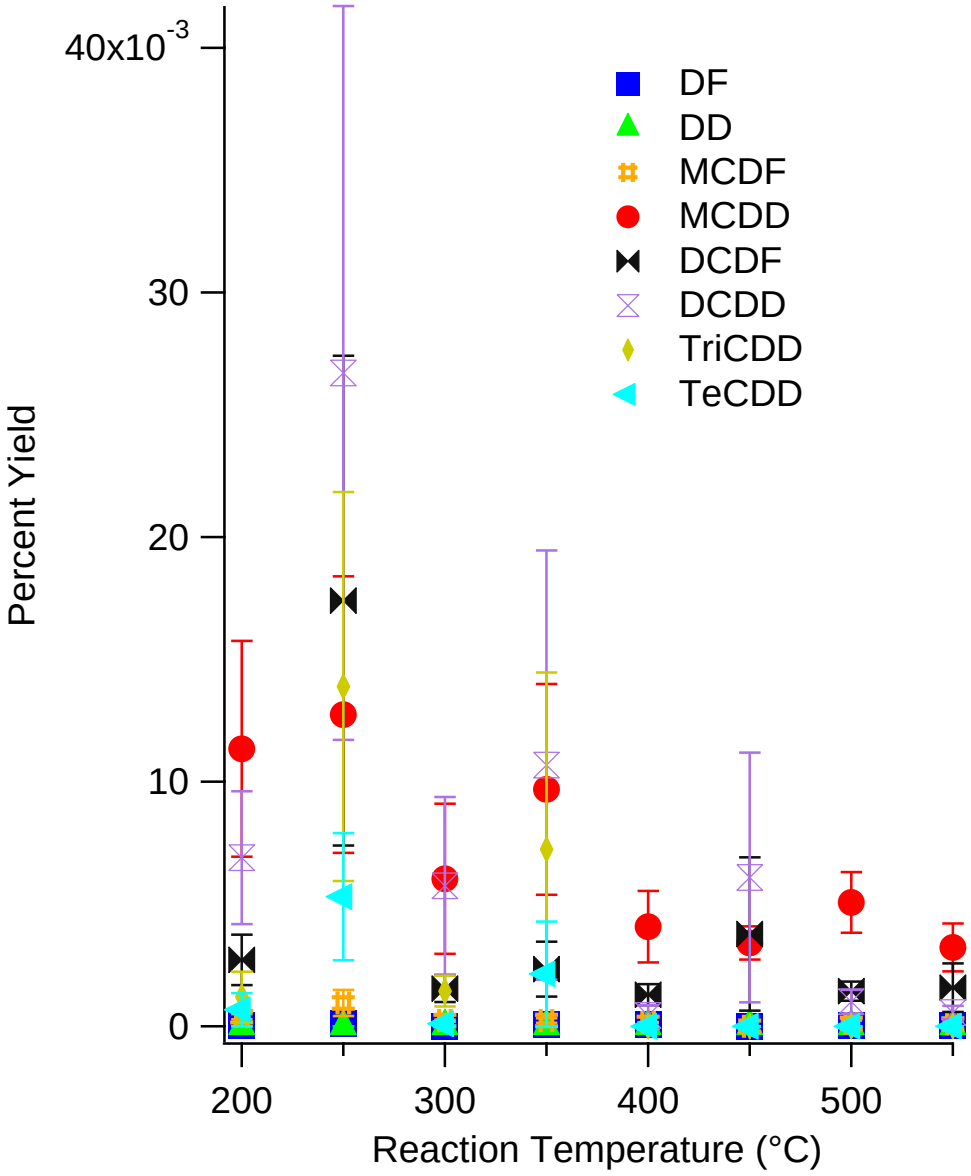

Figure 3.43. Major PCDD/F yields from the oxidation of 2-MCP over a 2.5% Fe_2O_3 + 2.5% CuO / silica surrogate.

Table 3.15. Dioxin and nondioxin products from the oxidation of 2-MCP over a 2.5% Fe_2O_3 + 2.5% CuO / silica surrogate.

	Reaction Temperature (^{0}C)						
	200	250	300	350	400	450	500
CBz	0.0022	0.0009	0.00094	0.0033	0.0011	0.003	0.0012
2-MCP	0.25	0.017	0.013	0.014	0.013	0.015	0.022
DCBz	0.00032	0.0012	0.0018	0.0036	0.0025	0.0021	3.8E-05
DCP	0.011	0.0035	0.0017	0.0015	0.00059	0.00066	0.00089
TriCBz	0.00011	0.0017	0.0019	0.0038	0.0052	0.0037	0.00051
TetraCBz	0.00025	0.0031	0.0023	0.0062	0.011	0.0069	0.0017
TriCP	0.039	0.051	0.0062	0.013	0.0035	0.0032	0.018
PentaCBz	0.00033	0.0018	0.00072	0.0021	0.0055	0.0038	0.0028
HexaCBz	0.00071	0.0082	0.00032	0.0019	0.0082	0.0073	0.01
DF	0.000041	0.00013	4.6E-06	9.7E-05	7.7E-05	bdl	3.6E-05
DD	2.40E-06	3.30E-06	2.00E-06	2.30E-06	1.90E-06	1.70E-06	2.30E-06
MCDF	0.00039	0.00095	0.00023	0.00026	0.00016	bdl	0.00012
MCDD	0.011	0.013	0.006	0.0071	0.0041	0.0034	0.0051
DCDF	0.0027	0.017	0.0015	0.0017	0.0013	0.0038	0.0014
DCDD	0.0069	0.027	0.0057	0.012	0.00045	0.0061	0.001
TriCDD	0.0012	0.014	0.0014	0.0096	bdl	bdl	bdl
TetraCDD	6.80E-04	5.30E-03	1.00E-04	2.90E-03	bdl	bdl	bdl
bdl - Below Detection Limit							

3.8 Thermal Degradation of 2-Monochlorophenol over a 4% Fe_2O_3 + 1% CuO / silica Surrogate

3.8.1 Pyrolytic Conditions

The product yields from the surface-mediated pyrolysis of 2-MCP over a 4% Fe_2O_3 + 1% CuO / silica surrogate are presented in Figures 3.44-3.46 as a function of temperature. The surrogate was fairly active in the destruction of 2-MCP precursor under pyrolytic conditions. Thermal degradation of 2-MCP was 90% at 200 ºC and increased to >99.9% at 450ºC.

The yields of chlorinated benzenes can be seen in Figure 3.44. The two most prevalent chlorinated benzenes were MCBz and HexaCBz, which exhibited slight increases in yields with increasing temperature and reached maximums of 0.07% and 0.2%, respectively, at 550^0C.

The yields of chlorinated phenols can be seen in Figure 3.45. DCP and TriCP were formed in extremely high concentrations at lower temperatures. DCP and TriCP reached maximums of 0.3% and 2.1%, respectively, at 250^0C.

The yields of PCDD/Fs can be seen in Figure 3.46. The 4% Fe_2O_3 + 1% CuO / silica surrogate was extremely active in the formation of PCDD/Fs from 250-300^0C. The most prevalent congeners were MCDD, DCDD, and DCDF with maximums yields of 3.6% at 275^0C, 0.5% at 300^0C, and 0.5% at 250^0C, respectively. Table 3.16 gives the yields of all chlorinated benzenes, phenols, and dioxin products.

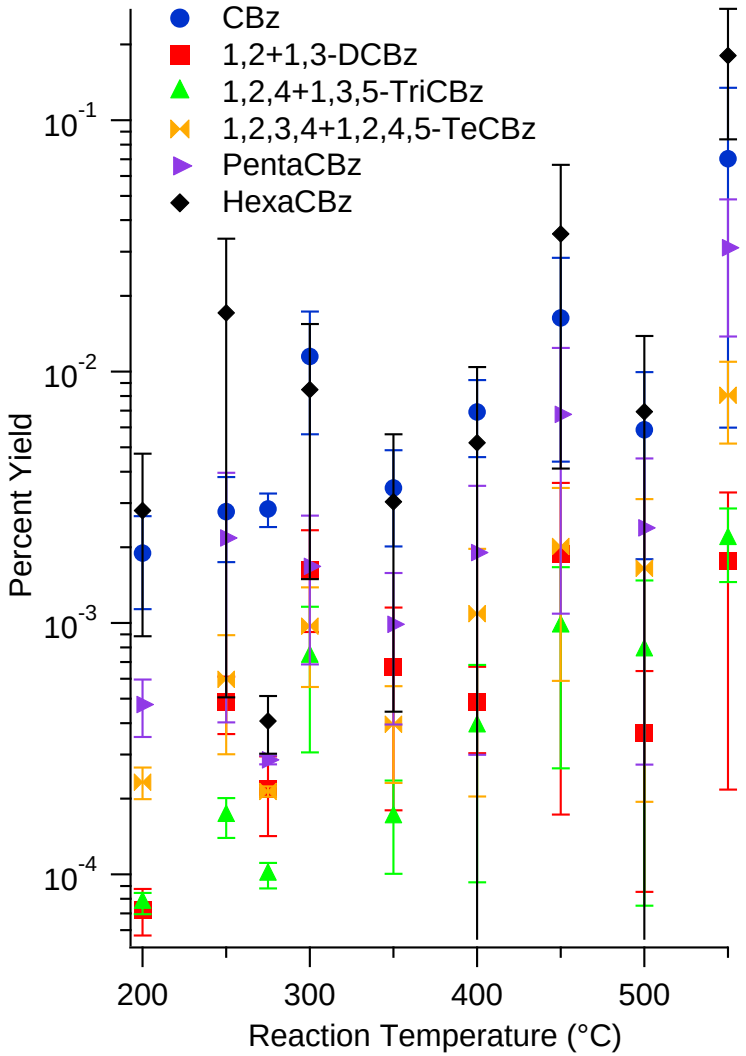

Figure 3.44. Chlorinated benzene yields from the pyrolysis of 2-MCP over a 4% Fe_2O_3 + 1% CuO / silica surrogate.

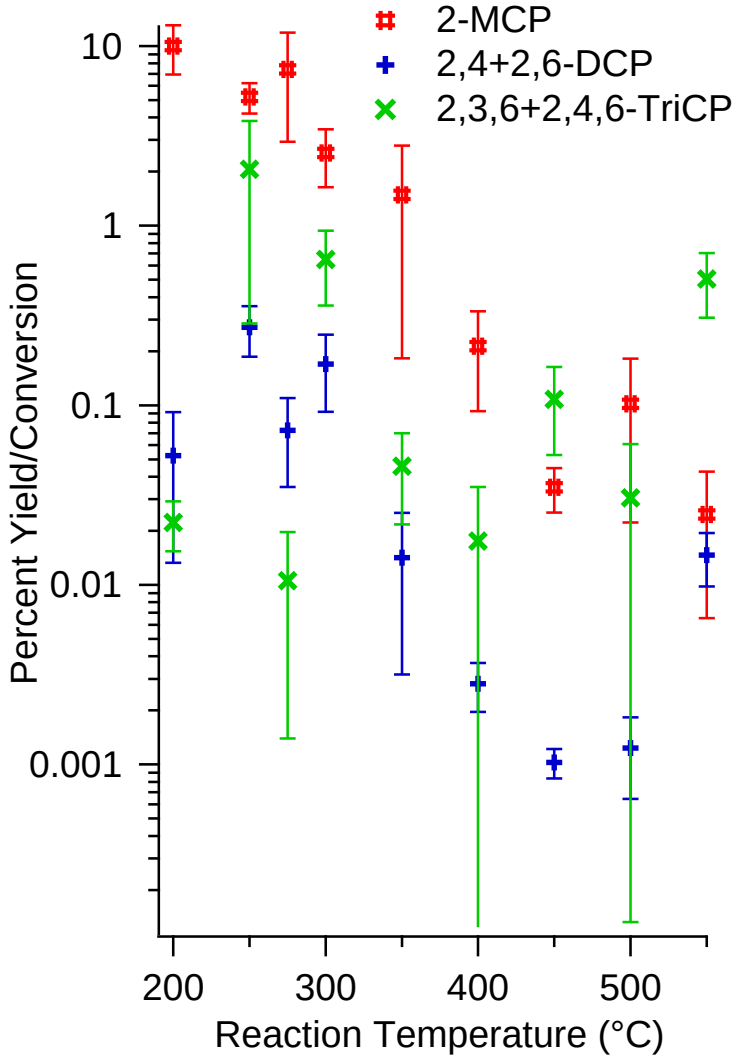

Figure 3.45. Chlorinated phenol yields and precursor conversion from the pyrolysis of 2-MCP over a 4% Fe_2O_3 + 1% CuO / silica surrogate.

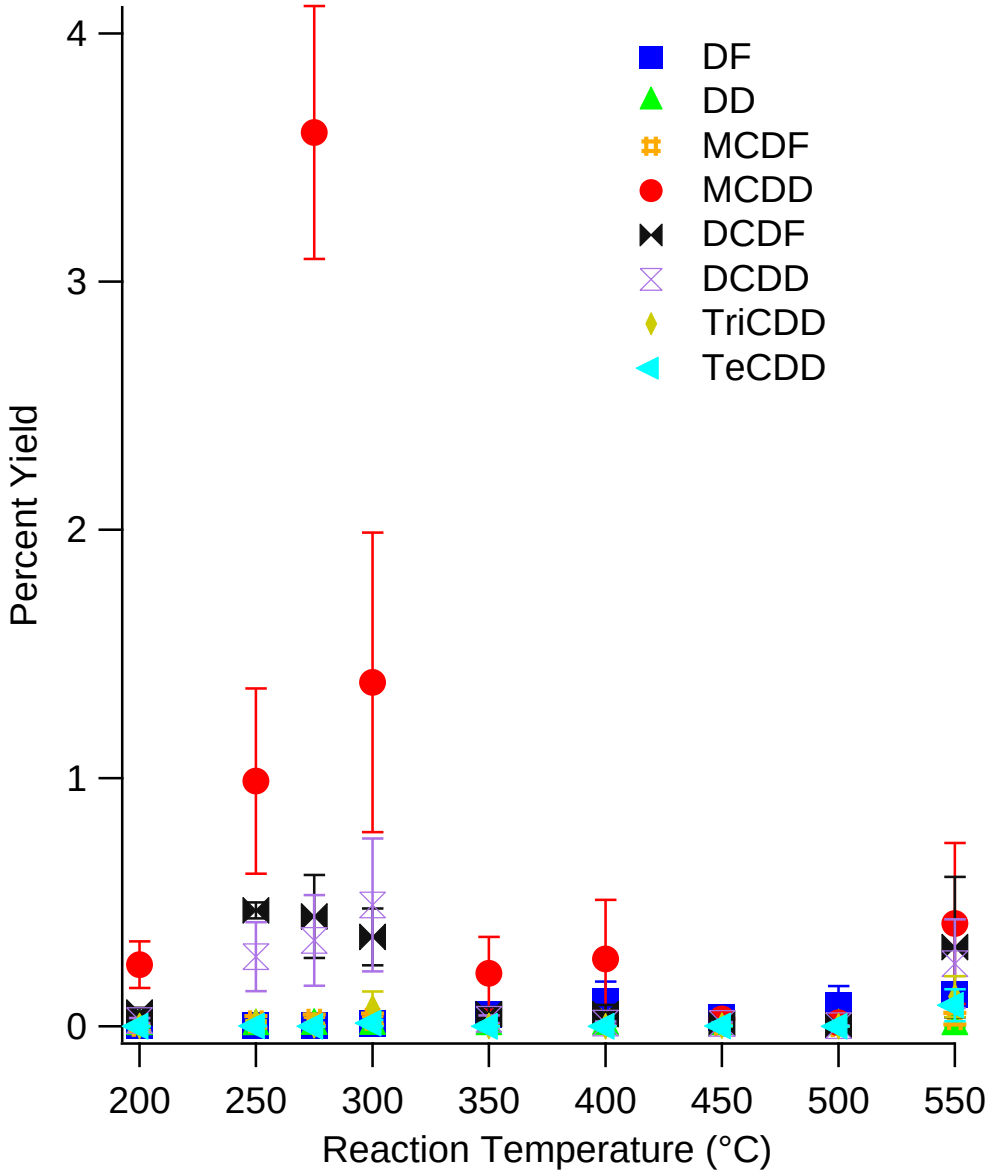

Figure 3.46. Major PCDD/F yields from the pyrolysis of 2-MCP over a 4% Fe_2O_3 + 1% CuO / silica surrogate.

Table 3.16. Dioxin and nondioxin products from the pyrolysis of 2-MCP over a 4% Fe_2O_3 + 1% CuO / silica surrogate.

	Reaction Temperature (^{0}C)						
	200	250	275	300	350	400	450
CBz	0.0019	0.0028	0.0028	0.011	0.0034	0.0069	0.016
2-MCP	10	5.2	7.4	2.5	1.5	0.21	0.035
DCBz	7.20E-05	0.00049	0.00022	0.0016	0.00067	0.00049	0.0019
DCP	0.052	0.27	0.072	0.17	0.014	0.0028	0.001
TriCBz	7.70E-05	0.00017	0.0001	0.00073	0.00017	0.00039	0.00097
TetraCBz	0.00023	0.0006	0.00021	0.00097	0.0004	0.0011	0.002
TriCP	0.022	2.1	0.011	0.65	0.046	0.018	0.11
PentaCBz	0.00047	0.0022	0.00029	0.0017	0.00099	0.0019	0.0068
HexaCBz	0.0028	0.017	0.00041	0.0085	0.003	0.0052	0.035
DF	0.00072	0.00081	0.00079	0.012	0.049	0.099	0.036
DD	9.90E-05	4.90E-04	8.30E-04	1.20E-03	4.60E-04	1.20E-03	2.50E-04
MCDF	0.0043	0.018	0.025	0.028	0.03	0.026	0.006
MCDD	0.25	0.99	3.6	1.4	0.21	0.27	0.03
DCDF	0.055	0.47	0.44	0.36	0.049	0.048	0.012
DCDD	0.023	0.28	0.35	0.49	0.028	0.013	0.011
TriCDD	0.00076	0.017	0.0042	0.075	0.0013	0	0.0029
TetraCDD	1.30E-04	1.70E-03	0	1.30E-02	0	0	6.70E-04
bdl - Below Detection Limit							

3.8.2 Oxidative Conditions

The product yields from the surface-mediated oxidation of 2-MCP over a 4% Fe_2O_3 + 1% CuO / silica surrogate are presented in Figures 3.47-3.49 as a function of temperature. This catalyst was similar to the other bimetallic catalysts and was extremely active in the degradation of 2-MCP precursor. Conversion of 2-MCP was >99.5% over the entire temperature range.

The yields of chlorinated benzenes can be seen in Figure 3.47. Total chlorinated benzene yield peaked between 350-400^{0}C with higher chlorinated species like TeCBz, PentaCBz, and HexaCBz reaching yields of 0.01% at 350^{0}C, 0.006% at 400^{0}C, and 0.01% at 400^{0}C, respectively.

The yields of chlorinated phenols can be seen in Figure 3.48. Chlorophenols were produced in higher concentrations than chlorobenzenes. TriCP had a maximum yield of 0.22% at 250^{0}C and exhibited a general decrease in yield with increasing temperature.

The yields of PCDD/Fs can be seen in Figure 3.49. Under oxidative conditions, the 4% Fe_2O_3 + 1% CuO / silica surrogate showed higher PCDD/F yields than the other bimetallic surrogates. DCDD, MCDD, and TriCDD were the most prevalent congeners with maximum yields of 0.2%, 0.1%, and 0.08%, respectively, at 250^{0}C. Table 3.17 gives the yields of all chlorinated benzenes, phenols, and dioxin products.

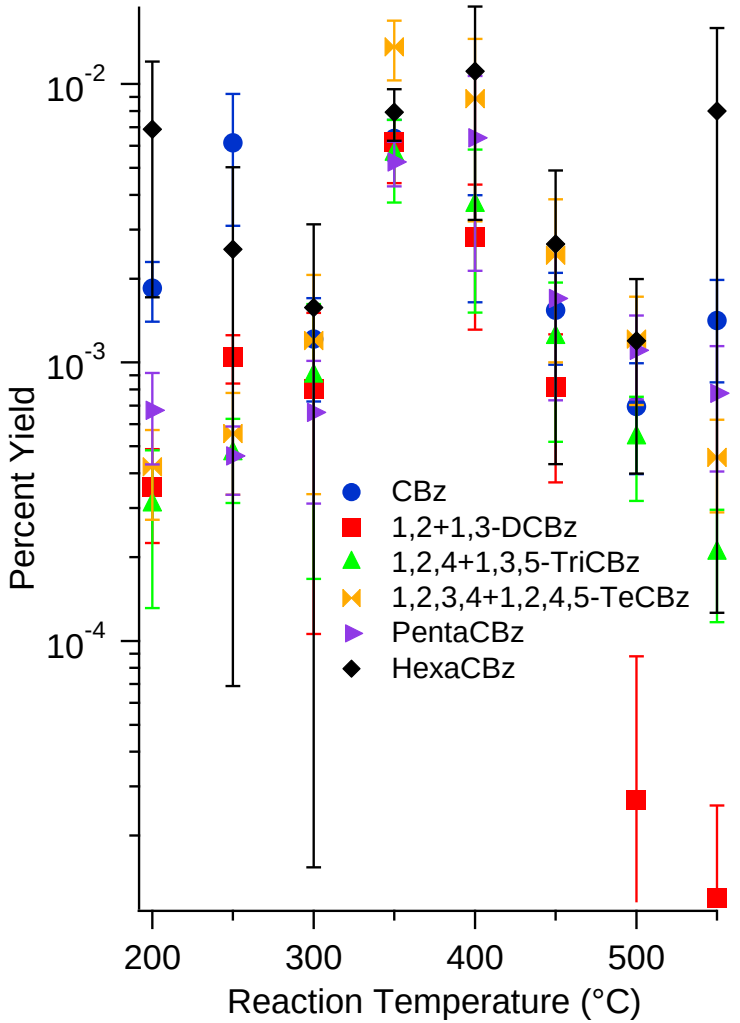

Figure 3.47. Chlorinated benzene yields from the oxidation of 2-MCP over a 4% Fe_2O_3 + 1% CuO / silica surrogate.

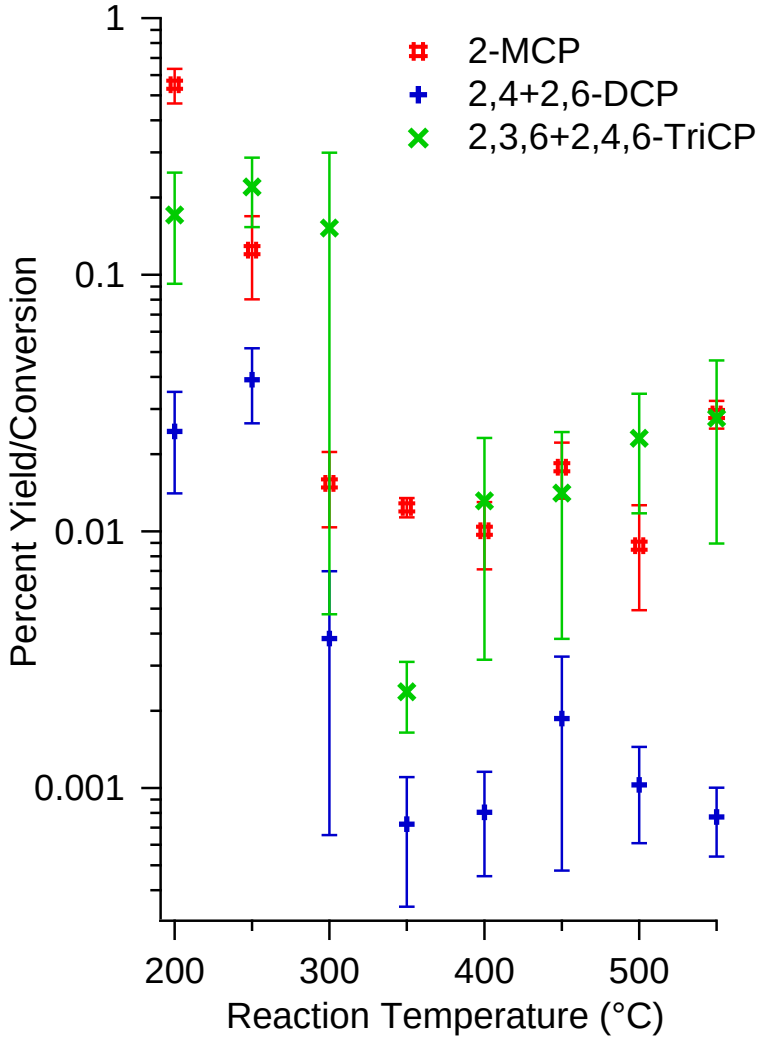

Figure 3.48. Chlorinated phenol yields and precursor conversion from the oxidation of 2-MCP over a 4% Fe_2O_3 + 1% CuO / silica surrogate.

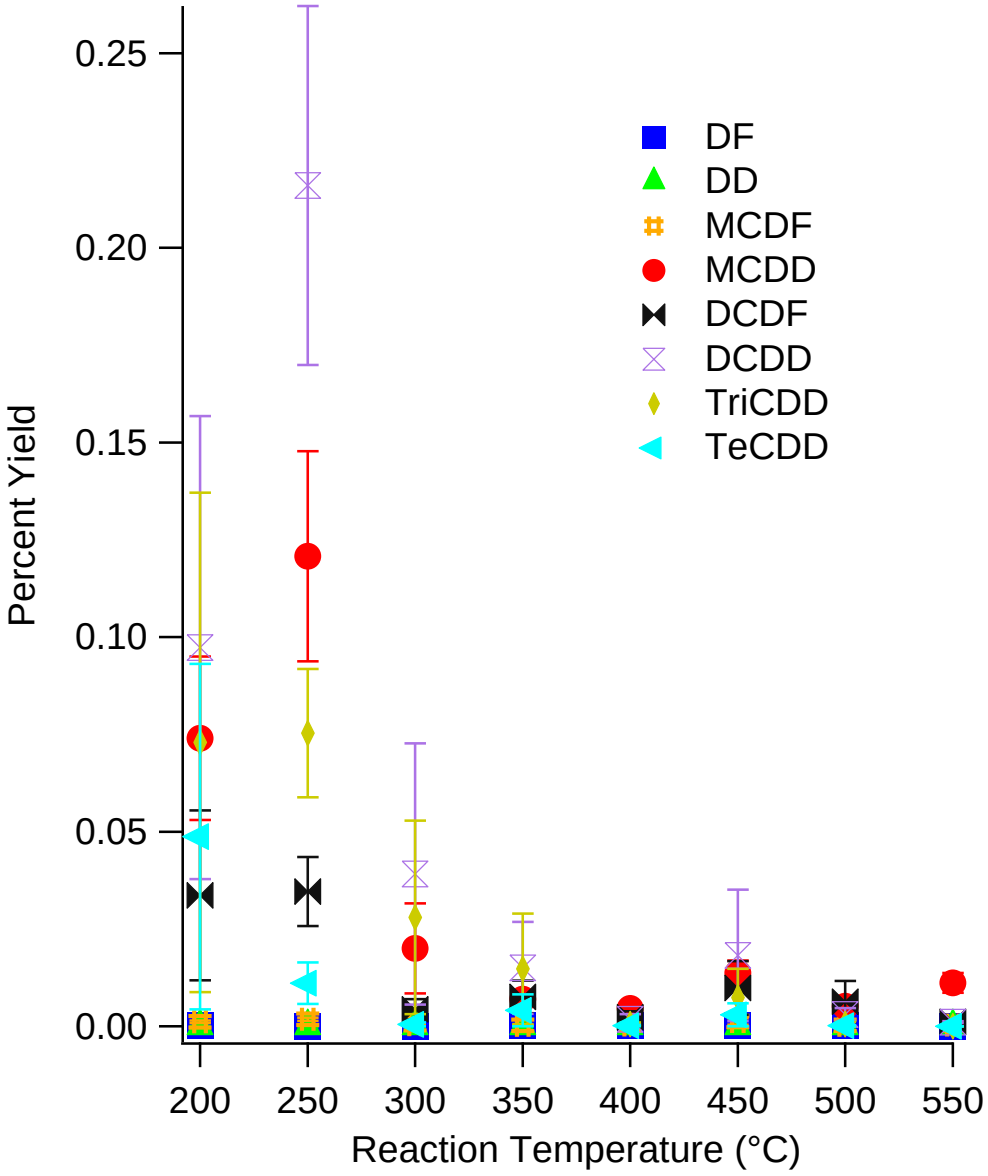

Figure 3.49. PCDD/F yields from the oxidation of 2-MCP over a 4% Fe_2O_3 + 1% CuO / silica surrogate.

Table 3.17. Dioxin and nondioxin products from the oxidation of 2-MCP over a 4% Fe_2O_3 + 1% CuO / silica surrogate.

	Reaction Temperature (^{0}C)						
	200	250	300	350	400	450	500
CBz	0.0018	0.0062	0.0012	0.0064	0.0028	0.0015	0.0007
2-MCP	0.55	0.12	0.015	0.012	0.01	0.018	0.0088
DCBz	0.00036	0.001	0.00081	0.0062	0.0028	0.00082	2.7E-05
DCP	0.025	0.039	0.0038	0.00072	0.0008	0.0019	0.001
TriCBz	0.00031	0.00047	0.00089	0.0056	0.0037	0.0012	0.00054
TetraCBz	0.00042	0.00056	0.0012	0.014	0.0089	0.0024	0.0012
TriCP	0.17	0.22	0.15	0.0024	0.013	0.014	0.023
PentaCBz	0.00067	0.00046	0.00066	0.0052	0.0064	0.0017	0.0011
HexaCBz	0.0069	0.0026	0.0016	0.0079	0.011	0.0027	0.0012
DF	0.000094	0.000034	0.000027	5.6E-05	0.00034	7.1E-05	0.00013
DD	5.90E-06	1.10E-05	3.50E-06	2.30E-06	2.10E-06	5.30E-06	2.30E-06
MCDF	0.0012	0.0018	0.00038	0.00023	0.0003	0.0012	0.00027
MCDD	0.074	0.12	0.02	0.007	0.0046	0.014	0.0052
DCDF	0.034	0.035	0.0044	0.0075	0.0023	0.0098	0.0063
DCDD	0.097	0.22	0.039	0.015	0.0018	0.018	0.0031
TriCDD	0.073	0.075	0.028	0.015	0.00055	0.0074	0.00054
TetraCDD	4.90E-02	1.10E-02	4.70E-04	4.10E-03	1.90E-04	3.00E-03	1.90E-04
bdl - Below Detection Limit							

3.9. References

1. Johnson, A.; Catalan, L. J. J.; Kinrade, S. D., Characterization and evaluation of fly-ash from co-combustion of lignite and wood pellets for use as cement admixture. *Fuel* **2010,** *89*, (10), 3042-3050.

2. Koukouzas, N.; Hämäläinen, J.; Papanikolaou, D.; Tourunen, A.; Jäntti, T., Mineralogical and elemental composition of fly ash from pilot scale fluidised bed combustion of lignite, bituminous coal, wood chips and their blends. *Fuel* **2007,** *86*, (14), 2186-2193.

3. Oberg, T.; Ohrstrom, T.; Bergstrom, J., Metal catalyzed formation of chlorinated aromatic compounds: a study of the correlation pattern in incinerator fly ash. *Chemosphere* **2007,** *67*, (9), S185-90.

4. Raclavska, H.; Raclavsky, K.; Matysek, D., Colour measurement as a proxy method for estimation of changes in phase and chemical composition of fly ash formed by combustion of coal. *Fuel* **2009,** *88*, (11), 2247-2254.

5. Rickard, W. D. A.; Williams, R.; Temuujin, J.; van Riessen, A., Assessing the suitability of three Australian fly ashes as an aluminosilicate source for geopolymers in high temperature applications. *Materials Science and Engineering: A* **2011,** *528*, (9), 3390-3397.

6. Addink, R.; Altwicker, E. R., Role of copper compounds in the de novo synthesis of polychlorinated dibenzo-p-dioxins/dibenzofurans. *Environ Eng Sci* **1998,** *15*, (1), 19-27.

7. Alderman, S. L.; Farquar, G. R.; Poliakoff, E. D.; Dellinger, B., An infrared and X-ray spectroscopic study of the reactions of 2-chlorophenol, 1,2-dichlorobenzene, and chlorobenzene with model cuO/silica fly ash surfaces. *Environmental science & technology* **2005,** *39*, (19), 7396-401.

8. Lomnicki, S.; Dellinger, B., A detailed mechanism of the surface-mediated formation of PCDD/F from the oxidation of 2-chlorophenol on a CuO/silica surface. *Journal of Physical Chemistry A* **2003,** *107*, (22), 4387-4395.

9. Lomnicki, S.; Truong, H.; Vejerano, E.; Dellinger, B., Copper oxide-based model of persistent free radical formation on combustion-derived particulate matter. *Environmental science & technology* **2008,** *42*, (13), 4982-8.

10. Nganai, S.; Lomnicki, S. M.; Dellinger, B., Formation of PCDD/Fs from the copper oxide-mediated pyrolysis and oxidation of 1,2-dichlorobenzene. *Environmental science & technology* **2011,** *45*, (3), 1034-40.

11. Gullett, B. K.; Linak, W. P.; Touati, A.; Wasson, S. J.; Gatica, S.; King, C. J., Characterization of air emissions and residual ash from open burning of

electronic wastes during simulated rudimentary recycling operations. *J Mater Cycles Waste* **2007,** *9*, (1), 69-79.

12. Nganai, S.; Lomnicki, S.; Dellinger, B., Ferric oxide mediated formation of PCDD/Fs from 2-monochlorophenol. *Environmental science & technology* **2009,** *43*, (2), 368-73.

13. Nganai, S.; Lomnicki, S.; Dellinger, B., Formation of PCDD/Fs from oxidation of 2-monochlorophenol over an Fe2O3/silica surface. *Chemosphere* **2012,** *88*, (3), 371-6.

Chapter IV. Discussion

Many researchers have shown before, that metal oxides catalyze the formation of PCDD/Fs.[1-3] Interactions between substituted aromatic precursors and metal oxide surfaces lead to the formation of surface-bound EPFRs, through the reduction of the metal active site.[4, 5] Condensation of EPFRs with each other or with gas phase precursors gives way to a PCDD/F.[1, 6-8]

4.1 PCDD/F Formation on Aluminas and Aluminosilicates

Decomposition profiles of 2-MCP over studied surfaces varied significantly (see Figure 4.1). The highest 2-MCP destruction yield was observed for γ-alumina (>99.9% destruction over studied temperature range) and the fly ash surrogate 5% Fe_2O_3/Silica (>90% destruction). It is evident, that these two catalysts are very active and catalytically oxidize 2-MCP on their surfaces at temperatures below 250 ^{0}C. The significantly higher surface area of γ-alumina is a contributing factor to its activity in the degradation of 2-MCP.

For the fly ash, α-alumina, and mullite, a gradual increase of 2-MCP degradation with increasing reaction temperature was observed, however, temperatures above 400 ^{0}C are required to achieve ~95% degradation. A close to linear dependence of 2-MCP degradation within the entire temperature range was observed for α-alumina, mullite, and fly ash (see Figure 4.1). Though the degradation at 250 ^{0}C was much lower for the fly ash, stronger temperature dependence resulted in higher conversions at temperatures above 450 ^{0}C.

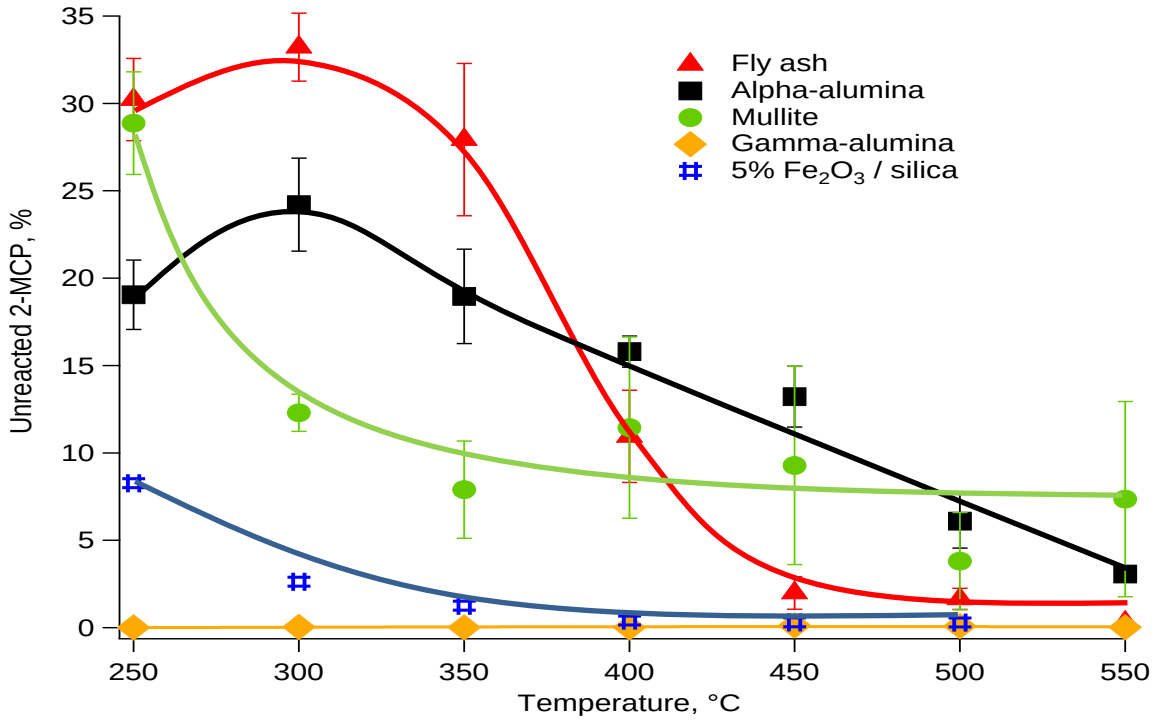

Figure 4.1. 2-MCP oxidative decomposition over the Fe_2O_3/silica surrogate, fly ash, α-alumina, mullite, and γ-alumina

The 2-MCP decomposition over fly ash differed from that of the Fe_2O_3/silica surrogate despite having a similar concentration of iron. Because iron is known to be particularly active in this temperature region, it seems likely that not all the iron in the fly ash may be available as active surface sites or it is present in a different coordination environment. This correlates with XPS results that show a weak iron signal under high-resolution scan. With a total surface area of 13.65m^2/g and a relatively small pore volume of 6.49x$10^{-3}$$cm^3$/g, the inner pore system of the studied fly ash is not significantly developed. While iron oxide could be present on the interior surface of the fly ash pores, and therefore hidden from XPS analysis, the available surface sites would be sparse and the average pore diameter (~19Å) would interfere with desorption of any PCDD/F products.

The high catalytic activity of γ-alumina is related to the surface sites in its crystal structure. Along with surface hydroxyl groups, γ-alumina has Al^{3+} Lewis acid sites that aid in adsorption of substituted organic species.[9, 10] High temperature pretreatment of the catalyst prior to the experiment removes hydroxyl coverage from the surface and increases the number of Al^{3+} sites available for adsorption of the precursor. Catalytic oxidation research suggests the catalytic activity of γ-alumina increases as the ratio of these two types of surface sites approaches one.[10, 11] Activation of the catalyst at 450 ºC prior to each experiment leads to approximately twice as many hydroxyl sites as Lewis acid sites.[12]

The lower activity of α-alumina and mullite, when compared to γ-alumina, is due to a difference in their active sites. The surface of α-alumina likely has a greater degree of hydroxyl group coverage and removing them to expose Al^{3+} Lewis acid sites could possibly require more extreme pretreatment conditions than on the γ-alumina surface. Lower catalytic activity on aluminas with higher ratios of hydroxyl groups to Lewis acid sites has been observed.[10, 11] The surface of mullite contains Si-bound hydroxyl groups and Al-bound hydroxyl groups. While chemisorption of 2-MCP can take place on the Si-bound hydroxyl groups to form chlorophenolate species[13, 14], electron transfer to form an EPFR does not occur. Al-bound hydroxyl groups would be the primary sites for EPFR formation on the mullite surface and condensation could involve chemisorbed species on Si-bound hydroxyl groups.

Destruction of 2-MCP resulted in formation of PCDD/Fs for all studied systems. Briefly, the surface-mediated mechanism for PCDD/F formation consists of the chemisorption of a precursor molecule to the catalytic surface to form an

environmentally persistent free radical (EPFR). The EPFRs are then able to react with each other to form PCDFs or upon further transformation react with gas-phase precursor molecules to form PCDDs.[1] According to this mechanism, only simple PCDDs and PCDFs such as dibenzo-*p*-dioxin (DD), 2-monochlorodibenzo-*p*-dioxin (2-MCDD), dibenzofuran (DF) and 4,6-dichlorodibenzofuran (4,6-DCDF) are anticipated to be formed from 2-MCP as a result of the direct condensation reactions. Indeed, such species were the dominant PCDD/F observed products, while small yields of higher chlorinated (tri- and tetraCDD) were also detected. The total PCDD/F product yields are presented in Figure 4.2 as a function of temperature under oxidative conditions.

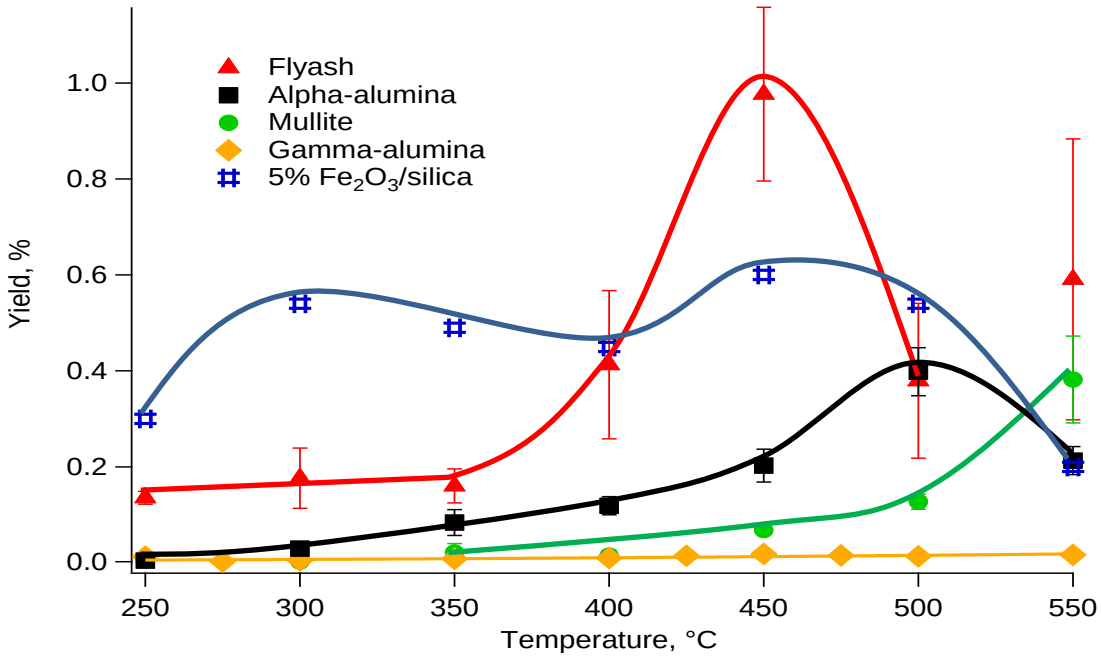

Figure 4.2. PCDD/F yields from the oxidation of 2-MCP over the Fe_2O_3/silica surrogate, fly ash, α-alumina, mullite, and γ-alumina

A stark contrast in the yields of PCDD/Fs was observed for different aluminas. The analysis of the reaction products for γ-alumina has indicated very low yields of

PCDD/Fs in the studied temperature region with a maximum at ~450 ^{0}C (0.01% yield of dibenzo-*p*-dioxin). Though the result is surprising, it is not entirely unanticipated. The high activity of γ-alumina, in the decomposition of 2-MCP, results in an unfavorable condition for surface condensation processes. It is likely that PCDD/F products are formed in the highly developed pore system – this is supported by observation of EPFR formation over γ-alumina.[15] With an average pore diameter of ~19 Å, precursor molecules are able to enter but PCDD/F products would be trapped ("ship-in-a-bottle" effect) and prone to secondary decomposition processes.

2-MCP oxidation over α-alumina produced PCDD/Fs with yields up to ~0.3% (see Figure 4.2). The maximum formation was observed at 500 ^{0}C, a temperature higher than the maximum yield temperatures for copper oxide and iron oxide surrogates (350 ^{0}C and 450 ^{0}C, respectively).[6-8] Smaller yields and shift of the maximum formation towards higher temperature indicates α-alumina is less active in the formation of PCDD/Fs compared to the transition metal ions such as copper and iron. However, in spite of its lower activity, aluminum-containing compounds are found in fly ash in concentrations many times higher than transition metals, therefore their contributions cannot be discounted. This is also true for mullite, which exhibited a similar yield of PCDD/Fs to α-alumina (~0.3% at 550 ^{0}C). The higher temperature of maximum yield compared to α-alumina indicates that mullite active sites have higher activation energy, likely due to the differences in the coordination environment of active sites. One can assume a similar mechanism of PCDD/F formation is taking place on both α-alumina and mullite surface as on transition metal oxides. Although future work using model fly ashes containing aluminas and aluminosilicates could better quantify the contributions

from these compounds, they could be the primary contributors to PCDD/F formation under certain incinerator conditions.

Formation of an EPFR contains a key step involving transfer of an electron from the chemisorbed precursor to the metal center, thereby reducing the metal.[1, 4, 5] Aluminum is less likely to accept an electron compared to transition metal oxides such as iron and copper. Patterson, et al. investigated the formation of surface-bound radicals on alumina. Reaction between phenol and γ-alumina yields phenoxyl radicals that are consistent with those formed on transition metal oxides.[15] The fate of the transferred electron was found to reside in F-centers. F-centers are crystallographic defects where a missing anion is replaced by an electron. These defects allow alumina to accept an electron from chemisorbed precursors and form surface-bound radicals. Decay of phenoxyl radicals on γ-alumina exhibit two distinct rates.[15] Phenoxyl radicals likely have different decay rates based on the identity of their alumina adsorption site. In γ-alumina, there are both Al^{3+} Lewis acid adsorption sites and hydroxyl groups that initiate hydrogen bonding.[9, 16, 17] The ratio of these sites is heavily dependent on pretreatment conditions, with higher temperatures leading to less hydroxyl groups and more Lewis acid sites.[12]

The EPA Test Burn Installation fly ash was used to compare the formation of PCDD/F with surrogate samples (see Figure 4.3). Observed maximum PCDD/F yield of ~1.0% at 450 ^{0}C is significantly higher than both mullite and α-alumina and even slightly higher than the Fe_2O_3/silica surrogate (a maximum yield of ~0.6%). This is surprising as iron oxide is known to strongly contribute to PCDD/F formation in the post-combustion cool zone. The studied fly ash contains iron, mullite, and amorphous

alumina. However, PCDD/F yields over fly ash are almost 80% higher compared to iron oxide surrogate and show a different formation temperature profile (see Figure 4.3). A further discourse between the activity of iron oxide and studied fly ash is more evident when comparing the congener pattern formed from 2-MCP reaction. Fly ashes produced mainly 2-MCDD, while iron oxide formed a mixture of 4,6-DCDF, DF, DD and 2-MCDD. Fly ash also formed small amounts of dichlorodibenzo-*p*-dioxin, a secondary chlorination product that also formed on all aluminum-containing catalysts. The congener profile from fly ash, containing secondary chlorination products and higher ratios of PCDD:PCDF, matches more closely to the congener profiles of the aluminas. The fly ash exhibits the higher yields of transition metal oxides and the congener profile of aluminum-containing compounds, implying synergistic effects involving transition metal oxides increasing the catalytic activity of aluminum active sites.

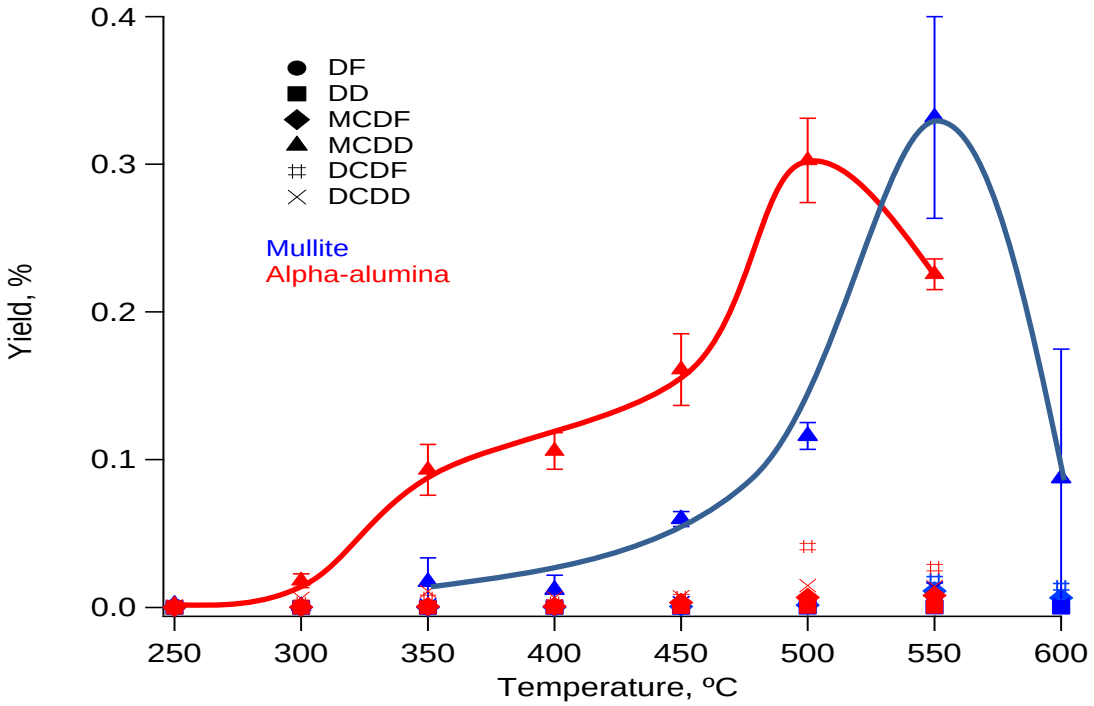

Figure 4.3. PCDD/F yields from the oxidation of 2-MCP over α-alumina and mullite

This observation is significant from the perspective of potential predictive models of PCDD/F formation based on fly ash composition as well as understanding the factors governing their yields. The presence of high concentration of metal (iron in this case) does not necessary translate to similar catalytic activity observed on pure metal oxide compositions. One of the potential explanations is surface availability of such metal oxides. Lab-made surrogates have their entire transition metal content on the surface and available for adsorption. In real fly ash, a portion of the metal oxides is contained within the particle, covered by other components, and is not available for precursor adsorption. At the same time, we have shown both alumina and aluminosilicates to affect the formation of PCDD/Fs.

4.2 Predicting PCDD/Fs in Fly Ash

The ability to predict PCDD/F yields on fly ash is extremely valuable as a way to lower costs and time in analyzing physical samples. The congener profile and PCDD/F yields from fly ash are related to the catalytic sites available on the fly ash surface. The components of fly ash, and their active sites, are directly related to incinerator feedstock makeup. The sum of PCDD/F yields from the Fe_2O_3/silica surrogate, α-alumina, and mullite is shown in Figure 4.4 alongside the total PCDD/F yield from fly ash. Currently referred to as the 'predicted yield,' this sum represents the three primary PCDD/F contributors found in this particular fly ash. The fly ash and the predicted yield share a similar maximum yield and temperature formation profile. The slight shift in the maximum is attributed to the higher temperatures required by aluminas and aluminosilicates to form PCDD/Fs. The high baseline at low temperatures seen in the predicted yield is due to higher concentrations of PCDFs resulting from Fe_2O_3 activity.

These results indicate that combustion-generated particulate matter can be viewed as a sum of its parts with regard to PCDD/F formation. The additive and possibly cooperative effects from the complex mixture of transition metals, alumina, and aluminosilicates leads to a significantly higher PCDD/F yield than any one component.

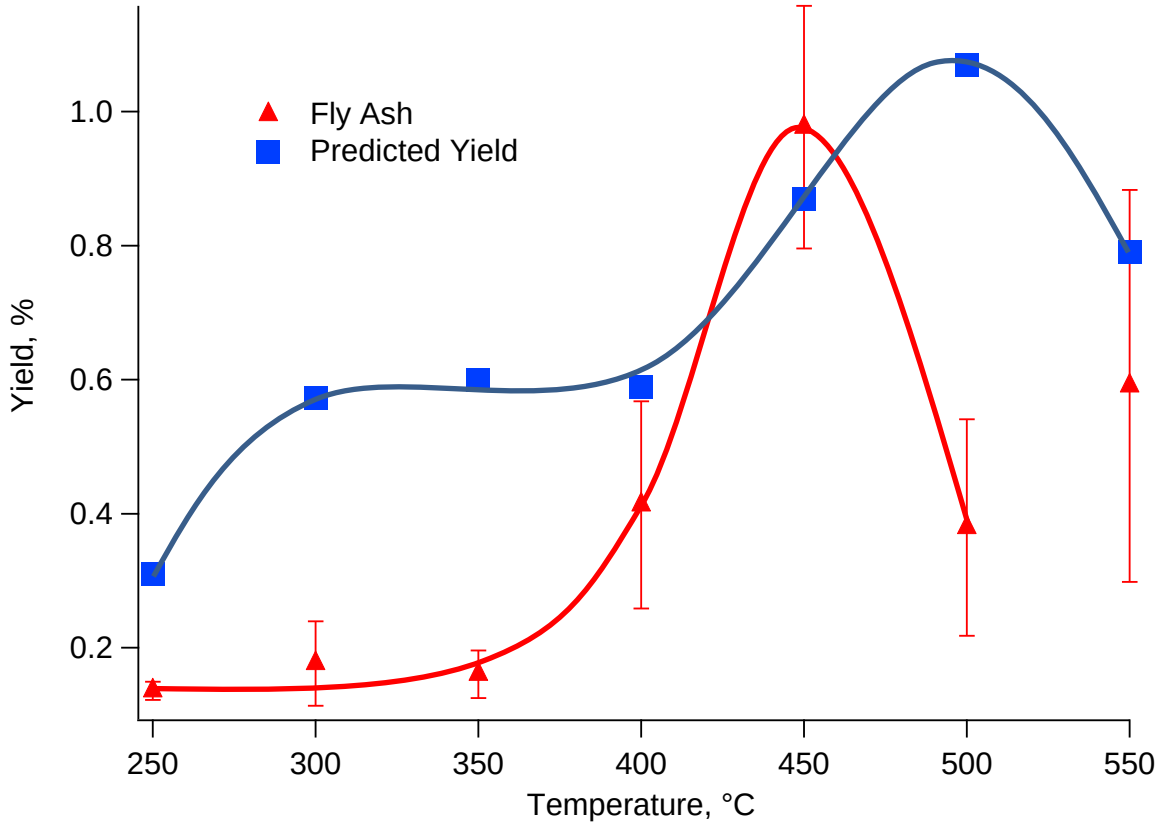

Figure 4.4. Comparison of PCDD/F yields from fly ash and predicted yields from a sum of studied fly ash components

For aluminas and aluminosilicates, which form a primary portion of the bulk structure of fly ash, the number of active sites far surpasses the concentration of organic species. For this reason, the PCDD/F yields from pure samples of aluminas and aluminosilicates were not adjusted before summing. For trace components, whose

number of active sites is more heavily dependent on their concentration on the fly ash surface, adjustments to the PCDD/F yields could lead to a more accurate prediction.

The sum of only three components should not detract from the large number of other factors that affect PCDD/F formation, including: surface area, catalytic site availability, reaction atmosphere, pressure, etc., but instead emphasize the importance of the fly ash chemical makeup on its ability to form PCDD/Fs. Once such effects are well understood, a mathematical equation can be designed that accurately identifies the expected PCDD/F surface concentrations and other quantifiable data like PCDD/PCDF ratios through input of the concentrations of various fly ash components. In a simple form, the equation will be a sum of yields from various components weighted based on each components concentration in the combustion system. Factors such as differing product profiles, surface availability, and catalytic synergy between components would allow the equation to grow to a more complex state.

4.3 Fe/Cu Synergy in PCDD/F Formation

Fly ash is a complex mixture of components whose concentration can vary widely based on incinerator feedstock. Knowing how multiple components affect each other, either synergistic or inhibitive, is paramount to understanding the formation of PCDD/Fs on fly ash surfaces. Synergistic effects between Fe and Cu in multicatalysis have been observed in a wide variety of applications.[18-25] Even in reactions where one catalyst was inactive on its own, synergistic effects were exhibited upon its addition to a bimetallic system.[19]

While most applications involve nanoparticles of metallic Fe and Cu, this work focused on Fe_2O_3 and CuO co-impregnated onto silica powder to simulate the structure of fly ash. Previous research involved monometallic fly ash surrogates containing 5% w/w of either Fe_2O_3 or CuO. For the sake of comparison, three bimetallic surrogates were made with a total of 5% w/w metal oxide and varying ratios of co-impregnated Fe_2O_3 and CuO. The three bimetallic surrogates contained Fe_2O_3:CuO ratios of 4, 1, and 0.25, which corresponds to Fe:Cu ratios of 1.8, 0.44, and 0.11, respectively.

The mechanism for EPFR formation on individual transition metal oxides has been thoroughly characterized.[4, 5, 26, 27] This mechanism can be applied to bimetallic surfaces as well. Intermediate species on bimetallic surfaces have not been investigated and their structure and lifetimes are unknown. On monometallic surrogates, phenoxyl-type radicals are the intermediates that condense to form PCDD/Fs. Phenoxyl-type radicals are likely formed on the bimetallic surrogates. The synergistic effects between the iron active sites and the copper active sites likely arise from the structure of the metal oxides on the surrogate surface. The proximity of the two metal oxides would affect the condensation of the surface-bound intermediates and the catalytic activity of the metal oxide active sites. Characterization of the surface of both fresh and used bimetallic surrogates using XPS and SEM-EDS would assist in gaining insight to the way in which the two metals influence each other when in close proximity.

In past research, monometallic Fe_2O_3 and CuO surrogates have exhibited different PCDD/F yields and congener profiles even when reacting with the same

precursor. In reactions involving 2-MCP, CuO surrogates yield congener profiles with much higher ratios of PCDDs. Fe_2O_3 surrogates yield approximately equal quantities of PCDDs and PCDFs, which also leads to higher overall PCDD/F yield than their CuO counterparts. Using this distinction, it is possible to determine how Fe and Cu are influencing the reaction in a bimetallic system.

The conversion of 2-MCP over the three studied bimetallic Fe/Cu surrogates is shown in Figures 4.5 and 4.6. For reference, previously obtained results from monometallic surrogates are also included on the graph. Under pyrolytic conditions, the

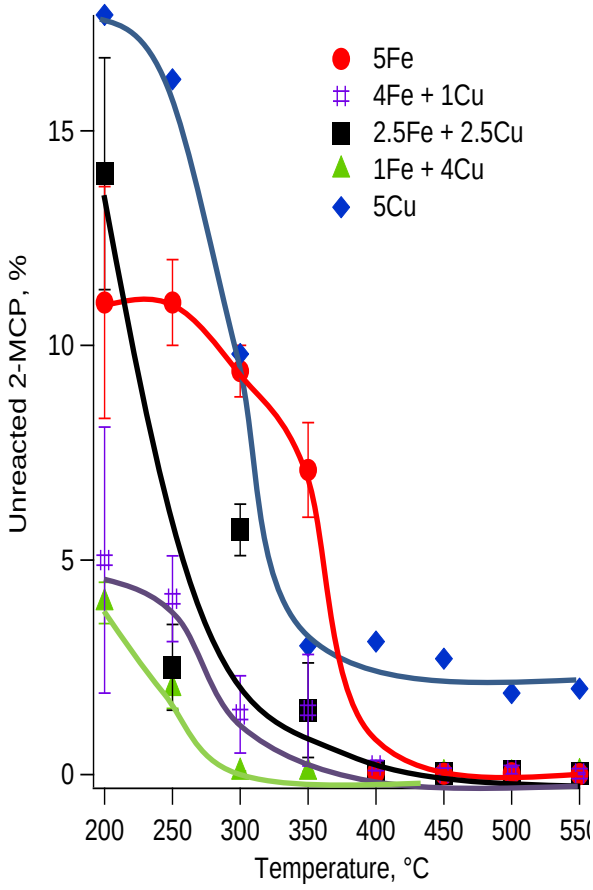

Figure 4.5. Pyrolytic degradation of 2-MCP over three bimetallic catalysts. Monometallic catalyst data for reference.

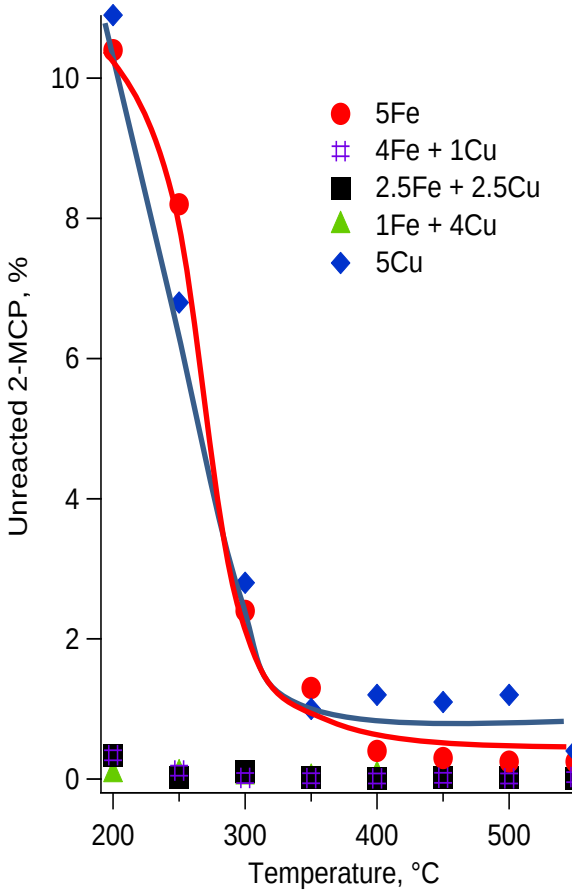

Figure 4.6. Oxidative degradation of 2-MCP over three bimetallic catalysts. Monometallic catalyst data for reference

bimetallic surrogates act in a similar manner to their monometallic counterparts in the catalytic oxidation of 2-MCP (see Figure 4.5). All three bimetallic surrogates are extremely catalytically active under oxidative conditions and convert >99.5% of the 2-MCP precursor across the entire measured temperature range (see Figure 4.6).

This significant increase in activity is exclusive to the bimetallic surrogates. Monometallic surrogates show only a small increase in activity between pyrolytic and oxidative conditions. The bimetallic cooperativity between the Fe_2O_3 and the CuO in oxidative conditions is expressed primarily through a fast 2-MCP destruction rate.

The total PCDD/F yields from the bimetallic surrogates are shown in Figure 4.7. There is an inverse relationship between the conversion of 2-MCP and the formation of PCDD/Fs. Under oxidative conditions, the rate of destruction of 2-MCP surpasses the rate of condensation of PCDD/F intermediates. Similar to γ-alumina, the bimetallic surrogates completely oxidize 2-MCP and its associated surface-bound intermediates before they can further react to form PCDD/Fs. The synergistic effects between the Fe_2O_3 and the CuO are easily seen under pyrolytic conditions by their high yields of PCDD/Fs. In the absence of oxygen, the rate of catalytic oxidation of 2-MCP is suppressed and the rate of condensation of surface species increases. A high concentration of PCDD/Fs is the result of more condensation of surface-bound intermediates. The yield of PCDD/Fs increases with increasing Fe_2O_3 concentration.

The congener profiles of the three bimetallic surrogates contains higher quantities of PCDDs than PCDFs. PCDD:PCDF ratios of 10 or more match results obtained from monometallic CuO surrogates, but the total PCDD/F yield shows a clear relationship

with increasing Fe_2O_3 concentration. Deng, et al., studying bimetallic catalyzed formation of carbon nanotubes, found that some metals are better at catalyzing nucleation and some are better at catalyzing growth of nanotubes.[20] By combining the best performing metal from each category, a bimetallic catalyst that exhibited the strengths of each metal was formed. Siriwardane, et al. found that mixtures of Fe_2O_3 and CuO were extremely active in the release of O_2 for chemical looping combustion, while individually Fe_2O_3 exhibited low activity and CuO experienced agglomeration problems.[25] In the Fe_2O_3 + CuO bimetallic catalysts studied in this work, CuO is influencing the congener profile while the synergistic effects of Fe_2O_3 are causing an overall increase in PCDD/F yield. EPFRs formed on CuO tend to undergo Eley-Rideal reactions with gas phase precursors to form higher yields of PCDDs. The addition of Fe_2O_3 does not affect this preference for Eley-Rideal type reactions but it does provide higher concentrations of EPFRs to undergo these condensation reactions with gas phase precursors, thereby leading to higher overall yields of total PCDD/Fs.

The location and structure of the transition metal oxides on the silica powder is currently unknown. Due to their synergistic effects, the Fe_2O_3 and CuO are likely in close proximity to each other in mixed nanoparticles on the surface of the fly ash surrogate. Wojciechowska, et al. showed that bimetallic catalysts of Cr2O3 and CuO experienced charge transfers from Cr to Cu.[28] The charge transfer goes to the metal with higher redox potential. Even if one component is inactive in reaction, as was the case with the Cr_2O_3/CuO catalyst, the synergistic effects still lead to an increase in catalytic activity for the active sites. In the case of the Fe/Cu bimetallic catalyst, charge

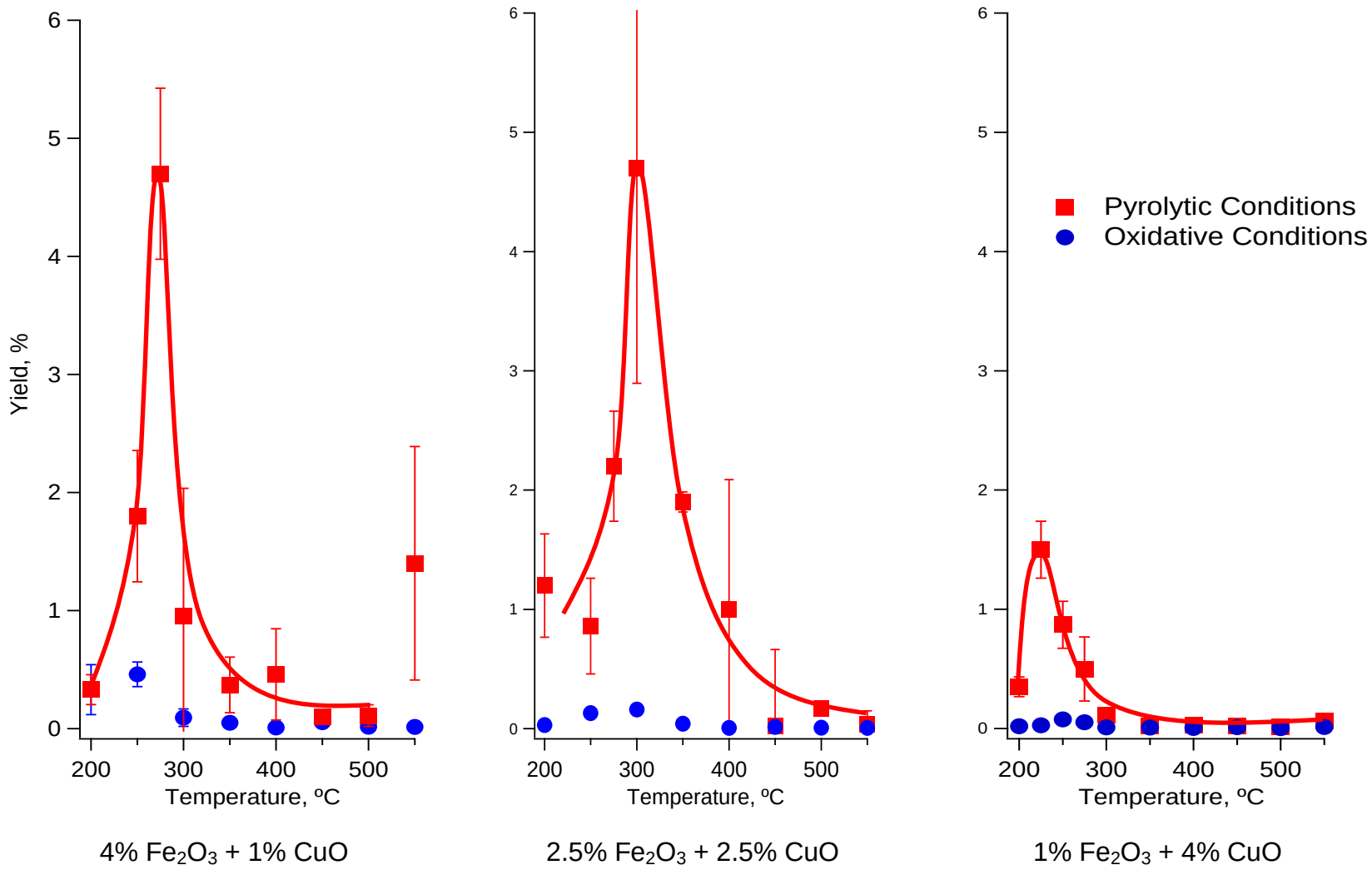

Figure 4.7. Total PCDD/F yields from the thermal degradation of 2-MCP over Fe/Cu bimetallic catalysts.

transfer would travel from Cu to Fe. After charge transfer, the highly oxidized Cu sites would be very catalytically active towards formation of surface-bound radicals.

4.4. Lab-scale vs. Full-scale Results

While an overall conversion of 5% precursor to dioxin may seem absurdly high to take place in a full-scale reactor, these synergistic reactions are only occurring in certain regions of an incineration system. In a well-mixed reactor, temperatures and oxygen concentration will be lower farther from the flame. 'Pyrolytic pockets' will develop that are poorly-mixed. Poorly-mixed regions are going to be oxygen starved and have cooler temperatures. Conditions in poorly-mixed regions are ideal for transition metal oxides to produce high yields of PCDD/Fs. Non-transition metal oxides, like aluminas and aluminosilicates, produce high yields of PCDD/Fs in the well-mixed regions when exposed to higher concentrations of oxygen and higher temperatures. Particulary high yields from bimetallic catalysts at low temperatures under pyrolytic conditions are a possible cause for unexplained PCDD/F formation in full-scale incinerators.

Comparing and contrasting individual lab-scale experiments to full-scale emissions leads to the false assumption that the two sets of results should match when in actuality, the full-scale system should be viewed as a wide range of conditions and reactions that would be almost impossible to mimic in a lab-scale experiment.

4.5 References

1. Lomnicki, S.; Dellinger, B., A detailed mechanism of the surface-mediated formation of PCDD/F from the oxidation of 2-chlorophenol on a CuO/silica surface. *Journal of Physical Chemistry A* **2003,** *107*, (22), 4387-4395.

2. Gullett, B. K.; Bruce, K. R.; Beach, L. O., The Effect of Metal-Catalysts on the Formation of Polychlorinated Dibenzo-Para-Dioxin and Polychlorinated Dibenzofuran Precursors. *Chemosphere* **1990,** *20*, (10-12), 1945-1952.

3. Olie, K.; Addink, R.; Schoonenboom, M., Metals as catalysts during the formation and decomposition of chlorinated dioxins and furans in incineration processes. *J Air Waste Manage* **1998,** *48*, (2), 101-105.

4. Lomnicki, S.; Truong, H.; Vejerano, E.; Dellinger, B., Copper oxide-based model of persistent free radical formation on combustion-derived particulate matter. *Environmental science & technology* **2008,** *42*, (13), 4982-8.

5. Vejerano, E.; Lomnicki, S.; Dellinger, B., Formation and stabilization of combustion-generated environmentally persistent free radicals on an Fe(III)2O3/silica surface. *Environmental science & technology* **2011,** *45*, (2), 589-94.

6. Nganai, S.; Lomnicki, S.; Dellinger, B., Ferric oxide mediated formation of PCDD/Fs from 2-monochlorophenol. *Environmental science & technology* **2009,** *43*, (2), 368-73.

7. Nganai, S.; Lomnicki, S.; Dellinger, B., Formation of PCDD/Fs from oxidation of 2-monochlorophenol over an Fe2O3/silica surface. *Chemosphere* **2012,** *88*, (3), 371-6.

8. Nganai, S.; Lomnicki, S. M.; Dellinger, B., Formation of PCDD/Fs from the copper oxide-mediated pyrolysis and oxidation of 1,2-dichlorobenzene. *Environmental science & technology* **2011,** *45*, (3), 1034-40.

9. Kim, S.; Byl, O.; Yates, J. T., Jr., Adsorption of triethylenediamine on Al2O3-III: Bonding to Lewis acid Al3+ sites. *The journal of physical chemistry. B* **2005,** *109*, (13), 6331-3.

10. Zhang, L.; Zheng, M.; Liu, W.; Zhang, B.; Su, G., A method for decomposition of hexachlorobenzene by gamma-alumina. *Journal of hazardous materials* **2008,** *150*, (3), 831-4.

11. Mawhinney, D. B.; Rossin, J. A.; Gerhart, K.; Yates, J. T., Adsorption and reaction of 2-chloroethylethyl sulfide with Al2O3 surfaces. *Langmuir : the ACS journal of surfaces and colloids* **1999,** *15*, (14), 4789-4795.

12. Thomas, J. K., Physical aspects of radiation-induced processes on SiO2, gamma-Al2O3, zeolites, and clays. *Chemical reviews* **2005,** *105*, (5), 1683-1734.

13. Alderman, S. L.; Dellinger, B., FTIR investigation of 2-chlorophenol chemisorption on a silica surface from 200 to 500 degrees C. *The journal of physical chemistry. A* **2005,** *109*, (34), 7725-31.

14. Pan, W.; Zhong, W.; Zhang, D.; Liu, C., Theoretical study of the reactions of 2-chlorophenol over the dehydrated and hydroxylated silica clusters. *The journal of physical chemistry. A* **2012,** *116*, (1), 430-6.

15. Patterson, M. C.; Keilbart, N. D.; Kiruri, L. W.; Thibodeaux, C. A.; Lomnicki, S.; Kurtz, R. L.; Poliakoff, E. D.; Dellinger, B.; Sprunger, P. T., EPFR formation from phenol adsorption on Al2O3 and TiO2: EPR and EELS studies. *Chem Phys* **2013,** *422*, 277-282.

16. Kim, S.; Byl, O.; Yates, J. T., Jr., The adsorption of triethylenediamine on Al(2)O(3)-I: a vibrational spectroscopic and desorption kinetic study of surface bonding. *The journal of physical chemistry. B* **2005,** *109*, (8), 3499-506.

17. Kim, S.; Byl, O.; Yates, J. T., Jr., The adsorption of triethylenediamine on Al(2)O(3)-II: hydrogen bonding to Al-OH groups. *The journal of physical chemistry. B* **2005,** *109*, (8), 3507-11.

18. Santos, M. M.; Schuchardt, U., The Synergistic Effect in Oxidative Lignin Degradation by the Biomimetic Gif System. *J Brazil Chem Soc* **1995,** *6*, (3), 257-260.

19. Schuchardt, U.; Pereira, R.; Krahembuhl, C. E. Z.; Rufo, M.; Buffon, R., Synergistic Effect of Iron and Copper Oxides Supported on Silica in the Room-Temperature Oxidation of Cyclohexane. *Appl Catal a-Gen* **1995,** *131*, (1), 135-141.

20. Deng, W. Q.; Xu, X.; Goddard, W. A., A two-stage mechanism of bimetallic catalyzed growth of single-walled carbon nanotubes. *Nano Lett* **2004,** *4*, (12), 2331-2335.

21. Zhu, N. R.; Luan, H. W.; Yuan, S. H.; Chen, J.; Wu, X. H.; Wang, L. L., Effective dechlorination of HCB by nanoscale Cu/Fe particles. *Journal of hazardous materials* **2010,** *176*, (1-3), 1101-1105.

22. Koutsospyros, A.; Pavlov, J.; Fawcett, J.; Strickland, D.; Smolinski, B.; Braida, W., Degradation of high energetic and insensitive munitions compounds by Fe/Cu bimetal reduction. *Journal of hazardous materials* **2012,** *219*, 75-81.

23. Shirakawa, E.; Ikeda, D.; Masui, S.; Yoshida, M.; Hayashi, T., Iron-Copper Cooperative Catalysis in the Reactions of Alkyl Grignard Reagents: Exchange Reaction with Alkenes and Carbometalation of Alkynes. *Journal of the American Chemical Society* **2012,** *134*, (1), 272-279.

24. He, M. S.; Chernov, A. I.; Obraztsova, E. D.; Jiang, H.; Kauppinen, E. I.; Lehtonen, J., Synergistic effects in FeCu bimetallic catalyst for low temperature growth of single-walled carbon nanotubes. *Carbon* **2013,** *52*, 590-594.

25. Siriwardane, R.; Tian, H. J.; Simonyi, T.; Poston, J., Synergetic effects of mixed copper-iron oxides oxygen carriers in chemical looping combustion. *Fuel* **2013,** *108*, 319-333.

26. Alderman, S. L.; Farquar, G. R.; Poliakoff, E. D.; Dellinger, B., Reaction of 2-chlorophenol with CuO: XANES and SEM analysis. *Proceedings of the Combustion Institute* **2005,** *30*, (1), 1255-1261.

27. Dellinger, B.; Loninicki, S.; Khachatryan, L.; Maskos, Z.; Hall, R. W.; Adounkpe, J.; McFerrin, C.; Truong, H., Formation and stabilization of persistent free radicals. *Proceedings of the Combustion Institute* **2007,** *31*, 521-528.

28. Wojciechowska, M.; Lomnicki, S.; Bartoszewicz, J.; Goslar, J., Characteristics of Cr2o3-Cuo/Mgf2 Catalysts and a Comparison with Cr2o3/Mgf2 and Cuo/Mgf2 Systems. *J Chem Soc Faraday T* **1995,** *91*, (14), 2207-2211.

Chapter V. Conclusions

Non-transition metals have been largely discounted in the past as nonparticipants in the formation of PCDD/Fs. While this may be true for some non-transition metals that are prevalent in fly ash, as in the case of SiO_2, other common components, such as aluminas and aluminosilicates, do play roles in PCDD/F formation. Particularly under oxidative conditions and at the higher temperatures of the cool zone range, aluminas and aluminosilicates can make significant contributions to PCDD/F formation. Specifically, α-alumina and mullite, both found in real world fly ash, exhibited maximum PCDD/F yields of 0.4% from the catalytic oxidation of 2-MCP. A real world fly ash sample containing both alumina and mullite reached a maximum of 1.0% PCDD/F yield. The mechanism for PCDD/F formation on aluminum-containing compounds has not been completely investigated. Similar to transition metal oxides, the initial step involving a surface-bound radical does take place on aluminas and therefore it can be inferred that condensation of surface-bound radicals is still the primary pathway for PCDD/F formation on these components.

The ability to predict PCDD/F yield from incineration systems would provide a fast and cheap alternative to real-time analysis for quantitative, and possibly qualitative, information about PCDD/F emissions. By taking into account the inorganic makeup of a fly ash, accurate predictions can be made about the PCDD/F concentration on the fly ash. This was very simply exhibited by summing the PCDD/F yields of α-alumina, mullite, and a Fe_2O_3/silica surrogate and comparing it to the real fly ash that contained alumina, mullite, and a similar concentration of Fe_2O_3. This simple sum matches

surprisingly close to the real fly ash in both total PCDD/F yield and temperature of maximum formation.

Model fly ash surrogates have been criticized for their inability to mimic real fly ash in the formation of PCDD/Fs. By studying Fe/Cu bimetallic surrogates, we have found that synergistic catalytic effects are one area of PCDD/F formation that has received little consideration. Fly ash is a complex mixture of many metals and studying them individually ignores their group interactions.

The mechanism of PCDD/F formation on bimetallic catalysts is still unknown but results indicate that copper sites are controlling the precursor condensation congener profiles matching those of monometallic copper oxide surrogates. The concentration of iron sites has a direct relationship with the total PCDD/F yield, indicating a synergistic effect that increases the activity of the copper sites.

The synergistic effects of Fe/Cu bimetallic surrogates under pyrolytic conditions are a step towards completing our understanding of PCDD/F formation. The development of pyrolytic pockets containing these cooperative metals in incineration systems is a likely cause of unexplained PCDD/F emission spikes.

Vita

Phillip Mackenzie Potter was born in July 1986 in Bell County, Texas. He attended Augusta State University in Augusta, Georgia where he received the degree of Bachelor of Science in Chemistry in 2009. Phillip Potter went on to further his chemistry education at Louisiana State University, joining the graduate program in the fall of 2009. He studied under Dr. Barry Dellinger, Patrick F. Taylor Chair of Environmental Chemistry and Director of the LSU Superfund Research Program (LSU-SRP). He is a candidate to receive a Doctor of Philosophy degree in Chemistry in May 2015.